Analysis of Stability and Viscous-Inviscid Interaction in Compressible Boundary Layers

A thesis presented for the degree of

Doctor of Philosophy of Imperial College

and the

Diploma of Imperial College

by

Thomas de Cointet

Department of Mathematics

Imperial College

180 Queen's Gate, London SW7 2BZ

OCTOBER 24, 2015

Table of contents

List of Figures

Abstract

This work belongs to the theory of fluid flows at high Reynolds number, characterised by low viscosity and, to a lesser extent, high speeds. It is a mathematically intensive field covering most aspects of applied mathematics, from Partial Differential equations to Numerical Analysis and Complex Analysis. Two of the central areas of research within this particular branch of fluid dynamics are the boundary-layer laminar-turbulent transition and the boundary-layer separation. Both of these phenomena have a high impact on the aerodynamic performance of aircraft wings, turbine blades and other fast-moving objects such as rockets. As a consequence, their study is relevant both for industrial applications and to the scientific community as a whole.

The mathematical element pertaining to the analysis of these two phenomena is the consistent use of asymptotic methods, such as matched asymptotic expansions and multiple-scales analysis. In particular, this work will be based on the viscous-inviscid interaction theory originally discovered by Lin (1955) and further developed by the work of Neiland (1969) and Stewartson & Williams (1969).

In the first chapter of this thesis, we will study the initial stages of the laminar-turbulent transition of a compressible boundary layer on a swept wing. The instability of interest will be the stationary crossflow vortex, which is known to be the main instability mode in three-dimensional boundary layers on a swept wing. We will focus on two specific aspects of the transition process, namely the receptivity and linear stability analysis of the flow. The receptivity mechanism introduced in our work is a roughness of size comparable with that of the boundary layer thickness. This justifies our restriction to the study of the inviscid instability of the flow and the use of the impermeability condition on the roughness.

The remaining two chapters are concerned with the viscous-inviscid interaction of the

boundary layer in the vicinity of a surface discontinuity. We will first study the behaviour of the subsonic flow exposed to the singular pressure gradient

$$\frac{\mathrm{d}p}{\mathrm{d}x} = \kappa(x_0 - x)^{-1/3}, \quad \text{as} \quad x \to x_0.$$

It forms when the body contour has a point $x = x_0$ near which

$$y_w = (x_0 - x)^{5/3}.$$

We will show how logarithmic terms need to be included in the solution. We then study a similar problem, this time in the context of an incoming transonic flow near a point of curvature discontinuity. We will show that in both cases the boundary layer experiences an "extreme acceleration".

Declaration

I certify that this thesis, and the research to which it refers, are the product of my own work, and that any ideas or quotations from the work of other people, published or otherwise, are fully acknowledged in accordance with the standard referencing practices of the discipline.

Signed:

Copyright

Acknowledgements

I would like first and foremost to thank Professor A. Ruban for his brilliant supervision throughout my PhD, and the Department of Mathematics, which supported me financially through the Roth Studentship. I am especially grateful for the moral support of my family and my girlfriend Ksenia, who stood behind me. I would also like to extend my thanks to my friends and colleagues at Imperial College, in particular to Curtis Banks, David Pryce, Joseph Maestri, Radu Cimpeanu, Jamie Nutter, Yang Tao, and Tomass Bernots.

Finally, my thoughts go to all my close friends who have been there for me throughout this time, especially Alexander Desneufbourgs, Pyer Sheard, Louis Kassar, Ivo Mihaylov and Omar Sindi.

This research was performed in the Laminar Flow Control Centre (LFC-UK) at Imperial College London. The centre is supported by EPSRC, Airbus UK and EADS Innovation Works.

Chapter 1

Introduction

The theory used and developed in this thesis is applicable to a wide range of flying objects such as planes, gliders or rockets. Our focus will nevertheless be on aircraft wings, such as ones found on commercial planes. We will restrict ourselves to the local analysis of some specific parts of the wing, as opposed to studying the wing as a whole. In particular, we will study the stagnation-line flow on a swept wing and the flow in the vicinity of a curvature discontinuity. We shall begin by a brief review of the origin of drag and two fundamental phenomena which contribute to its generation.

1.1 Origin of the drag on an aircraft wing

A plane in flight experiences four different forces, traditionally paired as follows: the weight of the aircraft pulls it down, while lift compensates to keep it airborne; the thrust coming from the engines pushes it forward while the drag opposes that motion. The aim of an aerodynamicist is to design wings and fuselage in such a way as to maximise lift while minimising the drag. It turns out that optimising the lift force is a much easier task than reducing the drag. This is partly due to the fact that lift is mostly an inviscid phenomenon and thus allows for simplified equations (the Euler equations) to be used.

In order to determine the drag force over a body, viscosity should be taken into account. In addition to the mathematical difficulty associated with solving the full Navier-Stokes equations, efforts at reducing drag are often hampered by technical requirements. For

example the wing shape, mostly designed to maximise the lift, cannot be globally modified without severely reducing performance and we must resort to small local modifications. Such an example would be the addition of vortex generators or arrays of roughnesses on the surface of the wing.

The drag experienced by an aircraft is composed of

- ◇ wave drag, which is caused by shockwaves forming in the flow at and above transonic speeds;
- ◇ induced drag, which is due to the generation of lift and wing tip vortices;
- ◇ form drag, due to the shape of the aircraft;
- ◇ skin friction drag, due to the friction of air against the surface of the aircraft.

We shall concentrate here on skin friction and form drag. Turbulence and flow separation, which will be the focus of our study, are two central phenomena in fluid dynamics that contribute to the generation of these two forms of drag. Indeed, the magnitude of the skin friction τ, defined as

$$\tau = \mu \frac{\partial u}{\partial y},$$

(where μ is the dynamic viscosity of the fluid and u represents the longitudinal component of the fluid velocity) is closely related to the state of the boundary layer, with laminar boundary layers having a lower skin friction than their turbulent counterparts. Similarly, it is known that the drastically modified pressure distribution observed in separated flows leads to an increase in form drag.

In an attempt to reduce both fuel consumption and carbon-dioxide emissions, a better understanding of the transition process and separation of the boundary layer is required. In this thesis, we will address both problems, and now proceed to give a brief description of the current status of research and the challenges we are facing.

1.2 Transition to Turbulence and the role of Receptivity

The vast majority of fluid flows encountered in nature are turbulent. It is thus necessary to understand how turbulence affects quantities such as the drag or the energy of a system.

An important aspect that is one of the main focus of current research is the actual transition from a laminar flow to a turbulent one.

1.2.1 Reynold's experiment

In 1883, Reynolds demonstrated the transition to turbulence in his famous experiment on pipe flow. His apparatus consisted of a tube placed horizontally within a large glass tank filled with water as shown on Figure 1.1.

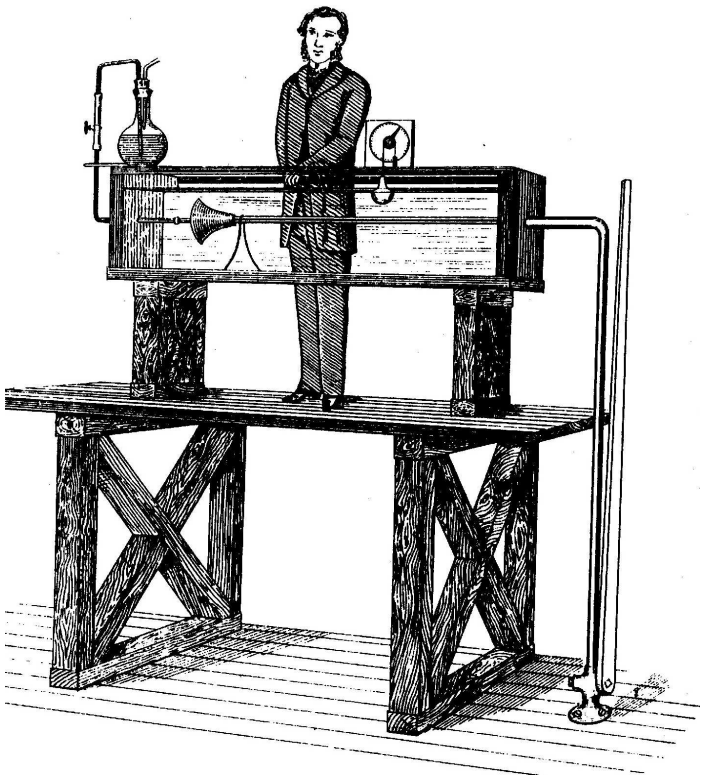

Figure 1.1: Reynold's apparatus.

One end of the tube was connected to a tap through which water flowed under the action of gravity as the tap was opened. The other end of the tube was open to the surrounding water, and fitted with a trumpet to reduce disturbances. Flow visualisation was performed with highly coloured water added to the flow in front of the trumpet. His experiment

showed that for low fluid velocities, the streak of colour extended in a perfectly straight line through the tube, as shown in Figure 1.2. This means that the flow remains steady, with the particles' trajectories being straight lines parallel to the tube axis. However, as the velocity is increased in small steps, the flow suddenly assumes an unsteady and irregular pattern, as depicted on Figure 1.3. Finally, as we further increase the velocity, the pattern seems to become random and 'chaotic', as seen on Figure 1.4 (Van Dyke 1982).

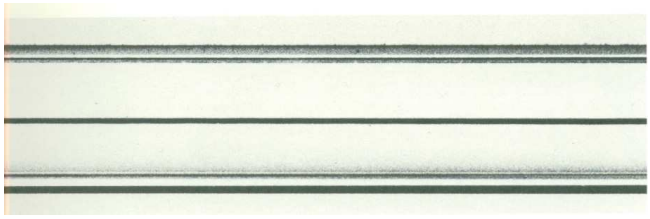

Figure 1.2: Laminar flow through the pipe.

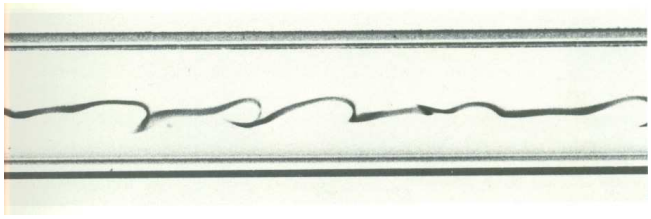

Figure 1.3: Transitional flow through the pipe.

Figure 1.4: Turbulent flow through the pipe.

Reynolds observed that this happened when the dimensionless parameter

$$\mathrm{Re} = \frac{\hat{u}_{\max} a}{\nu},$$

now called the Reynolds number after him, reaches a critical value $\mathrm{Re}_c \sim 13000$[1]. Here,

[1]It is interesting to note that linear stability predicts the flow to be linearly stable at all values of Re. This is because the analysis doesn't capture the small roughness always present on the surface of the wall.

ν represents the kinematic viscosity of the fluid, a is the diameter of the tube and $\hat{u}_{\max}$ the dimensional maximum velocity of the fluid that is reached at the tube axis. We now know that there are many factors affecting the so-called transition Reynolds number, including the presence of surface roughness, external noise and vibrations to cite but a few. This laminar-turbulent transition process is not limited to pipe flows. It was also discovered to take place in various other configurations, such as the flow on a flat plate, and a lot of research focuses on finding accurate measurement of the corresponding transition Reynolds number.

1.2.2 Subsequent research

Over a century has now passed since Reynolds introduced the basic ideas and concepts of what would become Hydrodynamic Stability Theory with his pipe-flow experiment. The advent of Computational Fluid Dynamics has enabled us to acquire deep insight in the study of turbulent flows. However, understanding the actual transition process whereby a flow loses stability and becomes turbulent remains a great challenge. The importance of predicting the onset of transition in a wide range of applications has brought its study to the forefront of research in fluid dynamics.

It is now known that in a 'quiet environment ', the transition to turbulence occurs due to an incipient instability of the basic flow field, and is provoked by the growth of instability waves in the boundary layer. Of particular interest to the aeronautical community is the boundary-layer transition of the flow over swept wings, which are standard on long range commercial aircrafts. It is currently understood to occur in four stages. The first one is referred to as 'receptivity'. Receptivity is concerned with the process by which external perturbations such as acoustic waves and surface roughness, are converted into instability modes of the flow. The second stage of the transition process is the linear growth (or decay) of the instability waves, which is predicted by the methods of Linear Stability Theory (Reed, Saric & Arnal 1996). The third stage is the nonlinear growth of the perturbations and the development of secondary instabilities. Finally, the last stage is the breakdown to turbulence. These stages are summarised in Figure 1.5.

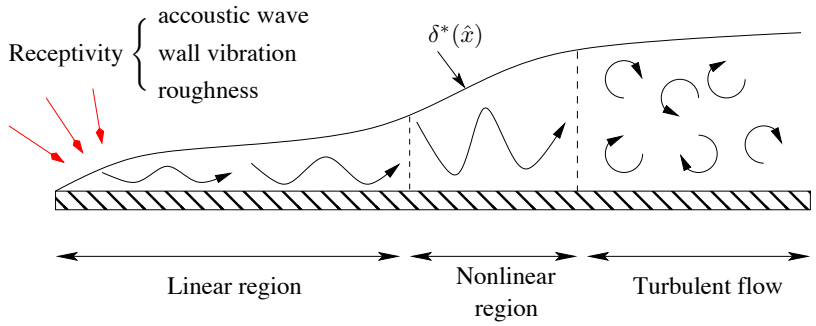

Figure 1.5: Laminar-turbulent boundary-layer transition. Here, $\delta^*(\hat{x})$ denotes the boundary-layer thickness.

Current attempts to delay transition have focused on the first two stages in order to try to limit the growth of linear instabilities. Most of the methods are based on the modification of the mean flow field. In particular, if the mean velocity profile has an inflection point, then according to the Rayleigh theorem, the flow is inviscidly unstable (Rayleigh 1879).The aim is then to alter the basic velocity profiles in such a way that those inflection points are either removed or displaced (for example through suction). Four types of instability mechanisms have been identified in swept wing flows: the leading edge instability at the attachment line; the Tollmien-Schlichting (TS) waves, which are streamwise instabilities; the Taylor-Görtler instability, occurring on concave parts of the wing; steady and unsteady crossflow vortices. A lot of effort was put into the study and control of swept wing instabilities in the past decades, and we now briefly describe some of the main results accomplished. A more in-depth discussion can be found in Saric & Reed (2004).

1.2.3 Instabilities in three-dimensional boundary layers

Effective control of attachment line instabilities can be achieved through either passive methods, such as the use of Gaster bumps, or active methods such as suction. This prevents the boundary layer flow from becoming turbulent from the leading edge and contaminating the flow downstream over the wing. The Görtler instability, which occurs on concave parts of the wings, can be controlled through profile design, by alternating convex and concave curvature, as shown by Benmalek & Saric (1994). There are many techniques to control the

growth of TS waves, one such technique being the tailoring of the airfoil shape to create a longer region of favourable pressure gradient, by increasing the distance between the stagnation point and the point of minimum pressure. However, this technique was found to make the boundary layer more susceptible to the crossflow instability. The latter one is now the focus of research in swept wing boundary-layer transition, and the subject of this study.

Whilst Linear Stability Theory is concerned with the development of the small amplitude instability waves, receptivity is concerned with their origin. The term was first used by Morkovin (1969). While there is no clear definition of receptivity, we understand it as being the mechanism that provides the link between the external forcing environment (such as free stream sound, vorticity or roughness), which creates the initial disturbance, and the instability waves which develop as a consequence. The task of determining the amplitude and spectral properties of the initial disturbance are of particular importance. These need to be taken into account in order to improve standard transition prediction methods such as the e^n method[2]. The traditional methods of Linear Stability Theory, which reduce the set of original equations to an eigenvalue problem, thus describing the normal modes of the system, are incapable of providing the required initial conditions. Instead, we need to solve an initial value problem, with some forcing terms coming either from the boundary conditions, or through inhomogeneous terms in the Navier-Stokes equations.

In the first chapter of this thesis, we will study the compressible flow over a swept wing. We will perform the standard Linear Stability Analysis of the flow, which leads to the derivation of the dispersion relation for crossflow vortices. We will then introduce a roughness element and show how the Receptivity Analysis enables us to calculate the initial amplitude and spectral properties of the disturbance waves. The remaining chapters are devoted to the viscous-inviscid interaction theory, to which we now turn our attention.

[2]Although this method provided satisfying results on the prediction of TS waves, it is less accurate in describing crossflow transition (White et al. 2001).

1.3 The development of Viscous-inviscid Interaction Theory

In Chapter 3 and 4, we will study the viscous-inviscid interaction which can be observed in the vicinity of a surface irregularity or curvature discontinuity. This is a vast subject, whose history we trace back in this section.

1.3.1 Classical Boundary-layer Theory

The study of fluid flows was developed extensively in the 18^{th} and 19^{th} century, through the work of Euler, Bernoulli and Helmholtz, to name but a few. The theory they built up is the basis of what is known as Classical Fluid Dynamics. The main contributions were done in inviscid flow theory, with famous examples such as the prediction of the lift force on a cylinder. An important discovery was the dependence of the properties of fluid flows on the fundamental dimensionless parameter called the Reynolds number. Introduced already in Section 1.2 in the context of hydrodynamic stability of pipe-flow, we define it now in a more general context as

$$\mathrm{Re} = \frac{\rho L V}{\mu}. \tag{1.1}$$

Here, ρ denotes the density of the fluid, μ is the dynamic viscosity of the fluid, and V is the velocity characteristic to the flow considered. L is a reference lengthscale of the problem. The Reynolds number thus represents the relative importance of inertial to viscous forces. In typical aerodynamic applications, the viscosity of air is small, and the Reynolds number Re proves to be very large, usually in the order of 10^6. Inviscid flow theory was developed by assuming that parameter Re^{-1} could be set to zero in the Navier-Stokes equations.This theory gave very satisfying results in the field of aerodynamics but also led to contradictions.

One famous contradiction in the theory is D'Alembert's Paradox, which is formulated as follow. Consider uniform fluid flow with free-stream velocity U past a cylinder of radius a. Then, inviscid potential flow theory predicts that the streamfunction should be given in polar coordinates by

$$\psi(r,\theta) = U\left(r - \frac{a^2}{r}\right)\sin\theta. \tag{1.2}$$

The corresponding streamline pattern is shown in Figure 1.6.

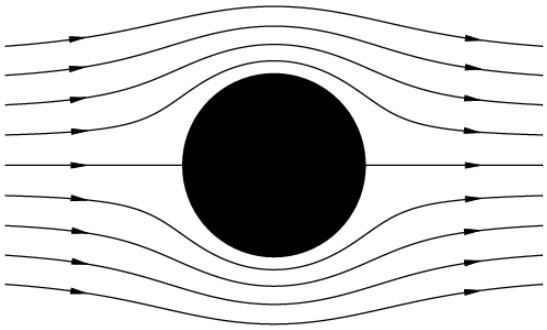

Figure 1.6: Streamlines of potential flow around a cylinder.

When comparing with experimental observations, depicted in Figure 1.7, one can see that the situation is very different. In Figure 1.7, the flow does not remain attached to the body at

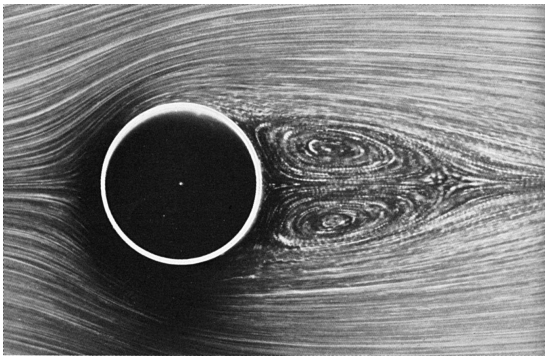

Figure 1.7: Experimental flow around a cylinder with Re=26, Taneda (1956).

the back of the cylinder. A region of re-circulating flow can be observed, leading to eddies which extend downstream if we increase the Reynolds number. The inviscid analysis also predicted that the drag on the cylinder should be zero, which contradicts experimental observations.

It was in 1904, during the 3rd International Congress of Mathematics held in Heidelberg, that Prandtl put forward the idea that would revolutionise the field of aeronautics, and that would help resolve the D'Alembert paradox. In his paper, he introduced the principle of singular perturbations, now used everywhere in Applied Mathematics, and explained the concept of boundary layers. Prandtl argued that no matter how small the viscosity is, there

is always a thin region adjacent to a rigid body surface, called the boundary layer, where viscous forces cannot be ignored and have to be taken into account. Prandtl was able to formulate the equations valid in this region. The method was later extended to a wide variety of situations, such as the flow past a wedge with different angles of attack (Falkner-Skan-Cooke), and stagnation point flow (Hiemenz flow). The development of boundary-layer theory enabled not only accurate predictions of the drag on solid surfaces, but helped our understanding of important flow phenomena, not least of which is flow separation. Even though it had been studied earlier, for example by Helmholtz (1868) in his attempt to describe flow past bluff bodies, it is in the context of boundary layers that the physical origin of flow separation was first explained.

To this aim, let us consider a body placed into a uniform fluid flow. As fluid particles move around the body, they are exposed to a pressure gradient. In the case of an adverse pressure gradient, where the pressure increases in the direction of flow, the particle's velocity should decrease, according to Bernoulli's law. This doesn't affect that much fluid particles outside the boundary layer, since they have high kinetic energy. However, as we get closer to the wall, fluid elements have much smaller velocity due to friction forces occurring in the boundary layer. Those fluid particles experience the same adverse pressure gradient[3], but their velocity is too small to overcome it. They come to a stop and then cause a region of reverse flow which separates from the body.

Separation has significant effects on the flow field as a whole, and especially on the pressure distribution around the body. For instance, in the case of an aerofoil at low angle of attack, we can usually make the following remarks (Anderson 2010):

- ◇ The pressure downstream of the leading edge of the aerofoil in a separated flow is higher than its attached counterpart, which results in a decrease in the lift force;
- ◇ The pressure at the trailing edge of the aerofoil tends to be smaller in the case of separated flow. This means that the pressure at the trailing edge is no longer able to compensate the one at the leading edge, and this results in an increase in drag. This particular type of drag is referred as pressure drag.

[3]One of the main results Blasius showed through the derivation of his equations is that pressure in the boundary layer doesn't change in the normal direction, and is thus determined by the outer inviscid analysis.

This shows the importance of the study of flow separation. One of the aims is to predict the location of the separation point x_s, which, following our discussion, is expected to occur at the point on the wall where the skin friction τ_w becomes zero

$$\tau_w = \mu_w \frac{\partial u}{\partial y}\bigg|_{y=0} = 0. \tag{1.3}$$

The other aim is to accurately model the behaviour of the flow in the vicinity of the separation point in order to calculate drag and lift.

1.3.2 The emergence of Triple Deck Theory

Unfortunately, the classical boundary layer theory developed by Prandtl, based on the Hierarchical approach, where the inviscid flow and the viscous flow are analysed independently of each other, cannot describe the separation process provoked by an adverse pressure gradient. It was shown by Landau & Lifshitz (1944) that as we approach the point x_s of zero skin friction, the classical boundary layer develops a singularity: the normal velocity component appears to experience unbounded growth as $x \to x_s$. This was further investigated by Goldstein (1948): in his work, he confirmed the ideas of Landau & Lifshitz but also showed that the solution found at the separation point could not be continued downstream. This discovery was of paramount importance and suggested that a whole new approach should be followed in order to study flow separation.

The investigation of the effect of an oblique shock wave impinging on an aerofoil is an interesting example where Prandtl's classical boundary layer theory fails. If we follow Prandtl's Hierarchical strategy, then we have to conclude (Ruban 2016) that in supersonic flow, no perturbations can propagate upstream of the intersection point, which is in total contradiction with the actual flow behaviour. Indeed, numerous experimental observations show that the flow actually separates upstream of the intersection point. This separation creates a displacement of the streamlines in the bottom of the inviscid region, producing a secondary oblique shockwave, giving rise to the 'λ-structure' sketched in Figure 1.8. While we do not go into details of the analysis of the 'λ-structure', we summarise the important

points which are relevant to us.

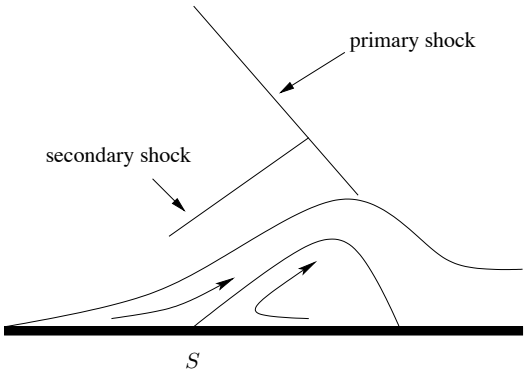

Figure 1.8: The λ-structure of the boundary layer, courtesy of Pr. Ruban.

It can be shown that the boundary layer comes into interaction with the external inviscid flow. In subsonic and supersonic flows, the width of this interaction region, which is situated around the separation point, can be estimated as $\mathrm{Re}^{-3/8}$. It is made up of three 'decks', each having a specific purpose in the viscous-inviscid interaction process. They are described as follows, from bottom to top:

- ◇ a viscous sublayer, with height estimated here as $\mathrm{Re}^{-5/8}$, where pressure variations are felt strongly, leading to a deformation of the streamlines in the vicinity of the body surface,
- ◇ a middle deck, of height estimated here as order $\mathrm{Re}^{-1/2}$, which transmits the displacement of the streamlines from the lower deck to the upper deck,
- ◇ an upper region, situated in the inviscid potential flow, which converts the displacement of streamlines into pressure perturbations; these are in turn impressed back on the boundary layer, thus creating a self-sustained process.

This mutual interaction between the boundary layer and the external inviscid flow taking place here is the key element that Prandtl and Goldstein were missing in their analysis. It enables upstream perturbations to propagate and removes the Goldstein singularity.

The theory of viscous-inviscid interaction is called 'triple deck theory', and was first formulated by Neiland (1969) and independently by Stewartson & Williams (1969), and Brown & Stewartson (1969). Triple deck theory has been successfully applied in describing many phenomena such as separation at the trailing edge of a thin aerofoil and separation of the boundary layer in hypersonic flow on a hot or cold wall (Sychev, Ruban & Korolev 1987). Early work was mainly concerned with self-induced separation. It was later found that singular adverse pressure gradients imposed on the boundary layer always lead to separation. In the case of subsonic or supersonic flows, these pressure gradients can be generated through discontinuities in curvature, corners, shock waves etc. Interestingly, it was found that such a singular pressure gradient can also occur in the analysis of transonic flows around the sonic point[4]. This will be the focus of Chapter 4.

1.3.3 Recent advances in Transonic Theory

The motivation behind our study of transonic flows comes from the fact that most commercial aircrafts fly at transonic speed when cruising. Despite the relevance and wide range of applications of transonic flow, it was not until the end of the forties that the subject started to develop, with the notable work of Frankl (1947), Kármán (1947) and Guderley (1947). The reluctance to study transonic flow was in part due to the mathematical difficulty of the equations, which comes from their inherent non-linearity. Moreover, the equations are of mixed type, reflecting the transition between subsonic flow, governed by an elliptic equation, and supersonic flow, described by a hyperbolic equation, making numerical methods difficult to implement.

The main achievement of classical transonic flow theory was the derivation of the Transonic Small Perturbation equation, also called Kármán-Guderley equation. It is based on a limiting process, whereby the Kármán parameter $K = (1-M_\infty^2)/\tau^{2/3}$ remains an order-one quantity as the Mach number of incoming unperturbed flow $M_\infty \to 1$ and the thickness of the body $\tau \to 0$. This equation was used extensively to study the far field behaviour of the transonic flow over a rigid body (Frankl 1947). In our work, we will show that this equation can be used to describe transonic flow in the vicinity of the sonic point, and self-similar

[4]The sonic point is the point on the body surface where the Mach number M=1.

solutions can be used to reduce it to an ODE, simplifying the analysis.

It is not surprising that due to the difficulty of the nonlinear transonic equations, little work has been done in the theory of transonic viscous-inviscid interaction. It is however of paramount importance for the aeronautical industry to further our understanding of the subject. Most of the literature published so far is concerned with situations where the external inviscid flow doesn't actually show its transonic nature, such as in the study of the flow near the trailing edge of a flat plate (Bodonyi & Kluwick, 1998). In these cases, the interaction problem is simplified, and an interaction law for the pressure can be derived. For the case of subsonic flow, the interaction law is given by the Cauchy integral of thin aerofoil theory, while in the supersonic case, it is given by the Ackeret formula. It was only at the beginning of the millennium that substantial progress was achieved in transonic interaction theory. Of particular interest to us are the recent works of Buldakov & Ruban (2002) and Yumashev (2012).

Buldakov & Ruban investigated in depth the transonic flow around the sonic point on a smooth body surface. The hodograph and the phase portrait method were used to analyse the inviscid transonic flow, and through the use of self-similar solutions it was found that a pressure gradient of the form

$$\frac{\mathrm{d}p}{\mathrm{d}x} \sim (-x)^{-1/3},$$

develops as we approach the sonic point. The main result of the research was the discovery of logarithmic terms in the expansion for the skin friction upstream of the interaction region, leading to an unusual behaviour of the flow in the interaction region. Furthermore, the solution proved to be non-unique.

The next step was to study a non-smooth body surface. Looking back to the work of Messiter & Hu (1975), it was proved that a discontinuity in curvature does not produce separation in subsonic and supersonic flow. Yumashev (2010) considered a similar problem, but focused his attention on the transonic regime. Depending on the ratio of the curvatures upstream and downstream of the singularity, different types of flow structures were observed in the transonic region: supersonic flows with a weak shock, supersonic flow decelerating to subsonic speed without a shock wave, and transonic Prandtl-Mayer flow. His

analysis led to the same form of the pressure gradient studied by Buldakov & Ruban (2002)

$$\frac{\mathrm{d}p}{\mathrm{d}x} = \kappa(-x)^{-1/3}. \tag{1.4}$$

Moreover, depending on the magnitude κ of the discontinuity, either linear or nonlinear behaviour is possible within the interaction region. Yumashev focused on the case where the curvature discontinuity is small, more specifically

$$\mathrm{Re}^{-1/6} \ll \kappa \ll \frac{1}{\log \mathrm{Re}}.$$

This approach enabled him to linearise the governing equations and find analytical solution in all of the decks of the interaction region. It was noted that for larger values of κ, separation might be observed, providing a big contrast with the results of Messiter & Hu (1975).

In the remaining two chapters of this thesis, we will investigate the subsonic and transonic flow past a discontinuity of curvature, where it will be assumed that the discontinuity is of order one. We will present a full analytical solution for the subsonic case, and numerical results for the transonic case. We hope that the strongly singular pressure gradient (1.4) provides an acceleration of the flow in the interaction region, combined with an increase in the wall skin friction. This would have the beneficial effect of delaying the onset of transition to turbulence and avoid early separation of the flow.

Chapter 2

Receptivity of Crossflow Vortices to Surface Roughness

2.1 The crossflow instability

The first chapter of this thesis is concerned with the receptivity of crossflow vortices to surface roughness on a swept wing. The crossflow instability is specific to 3D boundary layers. The crossflow profile (Figure 2.1) developing due to the combined effect of the sweep of the wing and the pressure gradient normally exhibits a so called 'generalised inflection point'. According to Rayleigh's theorem, under these conditions the flow is susceptible to inviscid instability. This instability takes the form of co-rotating vortices, nearly aligned with the inviscid stream lines. Both travelling and stationary vortices exist. Experiments have shown that at low level of free stream turbulence, which is typical of flight conditions, steady crossflow vortices dominate on a wing with sweep angle larger than 35 degrees (Deyhle & Bippes 1996). This motivates us to study the spatial development of those instabilities. The primary crossflow instability, as well as details of the nonlinear effects are now well documented (Arnal 1997, Reshotko 1997, Saric & Reed 2003). A good understanding of the receptivity process remains a big challenge, which we hope to tackle with this study.

The receptivity process of crossflow vortices needs to be contrasted with other typical instabilities. Ruban (1984) showed that Tollmien-Schlichting (TS) waves are very sensi-

tive to free stream sound and 2D roughness. In particular, an interaction between those two mechanisms was needed to generate the necessary scale conversion which leads to the development of a TS wave. The situation with crossflow vortices is quite different: instability can occur with just one type of disturbance. Moreover, mechanisms enhancing receptivity of TS waves, such as the combination of 2D roughness and acoustic waves, do not affect crossflow vortices. However, they turn out to be highly sensitive to 3D roughness and free stream vorticity. The experiments by Radeztsky et al. (1999) and Reibert et al. (1996) showed that a decrease of amplitude from 3.3μm to 0.2μm of arrays of micron-sized roughnesses placed on the surface of the airfoil resulted in a delay of transition from 45% to 65% chord. These studies showed that crossflow vortices were most receptive to roughnesses placed near the leading edge. Smaller 3D roughnesses placed further downstream, as well as 2D roughnesses had no effect. Furthermore the shape of the roughnesses didn't matter, only their spacing and height was important (Saric & Reed 2003). We will present a novel analytical approach to the receptivity to small surface roughness based on the impermeability boundary condition.

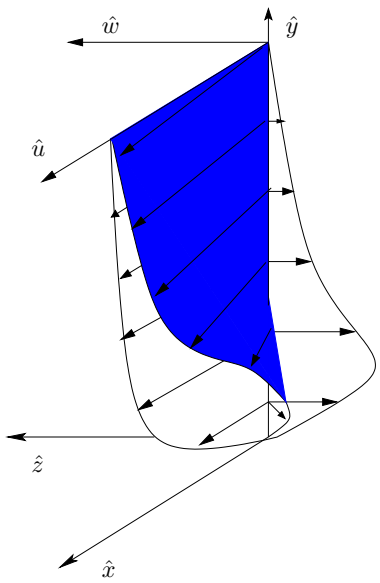

Figure 2.1: Crossflow profile in a swept-wing boundary layer.

We will start by applying the methods of linear stability theory to the study of the compressible flow of a perfect gas over a semi-infinite swept wing. The inviscid instability of the flow is considered, the role of viscosity being restricted to establishing the basic state velocity profile and having no effect (to leading order) on the perturbations. The compressible version of the Rayleigh equation in the case of spatially growing perturbation is then derived. This leads to an eigenvalue problem, whose eigenvalues and eigenfunctions are calculated numerically for a few basic velocity profiles. However, as noted earlier, linear instability theory does not give the initial amplitude for the development of the perturbations. This is the role of the receptivity analysis that we will conduct, through the introduction of a small wall roughness. The forcing term appearing in the boundary condition modifies the structure of the problem, and we are able to derive an analytical expression for the amplitude of the growing mode, through the use of the Fredholm Alternative. Finally, we will compare our results with the work of Choudhari & Duck (1996), which is based on the no-slip condition.

2.2 Linear Stability Analysis

Let us consider the flow of a compressible perfect gas over a swept wing, set at an angle χ to the incoming flow. We introduce a set of coordinate axes so that $\hat{z}$ runs parallel to the leading edge of the wing, and $\hat{x}$ is perpendicular to it. Coordinate $\hat{y}$ is chosen normal to the wing surface. Assuming the incoming flow has speed $V_\infty/\cos\chi$, we define the free-stream velocity vector $\mathbf{V} = (V_\infty, 0, V_\infty \tan\chi)$. The flow layout is depicted on Figure 2.2.

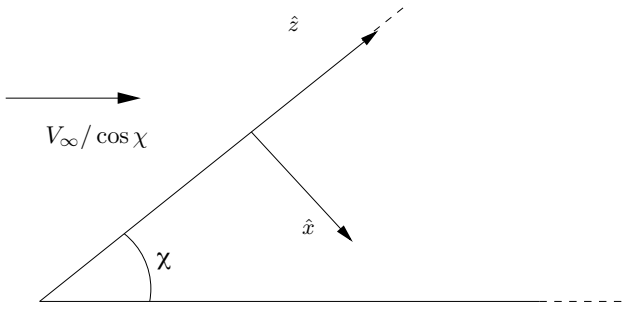

Figure 2.2: Coordinate system for the swept wing.

The flow is governed by the compressible Navier-Stokes equations, which are written in Cartesian coordinates as

$$\begin{aligned}\hat{\rho}\left(\hat{u}\frac{\partial\hat{u}}{\partial\hat{x}}+\hat{v}\frac{\partial\hat{u}}{\partial\hat{y}}+\hat{w}\frac{\partial\hat{u}}{\partial\hat{z}}\right)&=\\ &=-\frac{\partial\hat{p}}{\partial\hat{x}}+\frac{\partial}{\partial\hat{x}}\left\{\mu\left[\frac{4}{3}\frac{\partial\hat{u}}{\partial\hat{x}}-\frac{2}{3}\left(\frac{\partial\hat{v}}{\partial\hat{y}}+\frac{\partial\hat{w}}{\partial\hat{z}}\right)\right]\right\}+\\ &\quad+\frac{\partial}{\partial\hat{y}}\left[\mu\left(\frac{\partial\hat{u}}{\partial\hat{y}}+\frac{\partial\hat{v}}{\partial\hat{x}}\right)\right]+\frac{\partial}{\partial\hat{z}}\left[\mu\left(\frac{\partial\hat{u}}{\partial\hat{z}}+\frac{\partial\hat{w}}{\partial\hat{x}}\right)\right],\end{aligned}\tag{2.1}$$

$$\begin{aligned}\hat{\rho}\left(\hat{u}\frac{\partial\hat{v}}{\partial\hat{x}}+\hat{v}\frac{\partial\hat{v}}{\partial\hat{y}}+\hat{w}\frac{\partial\hat{v}}{\partial\hat{z}}\right)&=\\ &=-\frac{\partial\hat{p}}{\partial\hat{y}}+\frac{\partial}{\partial\hat{y}}\left\{\mu\left[\frac{4}{3}\frac{\partial\hat{v}}{\partial\hat{y}}-\frac{2}{3}\left(\frac{\partial\hat{u}}{\partial\hat{x}}+\frac{\partial\hat{w}}{\partial\hat{z}}\right)\right]\right\}+\\ &\quad+\frac{\partial}{\partial\hat{x}}\left[\mu\left(\frac{\partial\hat{u}}{\partial\hat{y}}+\frac{\partial\hat{v}}{\partial\hat{x}}\right)\right]+\frac{\partial}{\partial\hat{z}}\left[\mu\left(\frac{\partial\hat{v}}{\partial\hat{z}}+\frac{\partial\hat{w}}{\partial\hat{y}}\right)\right],\end{aligned}\tag{2.2}$$

$$\begin{aligned}\hat{\rho}\left(\hat{u}\frac{\partial\hat{w}}{\partial\hat{x}}+\hat{v}\frac{\partial\hat{w}}{\partial\hat{y}}+\hat{w}\frac{\partial\hat{w}}{\partial\hat{z}}\right)&=\\ &=-\frac{\partial\hat{p}}{\partial\hat{z}}+\frac{\partial}{\partial\hat{z}}\left\{\mu\left[\frac{4}{3}\frac{\partial\hat{w}}{\partial\hat{z}}-\frac{2}{3}\left(\frac{\partial\hat{v}}{\partial\hat{y}}+\frac{\partial\hat{u}}{\partial\hat{x}}\right)\right]\right\}+\\ &\quad+\frac{\partial}{\partial\hat{x}}\left[\mu\left(\frac{\partial\hat{u}}{\partial\hat{z}}+\frac{\partial\hat{w}}{\partial\hat{x}}\right)\right]+\frac{\partial}{\partial\hat{y}}\left[\mu\left(\frac{\partial\hat{v}}{\partial\hat{z}}+\frac{\partial\hat{w}}{\partial\hat{y}}\right)\right],\end{aligned}\tag{2.3}$$

$$\begin{aligned}\hat{\rho}\left(\hat{u}\frac{\partial\hat{h}}{\partial\hat{x}}+\hat{v}\frac{\partial\hat{h}}{\partial\hat{y}}+\hat{w}\frac{\partial\hat{h}}{\partial\hat{z}}\right)&=\hat{u}\frac{\partial\hat{p}}{\partial\hat{x}}+\hat{v}\frac{\partial\hat{p}}{\partial\hat{y}}+\hat{w}\frac{\partial\hat{p}}{\partial\hat{z}}+\\ &+\frac{1}{Pr}\left[\frac{\partial}{\partial\hat{x}}\left(\mu\frac{\partial\hat{h}}{\partial\hat{x}}\right)+\frac{\partial}{\partial\hat{y}}\left(\mu\frac{\partial\hat{h}}{\partial\hat{y}}\right)+\frac{\partial}{\partial\hat{z}}\left(\mu\frac{\partial\hat{h}}{\partial\hat{z}}\right)\right]+\\ &+\mu\left(\frac{\partial\hat{u}}{\partial\hat{y}}+\frac{\partial\hat{v}}{\partial\hat{x}}\right)^2+\mu\left(\frac{\partial\hat{u}}{\partial\hat{z}}+\frac{\partial\hat{w}}{\partial\hat{x}}\right)^2+\mu\left(\frac{\partial\hat{v}}{\partial\hat{z}}+\frac{\partial\hat{w}}{\partial\hat{y}}\right)^2+\\ &+\frac{4}{3}\mu\left[\left(\frac{\partial\hat{u}}{\partial\hat{x}}-\frac{\partial\hat{v}}{\partial\hat{y}}\right)\frac{\partial\hat{u}}{\partial\hat{x}}+\left(\frac{\partial\hat{v}}{\partial\hat{y}}-\frac{\partial\hat{w}}{\partial\hat{z}}\right)\frac{\partial\hat{v}}{\partial\hat{y}}+\left(\frac{\partial\hat{w}}{\partial\hat{z}}-\frac{\partial\hat{u}}{\partial\hat{x}}\right)\frac{\partial\hat{w}}{\partial\hat{z}}\right],\end{aligned}\tag{2.4}$$

$$\frac{\partial\hat{\rho}\hat{u}}{\partial\hat{x}}+\frac{\partial\hat{\rho}\hat{v}}{\partial\hat{y}}+\frac{\partial\hat{\rho}\hat{w}}{\partial\hat{z}}=0,\tag{2.5}$$

$$\hat{h}=\frac{\gamma}{\gamma-1}\frac{\hat{p}}{\hat{\rho}}.\tag{2.6}$$

Here, $\hat{u}, \hat{v}, \hat{w}$ represent the cartesian components of the velocity, $\hat{p}$ denotes the pressure, $\hat{\rho}$ the density and $\hat{h}$ the enthalpy. Parameter γ and μ represent the heat capacity ratio and viscosity of the fluid. The Prandtl number Pr is defined as

$$Pr = \frac{c_p \mu}{k},$$

where c_p is the specific heat at constant pressure and k the thermal conductivity.

The flow is viscous and must satisfy the no-slip conditions on the body surface. In the boundary-layer approximation, the Navier-Stokes equations written in cartesian coordinates are identical to the Navier-Stokes equations written in body fitted coordinates (Ruban & Gajjar 2014). As a result, the no-slip condition are written

$$\hat{u} = \hat{v} = \hat{w} = 0, \quad \text{at} \quad \hat{y} = 0. \tag{2.7}$$

In addition, we provide the matching conditions with the freestream

$$(\hat{u}, \hat{v}, \hat{w}, \hat{p}, \hat{\rho}, \hat{h}) \to (V_\infty, 0, V_\infty \tan\chi, \rho_\infty, p_\infty, h_\infty) \quad \text{as} \quad \hat{x}^2 + \hat{y}^2 + \hat{z}^2 \to \infty. \tag{2.8}$$

We introduce non-dimensional variables in the usual way

$$\begin{cases} \hat{x} = L\bar{x}, \quad \hat{y} = L\bar{y}, \quad \hat{z} = L\bar{z}, \\ \hat{u} = V_\infty u, \quad \hat{v} = V_\infty v, \quad \hat{w} = V_\infty w, \\ \hat{p} = p_\infty + \rho_\infty V_\infty^2 p, \quad \hat{\rho} = \rho_\infty \rho, \quad \hat{h} = V_\infty^2 h, \end{cases} \tag{2.9}$$

and define the Reynolds number as

$$\mathrm{Re} = \frac{\rho_\infty V_\infty L}{\mu}, \tag{2.10}$$

which is assumed to be large throughout this dissertation. Here, L represents a typical length-scale, and V_∞, ρ_∞ and p_∞ represent the free stream values of the velocity, density and pressure respectively. We denote the dynamic viscosity of the fluid by μ.

The first aim of this chapter is to investigate the stability of the flow. Our interest lies

into finding whether small perturbations to the basic state grow or decay. On a swept wing, these perturbations take the form of crossflow vortices, which are an inflection type of instability and are thus an inviscid phenomenon. The wavelength of these perturbations is known to be of the order of the thickness of the boundary layer δ^*, which can be estimated as $\delta^* = \mathrm{Re}^{-1/2}$ for a flat plate. Consequently, we look for a solution in the asymptotic form

$$\left.\begin{aligned} u &= U(\bar{x}, y, \bar{z}) + \delta u'(x, y, z) + \cdots, \\ v &= \mathrm{Re}^{-1/2} V(\bar{x}, y, \bar{z}) + \delta v'(x, y, z) + \cdots, \\ w &= W(\bar{x}, y, \bar{z}) + \delta w'(x, y, z) + \cdots, \\ \rho &= \rho_b(\bar{x}, y, \bar{z}) + \delta \rho'(x, y, z) + \cdots, \\ p &= P(\bar{x}, y, \bar{z}) + \delta p'(x, y, z) + \cdots, \\ h &= H(\bar{x}, y, \bar{z}) + \delta h'(x, y, z) + \cdots. \end{aligned}\right\} \tag{2.11}$$

The functions $(u', v', w', \rho', p', h')$ represent the perturbations to the base flow, which is denoted (U, V, W, ρ_b, P, H). Parameter δ is assumed small and arbitrary at this stage. The new 'inviscid' coordinates (x, y, z) are introduced through the scalings

$$x = \frac{\bar{x} - \bar{x}_0}{\mathrm{Re}^{-1/2}}, \quad y = \frac{\bar{y}}{\mathrm{Re}^{-1/2}}, \quad z = \frac{\bar{z} - \bar{z}_0}{\mathrm{Re}^{-1/2}}. \tag{2.12}$$

2.2.1 Computing the base flow

While our interest lies in analysing the behaviour of the perturbations, the base flow functions should still be accurately calculated as these appear as coefficients in the perturbation equations. We substitute asymptotic expansions (2.11) into the compressible Navier-Stokes equations (2.1)-(2.6), and this reduces them at leading order to the compressible boundary-layer equations. In this thesis, we shall restrict our attention to the front stagnation line of the wing. Near the attachment line, where compressibility are negligible the boundary-

layer equations take the form

$$U\frac{\partial U}{\partial \bar{x}} + V\frac{\partial U}{\partial y} + W\frac{\partial U}{\partial \bar{z}} = -\frac{\partial P}{\partial \bar{x}} + \frac{\partial^2 U}{\partial y^2}, \tag{2.13}$$

$$U\frac{\partial W}{\partial \bar{x}} + V\frac{\partial W}{\partial y} + W\frac{\partial W}{\partial \bar{z}} = -\frac{\partial P}{\partial \bar{z}} + \frac{\partial^2 W}{\partial y^2}, \tag{2.14}$$

$$\frac{\partial P}{\partial y} = 0, \tag{2.15}$$

$$\frac{\partial U}{\partial \bar{x}} + \frac{\partial V}{\partial y} + \frac{\partial W}{\partial \bar{z}} = 0. \tag{2.16}$$

The wing is assumed to be semi-infinite in the $\bar{z}$ direction, so we can disregard derivatives in $\bar{z}$, leading to the set of equations

$$U\frac{\partial U}{\partial \bar{x}} + V\frac{\partial U}{\partial y} = -\frac{\partial P}{\partial \bar{x}} + \frac{\partial^2 U}{\partial y^2}, \tag{2.17}$$

$$U\frac{\partial W}{\partial \bar{x}} + V\frac{\partial W}{\partial y} = \frac{\partial^2 W}{\partial y^2}, \tag{2.18}$$

$$\frac{\partial P}{\partial y} = 0, \tag{2.19}$$

$$\frac{\partial U}{\partial \bar{x}} + \frac{\partial V}{\partial y} = 0. \tag{2.20}$$

Equation (2.19) indicates that the pressure remains constant across the boundary layer. The matching condition with the external inviscid flow then requires that $P = P_e(\bar{x})$, where $P_e(\bar{x})$ denotes the inviscid pressure at the edge of the boundary layer. Similarly, we denote by $U_e(\bar{x})$ the streamwise velocity at the edge of the boundary layer.

Near the front stagnation line, we can assume that $U_e = \bar{x}$. Hence, using the Bernoulli equation, we find

$$\frac{\mathrm{d}P_e}{\mathrm{d}\bar{x}} = -\bar{x}.$$

Upon introducing the stream function ψ defined as usual by $\dfrac{\partial \psi}{\partial y} = U, \dfrac{\partial \psi}{\partial \bar{x}} = -V$, the $\bar{x}$-momentum equation becomes

$$\frac{\partial \psi}{\partial y}\frac{\partial^2 \psi}{\partial \bar{x}\partial y} - \frac{\partial \psi}{\partial \bar{x}}\frac{\partial^2 \psi}{\partial y^2} = \bar{x} + \frac{\partial^3 \psi}{\partial y^3}. \tag{2.21}$$

We look for a self-similar solution of the form

$$\psi = \bar{x}^{\alpha} f(\eta), \quad \eta = \frac{y}{\bar{x}^{\beta}}.$$

Substituting this into equation (2.21) shows that $\alpha = 1, \beta = 0$, and equation (2.21) reduces to the ordinary differential equation

$$f''' - \left(f'\right)^2 + f f'' + 1 = 0.$$

Finally, letting $W = g(y)$, the $\bar{z}$-momentum equation becomes

$$g'' + g' f = 0.$$

This results in the following system of equations

$$\begin{cases} f''' - (f')^2 + f f'' + 1 = 0, \\ g'' + g' f = 0, \end{cases} \tag{2.22}$$

which are solved using the boundary conditions

$$f(0) = f'(0) = 0, \quad f'(\infty) = 1, \quad g(0) = 0, \quad g'(\infty) = 0. \tag{2.23}$$

This task is performed numerically using a simple shooting method and an RK4 integrator. Further away from the attachment point, where compressibility effects become more pronounced, profiles from a compressible boundary-layer code are used (Mughal 1998). The boundary-layer data, which includes the velocity profiles U, W and the density ρ were provided to us by S. Mughal in raw form. These are shown in Figure 2.3.

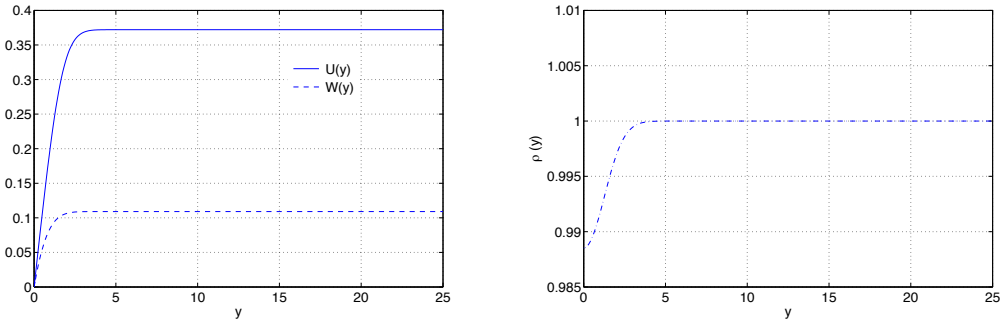

Figure 2.3: Basic velocity (left) and density profile (right) from CoBLc calculations.

2.2.2 Linearised compressible Euler equations

Let us now turn our attention to the linearised equations describing the behaviour of the small perturbations. Using the scalings (2.12), the viscous terms drop out from the Navier-Stokes equations. The momentum equations then take the form

$$\begin{aligned}
\rho_b\left(U\frac{\partial u'}{\partial x}+\frac{\partial U}{\partial y}v'+W\frac{\partial u'}{\partial z}\right)&=-\frac{\partial p'}{\partial x},\\
\rho_b\left(U\frac{\partial v'}{\partial x}+W\frac{\partial v'}{\partial z}\right)&=-\frac{\partial p'}{\partial y},\\
\rho_b\left(U\frac{\partial w'}{\partial x}+\frac{\partial W}{\partial y}v'+W\frac{\partial w'}{\partial z}\right)&=-\frac{\partial p'}{\partial z},
\end{aligned} \tag{2.24}$$

and the continuity, enthalpy and state equation read

$$\begin{aligned}
U\frac{\partial \rho'}{\partial x}+\frac{\partial \rho_b}{\partial y}v'+W\frac{\partial \rho'}{\partial z}&=-\rho_b\left(\frac{\partial u'}{\partial x}+\frac{\partial v'}{\partial y}+\frac{\partial w'}{\partial z}\right),\\
\rho_b\left(U\frac{\partial h'}{\partial x}+\frac{\partial H}{\partial y}v'+W\frac{\partial h'}{\partial z}\right)&=U\frac{\partial p'}{\partial x}+W\frac{\partial p'}{\partial z},\\
h'&=\frac{\gamma}{\gamma-1}\frac{p'}{\rho_b}-\frac{1}{(\gamma-1)M_\infty^2}\frac{\rho'}{\rho_b^2}.
\end{aligned} \tag{2.25}$$

These equations no longer include viscous terms, so the no-slip condition (2.7) should be dropped in favour of the impermeability condition. When analysing stagnation line flow,

this is written

$$v'(x,0,z)=0. \tag{2.26}$$

The condition at the edge of the boundary layer is

$$\lim_{y\to\infty} v'=0.$$

The base flow functions $U(\bar{x},y,\bar{z}), W(\bar{x},y,\bar{z})$ and $\rho_b(\bar{x},y,\bar{z})$ appearing as coefficients in equations (2.24)-(2.25) depend on the viscous variables $(\bar{x},y,\bar{z})$. Since equations (2.24)-(2.25) are written for functions depending on the inviscid variables (x,y,z), we need to re-expand U,W,ρ_b accordingly. Using the scalings (2.12), a Taylor expansion around $\bar{x}_0,\bar{z}_0$ gives

$$\begin{aligned}
U(\bar{x},y,\bar{z}) &= U(\bar{x}_0,y,\bar{z}_0)+O\left(\mathrm{Re}^{-1/2}\right),\\
W(\bar{x},y,\bar{z}) &= W(\bar{x}_0,y,\bar{z}_0)+O\left(\mathrm{Re}^{-1/2}\right),\\
\rho_b(\bar{x},y,\bar{z}) &= \rho_b(\bar{x}_0,y,\bar{z}_0)+O\left(\mathrm{Re}^{-1/2}\right).
\end{aligned}$$

This means that at leading order, we are freezing the basic profile at a specific location $(\bar{x}_0,\bar{z}_0)$ and the functions U,W,ρ_b locally only depend on the normal variable y.

Experimental observations suggest that the perturbations are periodic in the spanwise direction. Consequently, we look for a solution in the normal mode form

$$(u',v',w',p',\rho',h')=\left(\bar{u}(y),\bar{v}(y),\bar{w}(y),\bar{p}(y),\bar{\rho}(y),\bar{h}(y)\right)\mathrm{e}^{\sigma x+i\beta z}. \tag{2.27}$$

Since we are interested in the spatial development of the instabilities, we will assume that σ is complex and β is real. Thus the real part of σ, which we denote $\Re(\sigma)$, represents the growth rate of the instability wave. This turns equations (2.24)-(2.25) into a system of

ordinary differential equations

$$\begin{aligned}
\rho_b\big(\sigma U + i\beta W\big)\bar{u} + \rho_b\frac{\mathrm{d}U}{\mathrm{d}y}\bar{v} &= -\sigma\bar{p},\\
\rho_b\big(\sigma U + i\beta W\big)\bar{v} &= -\frac{\mathrm{d}\bar{p}}{\mathrm{d}y},\\
\rho_b\big(\sigma U + i\beta W\big)\bar{w} + \rho_b\frac{\mathrm{d}W}{\mathrm{d}y}\bar{v} &= -i\beta\bar{p},
\end{aligned} \tag{2.28}$$

and

$$\begin{aligned}
\big(\sigma U + i\beta W\big)\bar{\rho} + \frac{\mathrm{d}\rho_b}{\mathrm{d}y}\bar{v} &= -\rho_b\left(\sigma\bar{u} + \frac{\mathrm{d}\bar{v}}{\mathrm{d}y} + i\beta\bar{w}\right),\\
\rho_b\big(\sigma U + i\beta W\big)\bar{h} + \rho_b\frac{\mathrm{d}H}{\mathrm{d}y}\bar{v} &= \big(\sigma U + i\beta W\big)\bar{p},\\
\bar{h} &= \frac{\gamma}{\gamma-1}\frac{\bar{p}}{\rho_b} - \frac{1}{(\gamma-1)M_\infty^2}\frac{\bar{\rho}}{\rho_b^2}.
\end{aligned} \tag{2.29}$$

Here and throughout the rest of this chapter, we define the basic flow combination

$$f = \sigma U + i\beta W.$$

The functions $\bar{u}, \bar{v}, \bar{w}, \bar{\rho}$ and $\bar{h}$ can be eliminated to reduce the system of differential equations (2.28)-(2.29) to a single ordinary differential equation for the pressure perturbations

$$\bar{p}\,'' - \frac{\mathrm{d}}{\mathrm{d}y}\left(\log\bar{M}^2\right)\bar{p}\,' - \left(\bar{M}^2 + \beta^2 - \sigma^2\right)\bar{p} = 0, \tag{2.30}$$

where $\bar{M} = f\rho_b^{1/2}M_\infty$.

It is worth comparing equation (2.30) with the equation derived in Smith & Brown (1990). In their paper, Smith & Brown investigated the temporal instability of a two dimensional compressible boundary layer. They found that the pressure perturbations $\bar{p}$ satisfied the equation

$$\bar{p}'' - \frac{\mathrm{d}}{\mathrm{d}y}\left(\log\bar{M}^2\right)\bar{p}' - \alpha^2(1-\bar{M}^2)\bar{p} = 0,$$

where $\bar{M} = (U-c)\rho_b^{1/2}M_\infty$. In contrast, we are analysing the three dimensional spatial instability of the flow. The equations are nonetheless very similar.

The boundary conditions for equation (2.30) can be found by investigating the momentum

equations (2.28). Setting $y = 0$, and using the boundary conditions $\bar{v}(0) = U(0) = W(0) = 0$ leads to

$$\bar{p}(0) = 0, \quad \bar{p}\,'(0) = 0.$$

The first condition is characteristic of the spatial instability considered here and will be the one used to solve equation (2.30).

To understand this, we turn to the study of the temporal instability of the flow of Smith & Brown (1990). In their paper, the normal mode decomposition takes the form $Q(x, y, z, t) = \bar{Q}(y) \exp(i(\alpha x + \beta z) + ct)$, and the basic flow combination is written

$$\tilde{f} = \alpha U + \beta W - \omega, \quad c = -i\omega.$$

As a consequence, $\tilde{f}(0) \neq 0$. Substituting this into the momentum equations thus leads to $\bar{p}(0) \neq 0$, in contrast with our study. The second condition $\bar{p}\,'(0) = 0$ remains however valid for both problems and was used in Smith & Brown (1990). In order to distinguish the spatial analysis from the temporal analysis, we will dismiss it in favour of the former condition.

A second boundary condition should be applied far away from the wall, where it is expected that perturbations decay. We thus need to solve the second order ODE

$$\bar{p}\,'' - \frac{\mathrm{d}}{\mathrm{d}y}\left(\log \bar{M}^2\right)\bar{p}\,' - \left(\bar{M}^2 + \beta^2 - \sigma^2\right)\bar{p} = 0, \tag{2.31}$$

subject to the boundary conditions

$$\bar{p}\,(0;\sigma) = 0, \quad \lim_{y\to\infty} \bar{p}\,(y;\sigma) = 0. \tag{2.32}$$

Equation (2.31) together with boundary conditions (2.32) form an eigenvalue problem. For a given wavenumber β, we need to find σ and $\bar{p}(y;\sigma)$ such that (2.31) and (2.32) are satisfied, and the solution is not trivial. This problem will be solved numerically. Asymptotical properties of this equation, which serve as a starting point for the numerical calculations, can be found in Appendix A.

2.2.3 Numerical solution of the stability equation

The complete solution to the eigenvalue problem (2.31)-(2.32) is now sought numerically. The goal of this analysis is to find how the growth rate $\Re(\sigma)$ varies as a function of the spanwise wavenumber β. This is called the dispersion relation.

An efficient way to solve the problem is to use the 4^{th} order Runge-Kutta shooting method. We have to integrate from some large distance y_{inf}, where the behaviour of $\bar{p}$ can be calculated by analysing the asymptotic properties of equation (2.31), described in Appendix A. A first guess for the eigenvalue σ is chosen, for which the corresponding solution will likely not satisfy the boundary condition on the wall. The guess is then improved using the Newton-Raphson method until the wall boundary condition is satisfied.

The stability equation (2.31) is very sensitive to initial conditions. In order to find the correct guess for σ which will guarantee the convergence of the Newton-Raphson iteration process, we will use a global eigenvalue method to guide us towards the correct initial guess. The QZ factorisation is an algorithm that enables us to solve the generalised eigenvalue problem

$$Ax = \sigma Bx, \tag{2.33}$$

with the 'standard' case being when B is the identity matrix.

The starting point for this method are the linearised normal mode equations (2.28)-(2.29). The enthalpy can be eliminated by combining the energy and state equations, thus reducing by one the number of equations and variables. The remaining equations form a mix of differential and algebraic equations. In order to solve them, the domain is split into N points and the equations are discretised. A second order central difference scheme is used in the bulk of the domain. On the lower/upper boundaries, a third order forward/backward difference scheme is implemented, representing the boundary conditions on the wall and at infinity. In order to formulate boundary conditions and initialise all variables at the wall, we need expressions for $\bar{u}\,(0)\,, \bar{v}\,(0)\,, \bar{w}\,(0)\,, \bar{p}\,(0)$ and $\bar{\rho}\,(0)$. The common technique is to evaluate each equation in (2.28)-(2.29) at $y = 0$. However, this technique fails here since the basic flow profiles vanish at the wall, giving trivial results. To avoid this

problem, we differentiate each equation once, and then evaluate at $y = 0$. We define

$$\lambda_1 = U'(0), \quad \lambda_3 = W'(0).$$

The discretisation notation is $Q_0 = Q|_{y=0}$ and $Q_k = Q|_{y=k\Delta h}$, where Δh is the spacing between two adjacent grid points. The wall boundary conditions then take the form

$$\begin{cases} i\beta\lambda_3\,\bar{u}_0 + \lambda_1\bar{v}_0{}' + \sigma\left(\lambda_1\bar{u}_0 + \dfrac{\bar{p}_0{}'}{\rho_{b0}}\right) = 0, \\ \bar{v}_0 = 0, \\ i\beta\left(\lambda_3\bar{w}_0 + \dfrac{\bar{p}_0{}'}{\rho_{b0}}\right) + \lambda_3\bar{v}_0{}' + \sigma\lambda_1\bar{w}_0 = 0, \\ \bar{p}_0 = 0, \\ -i\beta\lambda_3\left(\bar{\rho}_0 - \rho_{b0}M_\infty^2\,\bar{p}_0\right) + \rho_{b0}{}'\bar{v}_0{}' + \sigma\left(\lambda_1\rho_{b0}M_\infty^2\bar{p}_0 - \lambda_1\bar{\rho}_0\right) = 0. \end{cases} \tag{2.34}$$

We use third order forward difference to compute $\bar{v}\,'(0)$

$$\bar{v}\,'(0) = \frac{-\frac{11}{6}\bar{v}_0 + 3\bar{v}_1 - \frac{3}{2}\bar{v}_2 + \frac{1}{3}\bar{v}_3}{h}.$$

In order to compute boundary conditions at infinity, we use the fact that

$$U \to U_e, \quad W \to W_e, \quad \rho_b \to 1, \quad \bar{v} \to 0,$$

leading to

$$\begin{cases} i\beta W_e\,\bar{u}_f + \sigma\left(U_e\bar{u}_f + \bar{p}_f\right) = 0, \\ \bar{p}_f = 0, \\ i\beta\left(W_e\,\bar{w}_f + \bar{p}_f\right) + \sigma U_e\bar{w}_f = 0, \\ i\beta\left(W_e\,\bar{\rho}_f + \bar{w}_f\right) + \sigma\left(\bar{u}_f + U_e\bar{\rho}_f\right) = 0, \\ i\beta W_e\left(\bar{\rho}_f - M_\infty^2\bar{p}_f\right) - \sigma\left(U_eM_\infty^2\bar{p}_f - U_e\bar{\rho}_f\right) = 0, \end{cases} \tag{2.35}$$

where subscript f denotes quantities evaluated at infinity. In practice, we used $y_{\text{inf}} = 25$. We then fill matrices A and B in order to bring (2.28)-(2.29) to the form described by equation (2.33).

Solving this system with the QZ algorithm implemented in Matlab then enables us to compute the full spectrum, giving all the eigenvalues σ for a given pair (β, M_∞) as well as the corresponding eigenfunctions. It is however slow and not accurate when N is small. This can be seen in Figure 2.7 where the boundary condition $\bar{p}'(0) = 0$ is satisfied, but we have $\bar{p}(0) \neq 0$. This issue can be resolved by increasing the number of grid points, but this drastically increases computing time. Thus, this method only serves as a starting point for our calculations.

We ran the QZ code for $\beta = 0.3$ and $M_\infty = 0.7$. The corresponding eigenvalue plot is displayed on Figure 2.4.

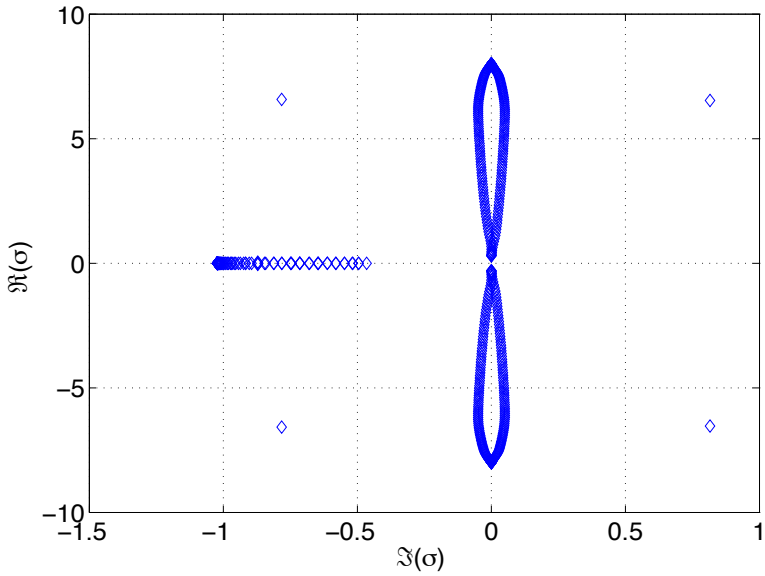

Figure 2.4: Eigenvalue computation from QZ method.

We notice four distinct features in this graph:

1. it is symmetric, which is to be expected with inviscid instability, where eigenvalues come in complex conjugate pairs;

2. the presence of two 'loops', corresponding to the continuous spectrum, which arises from the Fourier decomposition that led us to equations (2.28)-(2.29);

3. a line, where $\Re(\sigma) = 0$, corresponding to neutral modes;

4. four isolated points which are spurious roots.

In order to confirm the last remark, we increased the number of grid points from $N = 151$ to $N = 201$ and $N = 301$ and observed that these four points also moved, as shown on Figure 2.5.

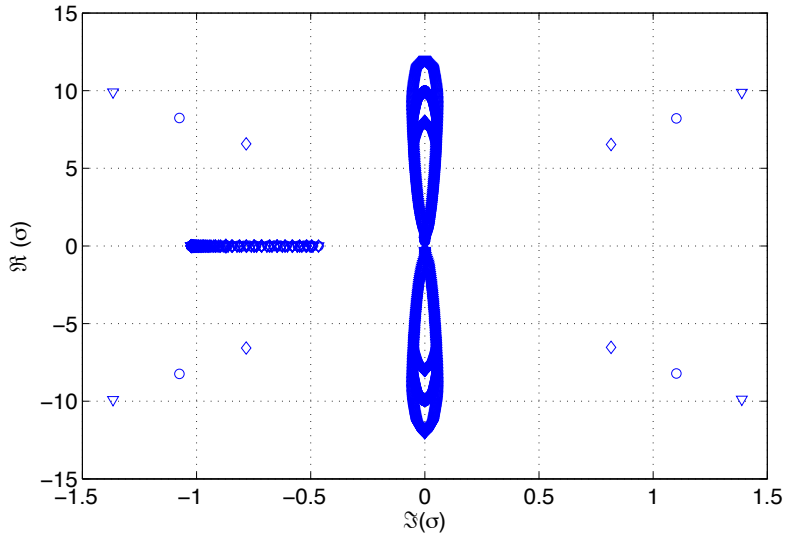

Figure 2.5: Calculations for $N = 151\,\diamond, 201\,\circ, 301\,\triangledown$.

The presence of both discrete and continuous spectrum is to be expected for this type of problems (Saric, Reed & Arnal 1994). The eigenvalues we want should be isolated ones, and we expect $\Re(\sigma)$ to be small. Zooming in close to the line $\Re(\sigma) = 0$, we find a single pair of eigenvalues, displayed on Figure 2.6. These are the relevant ones for the problem at hand. It should be noted that while the location of the spurious roots and the continuous spectrum varied with the number of points, as shown on Figure 2.5, this pair of eigenvalues does not move and is thus the one we are after. For this particular example when $\beta = 0.3$, we find the eigenvalue pair

$$\sigma = \pm 0.0473 - 0.8716\,\mathrm{i}.$$

These values were compared with the one obtained through a compressible linear stability

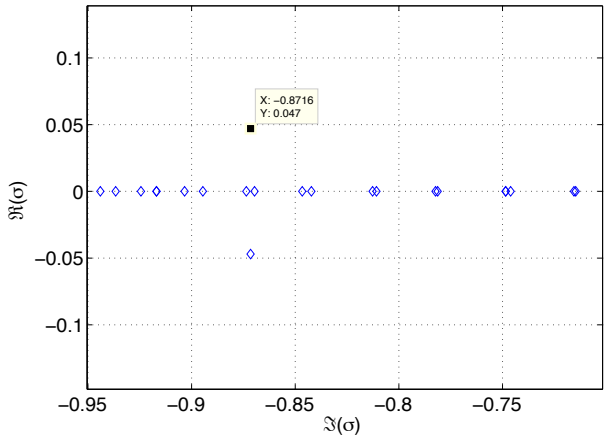

Figure 2.6: A closer look at the vicinity of the neutral line reveals a pair of eigenvalues.

solver (COPSE, Mughal 1998), developed independently. The results were found to agree to 4 decimal places. The eigenfunctions corresponding to this eigenvalue are shown in Figure 2.7, where for the sake of clarity we have plotted the absolute value of the perturbations rather than their real and imaginary part.

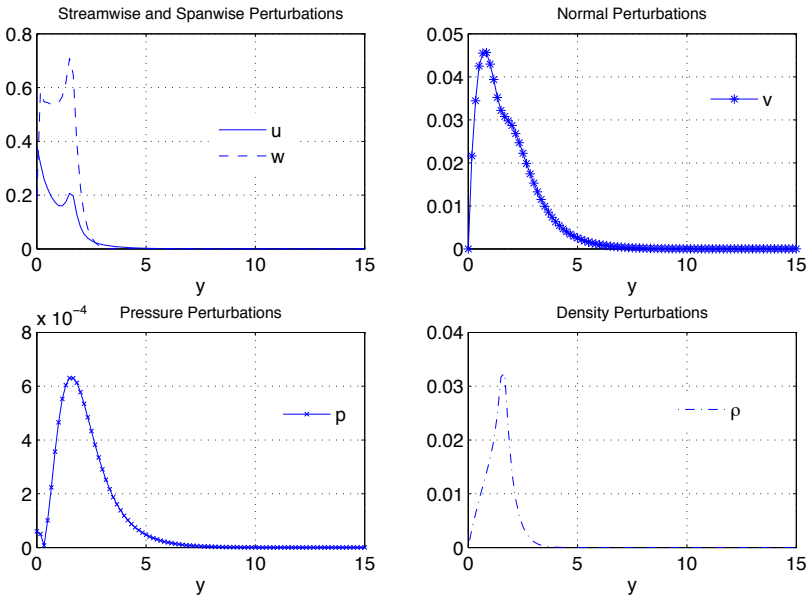

Figure 2.7: Eigenfunctions of the linear system.

The guess obtained for the eigenvalue now enables us to solve equation (2.31) precisely.

We start the numerical integration at some large value of y where the behaviour of $\bar{p}$ is known from the asymptotic formula described in Appendix A. We use the guess for σ obtained through the QZ method and we then numerically integrate (2.31) up to the wall $y = 0$ using a standard 4th order Runge-Kutta method. We then iterate this process until the boundary condition on the wall is satisfied, which is done by using the Newton-Raphson method. The code is assumed to converge when $|\bar{p}(0)| < 10^{-7}$.

We use once again the value $\beta = 0.3$, in which case the guess from the QZ method was $\sigma_g = +0.0473 - 0.8716\,\mathrm{i}$. The Newton-Raphson method converged after 4 iterations and we found

$$\sigma = +0.0478578 - 0.8694983\,\mathrm{i}.$$

The corresponding eigenfunction, normalised so that $\max \Re(p) = 1$, is plotted in Figure 2.8. We note that the boundary condition $\bar{p}(0) = 0$ is clearly satisfied, as well as the extra condition $\bar{p}\,'(0) = 0$.

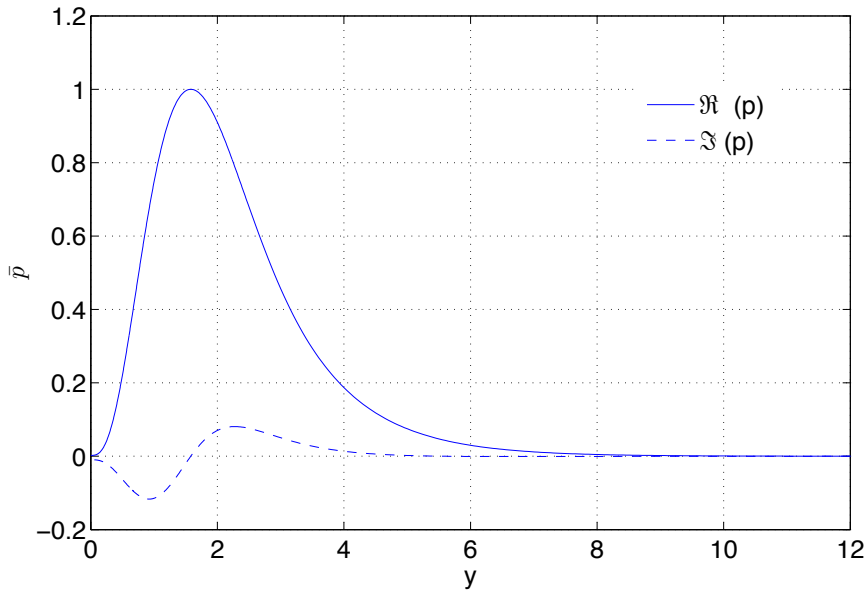

Figure 2.8: Normalised eigenfunctions for $\beta = 0.3, \sigma = +0.0478578 - 0.8694983\,\mathrm{i}$.

The full spectrum is then found by slightly increasing β at every step. Figure 2.9 shows a

comparison of the spectrum obtained via the QZ method and the Newton-Raphson method. There is a very good agreement between the two methods, the difference laying in the computational cost. Indeed, the QZ method was very slow and computationally intensive: it took about 40 hours to compute the solution at 20 values of β for a grid of size $N = 801$. In comparison, the Newton-Raphson method computed the solution at 4000 values of β, for a grid size $N = 1001$ in under 45 minutes. Notice that we were not able to calculate eigenvalues for $\beta < 0.025$ using the N-R technique. These can however still be estimated with the QZ method.

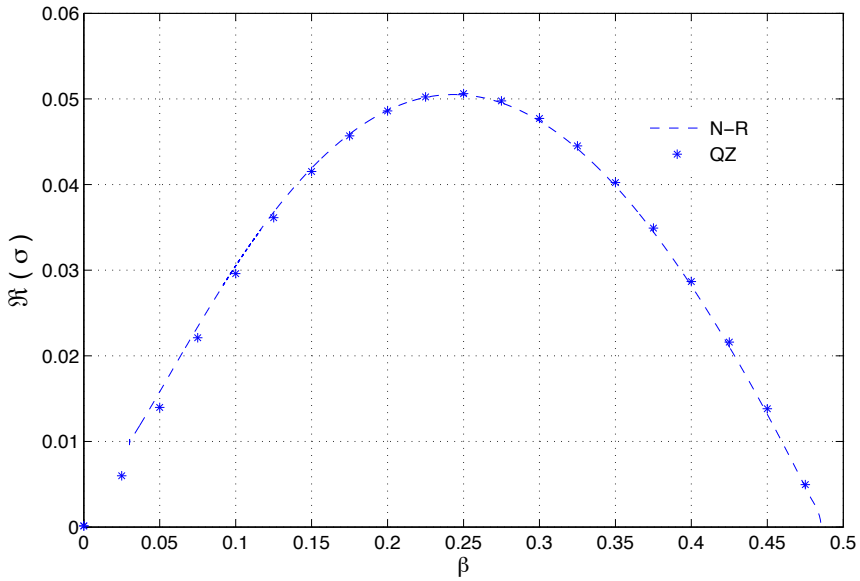

Figure 2.9: Comparison between QZ method and N-R method.

The calculation of the dispersion relation shown on Figure 2.9 is the main goal of the Linear Stability Analysis. It enables us to understand the range of spanwise wave number β for which the flow is unstable. We now turn to the mechanism that generated this instability wave, and try to determine its initial amplitude.

2.3 Receptivity Analysis

The linear instability analysis presented in the previous section enabled us to find the eigenvalues and eigenfunctions for our problem. However, since $\bar{p}$ satisfies a linear homogeneous equation with homogeneous boundary conditions, the amplitude of the perturbations is unknown at this stage. The source of perturbations should be specified in order to determine their amplitude and solve the receptivity problem. Let us assume that the perturbations are created by a small roughness of size ϵ situated downstream, at some distance L from the front stagnation point. In order to generate the correct resonance condition for the crossflow instability to take place, we have to assume that the longitudinal extent of this roughness is of the same order as the boundary-layer thickness $\delta^* = \mathrm{Re}^{-1/2}$ which develops on the wing. Hence, we shall represent the roughness shape by the equation

$$\bar{y}_w = \mathrm{Re}^{-1/2}\,\epsilon\,\eta(x,z), \tag{2.36}$$

where

$$x = \frac{\bar{x}-1}{\mathrm{Re}^{-1/2}}, \quad z = \frac{\bar{z}-1}{\mathrm{Re}^{-1/2}}.$$

We shall further assume the roughness to be periodic in the z-direction and so we write

$$\eta(x,z) = e^{\frac{1}{2}i\beta z}\,g(x). \tag{2.37}$$

The unusual factor of $1/2$ in the exponent will be made clear in the next section.

2.3.1 Formulation of the receptivity problem

In order to derive appropriate equations for the problem, we proceed in a similar fashion as Section 2.2. Starting from the compressible Navier-Stokes equations (2.1)-(2.6), we introduce the non dimensional variables

$$\begin{cases} \hat{x} = L\bar{x}, \quad \bar{y} = L\bar{y}, \quad \hat{z} = L\bar{z}, \\ \hat{u} = V_\infty u, \quad \hat{v} = V_\infty v, \quad \hat{w} = V_\infty w, \\ \hat{p} = p_\infty + \rho_\infty V_\infty^2 p, \quad \hat{\rho} = \rho_\infty \rho, \quad \hat{h} = V_\infty^2 h. \end{cases} \tag{2.38}$$

Assuming that $\epsilon \ll 1$, the flow is then studied using asymptotic expansions

$$\left.\begin{aligned} u &= U\left(\bar{x}, y, \bar{z}\right) + \delta(\epsilon) u'(x, y, z) + \cdots, \\ v &= \mathrm{Re}^{-1/2} V\left(\bar{x}, y, \bar{z}\right) + \delta(\epsilon) v'(x, y, z) + \cdots, \\ w &= W\left(\bar{x}, y, \bar{z}\right) + \delta(\epsilon) w'(x, y, z) + \cdots, \\ \rho &= \rho_b\left(\bar{x}, y, \bar{z}\right) + \delta(\epsilon) \rho'(x, y, z) + \cdots, \\ p &= P\left(\bar{x}, y, \bar{z}\right) + \delta(\epsilon) p'(x, y, z) + \cdots, \\ h &= H\left(\bar{x}, y, \bar{z}\right) + \delta(\epsilon) h'(x, y, z) + \cdots. \end{aligned}\right\} \tag{2.39}$$

The coordinates (x, y, z) are introduced as before through the scalings

$$x = \frac{\bar{x} - 1}{\mathrm{Re}^{-1/2}}, \quad y = \frac{\bar{y}}{\mathrm{Re}^{-1/2}}, \quad z = \frac{\bar{z} - 1}{\mathrm{Re}^{-1/2}}. \tag{2.40}$$

This leads again to the equations (2.24)-(2.25) of Section 2.2. We remind the reader that the perturbations equations take the form

$$\rho_b \left(U \frac{\partial u'}{\partial x} + \frac{\mathrm{d}U}{\mathrm{d}y} v' + W \frac{\partial u'}{\partial z} \right) = -\frac{\partial p'}{\partial x}, \tag{2.41}$$

$$\rho_b \left(U \frac{\partial v'}{\partial x} + W \frac{\partial v'}{\partial z} \right) = -\frac{\partial p'}{\partial y}, \tag{2.42}$$

$$\rho_b \left(U \frac{\partial w'}{\partial x} + \frac{\mathrm{d}W}{\mathrm{d}y} v' + W \frac{\partial w'}{\partial z} \right) = -\frac{\partial p'}{\partial z}. \tag{2.43}$$

and

$$U \frac{\partial \rho'}{\partial x} + \frac{\mathrm{d}\rho_b}{\mathrm{d}y} v' + W \frac{\partial \rho'}{\partial z} = -\rho_b \left(\frac{\partial u'}{\partial x} + \frac{\partial v'}{\partial y} + \frac{\partial w'}{\partial z} \right), \tag{2.44}$$

$$\rho_b \left(U \frac{\partial h'}{\partial x} + \frac{\mathrm{d}H}{\mathrm{d}y} v' + W \frac{\partial h'}{\partial z} \right) = U \frac{\partial p'}{\partial x} + W \frac{\partial p'}{\partial z}, \tag{2.45}$$

$$h' = \frac{\gamma}{\gamma - 1} \frac{p'}{\rho_b} - \frac{1}{(\gamma - 1) M_\infty^2} \frac{\rho'}{\rho_b^2}. \tag{2.46}$$

Following the same reasoning as in the previous chapter, the base flow functions U, W and ρ_b are Taylor expanded around the roughness location and thus are locally considered as functions of y only.

Unlike in Choudhari & Duck (1996), we shall assume that the roughness size is larger than the thickness of the viscous sublayer, as shown on Figure 2.10. We thus require $\epsilon \gg \mathrm{Re}^{-1/6}$. In this case, the viscous effects can be disregarded, and equations (2.41)-(2.46) should be solved with the impermeability condition on the wall. In Section 2.4, we will compare this approach with the work of Choudhari & Duck.

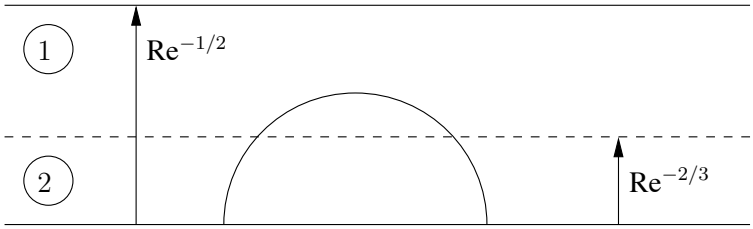

Figure 2.10: A roughness buried within the boundary layer, but larger than the viscous sublayer.

Upon introducing the small roughness described by (2.36), we now need to assume that parameter δ in (2.39) depends on ϵ. The relation $\delta(\epsilon)$ is found by investigating the boundary conditions. To this aim, we introduce the function $\phi = y - \epsilon\,\eta(x,z)$, so that the body surface is represented by the equation $\phi = 0$. This enables us to write the impermeability condition in the form

$$\mathbf{u}.\nabla\phi = 0 \quad \text{on} \quad \phi = 0. \tag{2.47}$$

We substitute the expansion (2.39), which leads to

$$\mathbf{u}.\nabla\phi = -\epsilon U\frac{\partial\eta}{\partial x} - \epsilon W\frac{\partial\eta}{\partial z} - \delta\epsilon\frac{\partial\eta}{\partial x}u' + \delta v' - \delta\epsilon\frac{\partial\eta}{\partial z}w' + \cdots . \tag{2.48}$$

On $\phi = 0$, we have $y = \epsilon\,\eta(x,z)$ and we can use Taylor expansion for U, W and $\mathbf{u}'$ as follows

$$\begin{cases} U = \epsilon\,\eta(x,z)U'(0) + \cdots , \\ W = \epsilon\,\eta(x,z)W'(0) + \cdots , \\ \mathbf{u}' = \mathbf{u}'(x,0,z) + \epsilon\,\eta(x,z)\dfrac{\partial\mathbf{u}'}{\partial y}\bigg|_{y=0} + \cdots , \end{cases} \tag{2.49}$$

where we used the fact that the basic flow satisfies the no-slip condition $U(0) = W(0) = 0$.

This leads to the equation

$$-\epsilon^2\left(U'(0)\eta\frac{\partial\eta}{\partial x}+W'(0)\eta\frac{\partial\eta}{\partial z}\right)+\delta v'(x,0,z)+O(\epsilon\,\delta)=0. \tag{2.50}$$

According to the principle of least degeneration, we need to set $\delta=\epsilon^2$. The linearised boundary conditions in the presence of a small roughness then reduces at leading order to

$$v'(x,0,z)=U'(0)\eta\frac{\partial\eta}{\partial x}+W'(0)\eta\frac{\partial\eta}{\partial z}. \tag{2.51}$$

We now substitute (2.37) in the boundary condition (2.51) to yield

$$v'(x,0,z)=e^{i\beta z}\left(U'(0)g(x)\frac{\mathrm{d}g}{\mathrm{d}x}+\frac{1}{2}i\beta W'(0)g^2(x)\right). \tag{2.52}$$

We note here that the wave number of the perturbation appears to be twice the value of the original roughness period, given in equation (2.37). This is because the boundary condition (2.51) is a nonlinear function of the roughness shape. This is one of the main results of this analysis.

Thus, our task is to solve equations (2.41)-(2.46) subject to condition (2.52) at $y=0$ and the condition of attenuation of the perturbations at $y\to\infty$. Due to the fact that the roughness is periodic in z, the solution to equations (2.41)-(2.46) is assumed to be periodic in the span wise direction. This motivates us to look for a solution in the form

$$\mathbf{q}'(x,y,z)=\tilde{\mathbf{q}}(x,y)\,\mathrm{e}^{i\beta z}, \tag{2.53}$$

where $\mathbf{q}$ represents the vector of fluid dynamic variables $\mathbf{q}=(u,v,w,p,\rho,h)$. We substitute this into the linearised equations (2.41)-(2.46), which leads to the set of equations

$$\begin{aligned}
&\rho_b U\frac{\partial\tilde{u}}{\partial x}+\rho_b i\beta W\tilde{u}+\rho_b\frac{\mathrm{d}U}{\mathrm{d}y}\tilde{v}=-\frac{\partial\tilde{p}}{\partial x},\\
&\rho_b U\frac{\partial\tilde{v}}{\partial x}+\rho_b i\beta W\tilde{v}=-\frac{\partial\tilde{p}}{\partial y},\\
&\rho_b U\frac{\partial\tilde{w}}{\partial x}+\rho_b i\beta W\tilde{w}+\rho_b\frac{\mathrm{d}W}{\mathrm{d}y}\tilde{v}=-i\beta\tilde{p},
\end{aligned} \tag{2.54}$$

$$
\begin{aligned}
&U\frac{\partial\tilde{\rho}}{\partial x}+i\beta W\tilde{\rho}+\frac{\mathrm{d}\rho_b}{\mathrm{d}y}\tilde{v}=-\rho_b\left(\frac{\partial\tilde{u}}{\partial x}+\frac{\partial\tilde{v}}{\partial y}+i\beta\tilde{w}\right),\\
&\rho_b U\frac{\partial\tilde{h}}{\partial x}+\rho_b i\beta W\tilde{h}+\rho_b\frac{\mathrm{d}H}{\mathrm{d}y}\tilde{v}=U\frac{\partial\tilde{p}}{\partial x}+i\beta W\tilde{p},\\
&\tilde{h}=\frac{\gamma}{\gamma-1}\frac{\tilde{p}}{\rho_b}-\frac{1}{(\gamma-1)M_\infty^2}\frac{\tilde{\rho}}{\rho_b^2}.
\end{aligned}
\tag{2.55}
$$

Taking into account the analysis conducted in Section 2.2, which showed that the perturbations grow exponentially downstream of the roughness, we shall apply the Laplace transform to equations (2.54)-(2.55) in the stream wise direction x. Recall that the Laplace transform of a function $\phi(x)$ is given by

$$\mathcal{L}(\phi)=\bar{\phi}(\sigma)=\int_0^\infty\phi(x)\,\mathrm{e}^{-\sigma x}\,\mathrm{d}x.$$

This is well defined provided that there exist positive constants C and a such that

$$|\phi(x)|\le C\,\mathrm{e}^{ax}\quad\text{for all}\quad\Re(\sigma)>a.$$

The formula for the Laplace transform of the derivative is

$$\mathcal{L}\left(\frac{\partial\phi}{\partial x}\right)=\sigma\bar{\phi}-\phi\big|_{x=0}.$$

Assuming, subject to subsequent confirmation, that the presence of the hump doesn't influence the perturbations upstream, we can set

$$\tilde{u}(0,y)=\tilde{v}(0,y)=\tilde{w}(0,y)=0,$$

with similar relations for the other flow variables. The resulting equations are then similar

to the ones derived in Section 2.2

$$\begin{aligned}
&\rho_b\big(\sigma U + i\beta W\big)\bar{u} + \rho_b \frac{\mathrm{d}U}{\mathrm{d}y}\bar{v} = -\sigma\bar{p},\\
&\rho_b\big(\sigma U + i\beta W\big)\bar{v} = -\frac{\mathrm{d}\bar{p}}{\mathrm{d}y},\\
&\rho_b\big(\sigma U + i\beta W\big)\bar{w} + \rho_b \frac{\mathrm{d}W}{\mathrm{d}y}\bar{v} = -i\beta\bar{p}.
\end{aligned} \tag{2.56}$$

$$\begin{aligned}
&\big(\sigma U + i\beta W\big)\bar{\rho} + \frac{\mathrm{d}\rho_b}{\mathrm{d}y}\bar{v} = -\rho_b\left(\sigma\bar{u} + \frac{\mathrm{d}\bar{v}}{\mathrm{d}y} + i\beta\bar{w}\right),\\
&\rho_b\big(\sigma U + i\beta W\big)\bar{h} + \rho_b \frac{\mathrm{d}H}{\mathrm{d}y}\bar{v} = \big(\sigma U + i\beta W\big)\bar{p},\\
&\bar{h} = \frac{\gamma}{\gamma-1}\frac{\bar{p}}{\rho_b} - \frac{1}{(\gamma-1)M_\infty^2}\frac{\bar{\rho}}{\rho_b^2}.
\end{aligned} \tag{2.57}$$

The transformation (2.53) and Laplace transform should also be applied to the boundary condition (2.51), which, together with decay condition at infinity, take the form

$$\bar{v}(0;\sigma) = \frac{1}{2}\big(\lambda_1\sigma + i\lambda_3\beta\big)\int_0^{+\infty} \mathrm{e}^{-\sigma x}\left[g(x)\right]^2 \mathrm{d}x, \quad \lim_{y\to\infty}\bar{v}(y;\sigma) = 0, \tag{2.58}$$

where $\lambda_1 = U'(0), \lambda_3 = W'(0)$. The boundary conditions are formulated for $\bar{v}$ which motivates us to reduce the system of differential equations (2.56)-(2.57) to a single second order differential equation for $\bar{v}$. Following a similar procedure as in Section 2.2, we introduce functions

$$f = \sigma U + i\beta W, \quad q = f^2 M_\infty^2 + \frac{\beta^2 - \sigma^2}{\rho_b},$$

and equations (2.56)-(2.57) are reduced to

$$\bar{v}\,'' - \frac{q'}{q}\,\bar{v}\,' - \left(\frac{f''}{f} + \rho_b q - \frac{f'}{f}\frac{q'}{q}\right)\bar{v} = 0. \tag{2.59}$$

The task is now to find a function $\bar{v}(y;\sigma)$ satisfying equation (2.59) and boundary conditions (2.58). Once this is done, the original perturbation velocity v' is recovered through

the inverse Laplace transform

$$v'(x,y,z) = e^{i\beta z}\frac{1}{2\pi i}\int_{a-i\infty}^{a+i\infty}\bar{v}(y;\sigma)e^{\sigma x}\mathrm{d}\sigma, \tag{2.60}$$

with a being to the right of all the singularities of $\bar{v}$ in the complex σ-plane. This integral can be evaluated by using the Residue theorem. To this aim, we need to calculate the poles of the integrand $\bar{v}(y;\sigma)e^{\sigma x}$ in the complex σ-plane. This is the task of the next subsection.

2.3.2 Analytical solution of the receptivity problem

Following a brief introduction to crossflow vortices, the second section of this chapter was concerned with the linear stability of the flow, leading to a set of homogeneous equation and boundary conditions, namely the pressure equation (2.31) and its associated boundary conditions (2.32). The amplitude of the disturbance could not be determined, but we could find the growth rate σ. Now that we have added forcing into the system through the boundary conditions, we can expect to be in a position to calculate the initial amplitude.

Indeed, this type of situation has been studied extensively in physical sciences (for example in the context of wave or quantum mechanics): a given homogenous problem, depending on a parameter λ, might only have a solution for a certain set of eigenvalues $\{\lambda_n\}$. This solution involves an undetermined constant, usually referred to as the amplitude. If we add some forcing term through a non-zero boundary condition or inhomogeneous terms in the equation, the eigenvalue constraint disappears and a solution can be constructed for any value of parameter λ. Moreover, using adjoint methods and the Fredholm alternative, it is possible to calculate the aforementioned unknown amplitude. It can however be shown that the general solution $f(x;\lambda)$ then develops poles at $\lambda = \lambda_n$. This is not a problem for us since we are actually interested in studying those poles in order to use the Residue Theorem. We will use a Laurent expansion to find the solution, this method being justified and demonstrated through a simplified example in Appendix B.

This discussion motivates us to look for a solution to equation (2.59) and boundary

conditions (2.58) in the form

$$\bar{v}(y;\sigma) = \frac{1}{\sigma-\sigma_0}\, v_0(y) + v_1(y) + O(\sigma-\sigma_0) \quad \text{as} \quad \sigma \to \sigma_0, \tag{2.61}$$

where we assume, subject to subsequent confirmation, that σ_0 is the eigenvalue of the homogeneous problem (2.31)-(2.32). By definition, the residue of the integrand in the inverse Laplace transform (2.60) is $v_0(y)\,\mathrm{e}^{\sigma_0 x}$. Our task is now to find function $v_0(y)$. We define $\delta = \sigma - \sigma_0$ and substitute expansion (2.61) into equation (2.59). The first and second order equations in the approximation in powers of δ are

$$\left[\frac{\mathrm{d}^2}{\mathrm{d}y^2} - \frac{q_0'}{q_0}\frac{\mathrm{d}}{\mathrm{d}y} - \left(\frac{f_0''}{f_0} + \rho_b q_0 - \frac{f_0'}{f_0}\frac{q_0'}{q_0}\right)\right] v_0 = 0, \tag{2.62}$$

$$\left[\frac{\mathrm{d}^2}{\mathrm{d}y^2} - \frac{q_0'}{q_0}\frac{\mathrm{d}}{\mathrm{d}y} - \left(\frac{f_0''}{f_0} + \rho_b q_0 - \frac{f_0'}{f_0}\frac{q_0'}{q_0}\right)\right] v_1 = \Lambda. \tag{2.63}$$

The functions f_0 and q_0 are defined by $f_0 = f(y;\sigma_0)$, $q_0 = q(y;\sigma_0)$, and the right hand side in (2.63) is given by

$$\Lambda = \frac{1}{q_0}\left(Q' - \frac{q_0'}{q_0}Q\right)v_0' + \left[\frac{1}{f_0}\left(U'' - \frac{f_0''}{f_0}U\right) + \rho_b Q + \right.$$
$$\left. + \frac{1}{f_0}\frac{1}{q_0}\left(f_0'Q' - f_0'\frac{q_0'}{q_0}Q + q_0'U' - q_0'\frac{f_0'}{f_0}U\right)\right] v_0.$$

As expected, it depends both on v_0 and v_0'. Finally, the function Q in the above equation is defined as

$$Q = 2M_\infty^2 f_0 U - 2\frac{\sigma_0}{\rho_b}.$$

The asymptotic expansion (2.61) for $\bar{v}$ should be substituted into the boundary conditions (2.58) as well. This results in

$$\begin{cases} v_0(0) = 0, & \lim\limits_{y\to\infty} v_0 = 0, \\ v_1(0) = C, & \lim\limits_{y\to\infty} v_1 = 0, \end{cases} \tag{2.64}$$

where

$$C = \frac{1}{2}\Big(\lambda_1\sigma_0 + i\lambda_3\beta\Big) \int_0^{+\infty} \mathrm{e}^{-\sigma_0 x}\,[g(x)]^2\,\mathrm{d}x. \tag{2.65}$$

The asymptotic expansion (2.61) has split the problem into two, one homogeneous and the other non homogeneous due to the presence of the right hand side Λ.

To progress in the analysis of the problem, it is convenient to express the differential operators on the left hand side of (2.62)-(2.63) in self-adjoint form. Any second order ODE can be put into Sturm-Liouville form, which is self-adjoint. Given the equation

$$p(x)y'' + q(x)y' + r(x)y = h(x), \tag{2.66}$$

this is done by multiplying both sides of (2.66) by the integrating factor

$$I = \exp\left(\int^x q(t)/p(t)\mathrm{d}t\right).$$

In our case, the integrating factor is

$$\exp\left(-\int \log(q_0(t))'\,\mathrm{d}t\right) = \frac{1}{q_0}.$$

Using this transformation, the set of equations (2.62)-(2.63) becomes

$$\begin{aligned}
&\left(\frac{v_0'}{q_0}\right)' - \frac{1}{q_0}\left(\frac{f_0''}{f_0} + \rho_b q_0 - \frac{f_0'}{f_0}\frac{q_0'}{q_0}\right) v_0 = 0,\\
&\left(\frac{v_1'}{q_0}\right)' - \frac{1}{q_0}\left(\frac{f_0''}{f_0} + \rho_b q_0 - \frac{f_0'}{f_0}\frac{q_0'}{q_0}\right) v_1 = \frac{\Lambda}{q_0}.
\end{aligned} \tag{2.67}$$

Combining (2.67) with the corresponding boundary conditions (2.64), we have

$$\begin{cases}
L_{\mathrm{sa}} v_0 = 0, & v_0(0) = 0, \quad \lim\limits_{y\to\infty} v_0 = 0,\\
L_{\mathrm{sa}} v_1 = \dfrac{\Lambda}{q_0}, & v_1(0) = C, \quad \lim\limits_{y\to\infty} v_1 = 0,
\end{cases} \tag{2.68}$$

The first line in (2.68) corresponds to the problem (2.31)-(2.32) solved in Section 2.2, cast in terms of the normal velocity instead of pressure. This confirms our assumption that

σ_0 needs to be chosen as the eigenvalue of the homogeneous problem. The second problem in (2.68) is inhomogeneous due to the forcing appearing in the boundary condition at the wall. The Fredholm alternative tells us that a solution only exists if a certain solvability condition is satisfied. It will enable us to determine the crossflow vortices. We define the inner product

$$< \phi, \psi >= \int_0^\infty \phi(t)\psi(t)\mathrm{d}t.$$

The solvability condition is found as follows: assuming a solution v_1 exists, we take the inner product of the equation with v_0, the solution of the homogenous problem. This is expressed as

$$< L_{sa}v_1, v_0 >=< \frac{\Lambda}{q_0}, v_0 > . \tag{2.69}$$

Using integration by parts on the left hand side, we get

$$< L_{\mathrm{sa}}v_1, v_0 >= \left[\frac{v_1'v_0 - v_1v_0'}{q_0}\right]_0^\infty + < v_1, L_{\mathrm{sa}}v_0 > . \tag{2.70}$$

Since v_0 satisfies the first equation, i.e. $L_{\mathrm{sa}}v_0 = 0$, the second term on the right hand side of (2.70) disappears and we are just left with the boundary terms in square brackets. Equating this with the right hand side of (2.69) leads to

$$\left[\frac{v_1'v_0 - v_1v_0'}{q_0}\right]_0^\infty =< \frac{\Lambda}{q_0}, v_0 > . \tag{2.71}$$

This is the solvability condition that we require.

Let $A = \max(v_0)$ and write $v_0 = A\hat{v}_0$, with $\hat{v}_0 = v_0/A$. According to the set of boundary conditions in (2.68), the only non-zero boundary term in (2.71) comes from $v_1(0)$, the forcing due to the presence of the roughness. The solvability condition (2.71) reduces to

$$\frac{v_1(0)}{q_0(0)}A\,\hat{v}_0\,'(0) = \int_0^{+\infty} \frac{\Lambda}{q_0}\,A\,\hat{v}_0\,\mathrm{d}y. \tag{2.72}$$

The function Λ on the right hand side of (2.72) contains only linear combinations of v_0, v_0' and we can thus extract a factor of A from it. The term $v_1(0)$ is given by the boundary

conditions (2.65). Rearranging equation (2.72), we find that A is given by

$$A = \frac{v_1(0)\hat{v}_0{}'(0)}{q_0(0)\int\limits_0^{+\infty} \Lambda\hat{v}_0/q_0\,\mathrm{d}y}. \tag{2.73}$$

We now return to the task of recovering the original perturbation v' through the integral

$$v'(x,y,z) = e^{i\beta z}\frac{1}{2\pi i}\int\limits_{a-i\infty}^{a+i\infty} \bar{v}(y;\sigma)e^{\sigma x}\mathrm{d}\sigma. \tag{2.74}$$

The solution to our problem was sought in the asymptotic expansion

$$\bar{v}(y;\sigma) = \frac{A}{\sigma-\sigma_0}\,\hat{v}_0(y) + v_1(y) + \ldots \quad \text{as} \quad \sigma \to \sigma_0.$$

The integrand thus contains a simple pole at $\sigma = \sigma_0$, with residue

$$\mathrm{Res}\left(\bar{v}\,\mathrm{e}^{\sigma x}\right) = A\,\hat{v}_0(y)\,\mathrm{e}^{\sigma_0 x}\,.$$

The contour can be closed by using a large semi circle of radius R, as sketched in Figure 2.11, and the integral can then be evaluated using the Residue Theorem in the limit $R \to \infty$. Jordan's Lemma is used to estimate the value of the integral on the arc of the circle, with its contribution vanishing to 0 as we let the radius $R \to \infty$.

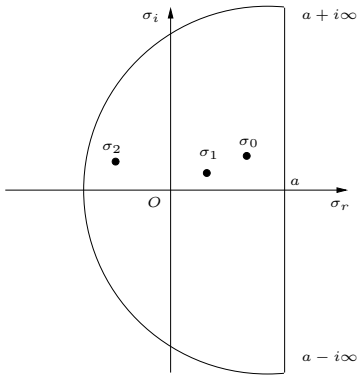

Figure 2.11: Integration contour for the inverse Laplace transform (2.74).

We then have

$$\int_{a-i\infty}^{a+i\infty} \bar{v}(y;\sigma)e^{\sigma x}\mathrm{d}\sigma = 2\pi i \sum_{\sigma=\sigma_i} \mathrm{Res}\big(\bar{v}(y;\sigma)e^{\sigma x}\big), \tag{2.75}$$

the sum being taken over the singularities σ_i. We are however only interested in the behaviour at large values of x, in which case we keep only the term which gives the largest growth rate in the sum. The perturbations far downstream are then written

$$v'(x,y,z) = \mathcal{K}(\beta)\left[\int_0^\infty \mathrm{e}^{-\sigma_0 x}\left[g(x)\right]^2 \mathrm{d}x\right] \hat{v}_0(y)\,\mathrm{e}^{i\beta z+\sigma_0 x} + \cdots, \quad \text{as} \quad x\to\infty, \tag{2.76}$$

with the receptivity coefficient $\mathcal{K}(\beta)$ given by

$$\mathcal{K}(\beta) = \frac{1}{2}\frac{(\lambda_1\sigma_0 + \lambda_3 i\beta)\,\hat{v}_0\,'(0)}{q_0(0)\int_0^{+\infty} \Lambda\hat{v}_0/q_0\,\mathrm{d}y}.$$

The formula (2.76) expresses the dependence of the downstream growing vortex on the receptivity coefficient $\mathcal{K}(\beta)$ and the Laplace transform of the roughness shape in the square brackets.

We define the amplitude $\mathcal{A}_{\text{inv}}$ of the vortex, obtained using the impermeability condition, as the receptivity coefficient $\mathcal{K}(\beta)$ multiplied by the Laplace transform of the square of the roughness

$$\mathcal{A}_{\text{inv}} = \mathcal{K}(\beta)\left[\int_0^\infty \mathrm{e}^{-\sigma_0 x}\left[g(x)\right]^2 \mathrm{d}x\right]. \tag{2.77}$$

The amplitude function (2.77) is calculated numerically, and its magnitude $|\mathcal{A}_{\text{inv}}(\beta)|$ is shown on Figure 2.12. The roughness shape $g(x)$ was assumed to take the standard Gaussian form

$$g(x) = \mathrm{e}^{-x^2}.$$

In order to perform the numerical calculations, we used one of the boundary-layer velocity profiles generated through the CoBL code of Mughal (1998). The distance s along the wing is $s = 0.0006759$ and the freestream Mach number is $M_\infty = 0.07317$. In this setting, a

growing instability wave, corresponding to $\Re(\sigma) \neq 0$, is observed when $\beta \in [0, 0.475]$.

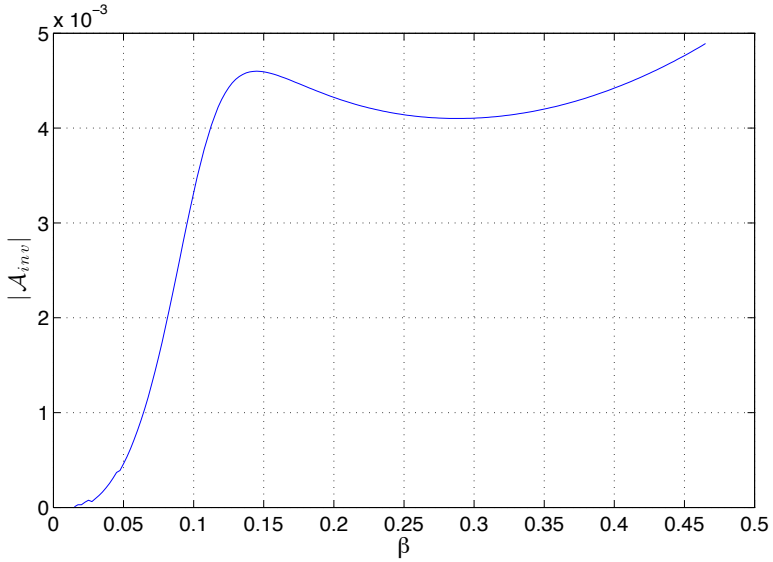

Figure 2.12: Amplitude of crossflow vortex $|\mathcal{A}_{\text{inv}}|$ as a function of the wavenumber β.

The results obtained in Figure 2.12 are very similar to the ones found in Choudhari & Streett (1990) and Choudhari (1994). At low values of the wavenumber β, the amplitude of the crossflow vortices is small. Then, as β increases to 0.125, the amplitude increases drastically and attains a local maximum. The amplitude then decreases slowly until β reaches the value 0.28. This is followed by a region of slow increase and the amplitude reaches a global maximum towards the end of the spectrum when $\beta = 0.475$. At larger values of β, the growth rate $\Re(\sigma)$ is zero and we no longer observe growing vortices.

On Figure 2.13, we present the results obtained as we increase slightly the distance s along the wing. We first observe that the spanwise wavenumber range β for which crossflow vortices develop also increases. The shape of the amplitude is magnified, and in particular its maximum increases in magnitude. Furthermore, we note that the location of this maximum is located at a higher wavenumber β.

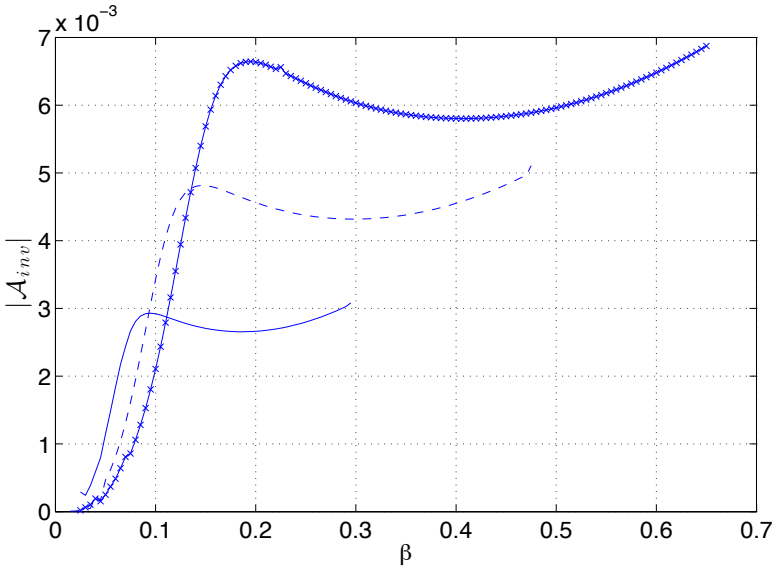

Figure 2.13: Amplitude of crossflow vortex at different locations along the wing (impermeability): $s = 0.0004167, M_\infty = 0.0442322$ (—); $s = 0.0006759, M_\infty = 0.0731715$ (−−); $s = 0.0009823, M_\infty = 0.1094626$ (-×-).

The inviscid approach, which used the impermeability condition to determine the amplitude of the crossflow vortices, showed two new distinct features. Firstly, the wavenumber of the growing vortex appears to be twice the value of the roughness wavenumber and secondly, the perturbations are proportional to the square of the roughness size. We now compare this to results obtained when $\epsilon \sim \mathrm{Re}^{-1/6}$, in which case viscosity should be reintroduced.

2.4 Viscous approach to the study of crossflow vortices

The previous section was concerned with the inviscid instability of crossflow vortices on a swept flat plate. The physical mechanism used to trigger this instability was the introduction of a surface roughness. Mathematically, the presence of the roughness adds forcing terms through the boundary condition. These forcing terms are what enables us to formulate the receptivity problem.

The longitudinal extent of the roughness was assumed to be of the order of the boundary-

layer thickness, estimated to be of order $\mathrm{Re}^{-1/2}$, and the height of the roughness (denoted by ϵ) was assumed to be small to ensure that the forcing is in resonance with the crossflow instability. Coordinates $\bar{x}, \bar{y}$ and $\bar{z}$ were all scaled with δ^* and the perturbations were of the order of ϵ^2. The latter gives us the correct conditions to get the required forcing in the impermeability boundary condition.

In Section 2.3, we assumed that the roughness height ϵ is small, but larger than the thickness of the viscous layer forming on the surface of the roughness. The latter may be estimated as $y \sim \mathrm{Re}^{-2/3}$. Here, we shall discuss the case when the roughness height is small compared with that of the viscous sublayer, as sketched on Figure 2.14.

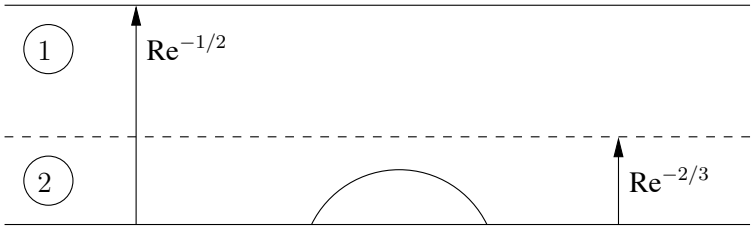

Figure 2.14: A roughness within the viscous sublayer.

To this aim, we need to impose some restriction on the roughness shape. Its longitudinal extent remains of order δ^*, and hence so do coordinates $\bar{x}$ and $\bar{z}$. Let us assume

$$\bar{y}_w = \mathrm{Re}^{-2/3}\, \epsilon\eta(x, z).$$

It is then necessary to scale $\bar{y}$ accordingly and leads to the presence of a viscous sublayer whose thickness we denote $\delta^\star$. This approach enables us to satisfy the no-slip condition.

2.4.1 Derivation of the viscous sublayer scalings

We start from the Navier-Stokes equations (2.1)-(2.6) written in terms of the non-dimensional variables $(\bar{x}, \bar{y}, \bar{z})$. The inviscid approach to the problem was based on the following

asymptotic expansion, valid in the main part of the boundary layer[1]

$$\left.\begin{aligned} u &= U\left(\bar{x}, y, \bar{z}\right) + \delta(\epsilon)\, u'(x, y, z) + \cdots, \\ v &= \mathrm{Re}^{-1/2}\, V\left(\bar{x}, y, \bar{z}\right) + \delta(\epsilon)\, v'(x, y, z) + \cdots, \\ w &= W\left(\bar{x}, y, \bar{z}\right) + \delta(\epsilon)\, w'(x, y, z) + \cdots. \end{aligned}\right\} \tag{2.78}$$

According to (2.12), the 'inviscid' coordinates were defined by

$$x = \frac{\bar{x} - 1}{\mathrm{Re}^{-1/2}} = O(1), \quad y = \frac{\bar{y}}{\mathrm{Re}^{-1/2}} = O(1), \quad z = \frac{\bar{z} - 1}{\mathrm{Re}^{-1/2}} = O(1). \tag{2.79}$$

To analyse the viscous sublayer, we first note that when y is small, the basic velocity components U and W behave as

$$\begin{aligned} U(\bar{x}, y, \bar{z}) &= \lambda_1 y + \cdots, \\ W(\bar{x}, y, \bar{z}) &= \lambda_3 y + \cdots, \end{aligned} \tag{2.80}$$

where $\lambda_1 = U_y|_{y=0}, \lambda_3 = W_y|_{y=0}$. Provided that the roughness height ϵ is small, the bump only produces small perturbations to the incoming Blasius flow. This motivates an asymptotic expansion in the viscous sublayer in the form

$$\left.\begin{aligned} u &= \lambda_1 y + \epsilon^\star\, U'(x_\star, y_\star, z_\star) + \cdots, \\ v &= \epsilon^\star\, \gamma\, V'(x_\star, y_\star, z_\star) + \cdots, \\ w &= \lambda_3 y + \epsilon^\star\, W'(x_\star, y_\star, z_\star) + \cdots. \end{aligned}\right\} \tag{2.81}$$

The small parameter $\epsilon^\star$ used here is different from parameter ϵ used in (2.78). The 'viscous' coordinates $(x_\star, y_\star, z_\star)$ appearing in (2.81) are defined through

$$x_\star = \frac{\bar{x} - 1}{\mathrm{Re}^{-1/2}} = O(1), \quad y_\star = \frac{\bar{y}}{\delta^\star} = O(1), \quad z_\star = \frac{\bar{z} - 1}{\mathrm{Re}^{-1/2}} = O(1), \tag{2.82}$$

with parameter $\delta^\star = \delta^\star(\mathrm{Re}) \ll 1$. It is important to realise that coordinates $x_\star$ and $z_\star$ are indistinguishable from the coordinates x and z used in Section 2.2 and 2.3. The change in

[1]For the purpose of this analysis, we will neglect the influence of compressibility effects, which are assumed to be negligible in the viscous sublayer.

notation is to emphasise that the domain of validity of (2.82) is the viscous sublayer.

Using the scaling (2.82) and combining this with (2.79) , we may rewrite the normal coordinate $y = \mathrm{Re}^{1/2}\,\delta^\star y_\star$ and substitute expansions (2.81) into the $\bar{x}$-momentum equation, which is written

$$u\frac{\partial u}{\partial \bar{x}} + v\frac{\partial u}{\partial \bar{y}} + w\frac{\partial u}{\partial \bar{z}} = -\frac{\partial p}{\partial \bar{x}} + \frac{1}{\mathrm{Re}}\frac{\partial u^2}{\partial \bar{y}^2}.$$

We estimate the convective term as

$$u\frac{\partial u}{\partial \bar{x}} = \epsilon^\star\,\delta^\star\,\mathrm{Re}^{1/2}\,y_\star\frac{\Delta U'}{\mathrm{Re}^{-1/2}\,\Delta x_\star} + \cdots,$$

while the viscous term on the right hand side of this equation is

$$\frac{1}{\mathrm{Re}}\frac{\partial^2 u}{\partial \bar{y}^2} = \frac{1}{\mathrm{Re}}\frac{\epsilon^\star}{\delta^{\star 2}}\frac{\Delta U'}{\Delta y_\star^2} + \cdots.$$

The required balance to retain viscosity is then

$$\mathrm{Re}\,\delta^\star \sim \frac{1}{\delta^{\star 2}\,\mathrm{Re}}, \tag{2.83}$$

which is easily solved to give $\delta^\star = \mathrm{Re}^{-2/3}$. In order to find the order of magnitude γ of normal velocity perturbations, we substitute (2.81) into the continuity equation,

$$\frac{\partial u}{\partial \bar{x}} + \frac{\partial v}{\partial \bar{y}} + \frac{\partial w}{\partial \bar{z}} = 0,$$

and balancing terms gives

$$\gamma = \delta^\star\,\mathrm{Re}^{1/2} = \mathrm{Re}^{-1/6}.$$

The solution in the viscous sublayer is then sought in the form

$$\left.\begin{aligned} u &= \mathrm{Re}^{-1/6}\,\lambda_1 y_\star + \epsilon^\star U'(x_\star, y_\star, z_\star) + \cdots, \\ v &= \epsilon^\star\,\mathrm{Re}^{-1/6}\,V'(x_\star, y_\star, z_\star) + \cdots, \\ w &= \mathrm{Re}^{-1/6}\,\lambda_3 y_\star + \epsilon^\star W'(x_\star, y_\star, z_\star) + \cdots, \\ p &= \epsilon^\star\,\mathrm{Re}^{-1/6}\,P'(x_\star, z_\star) + \cdots. \end{aligned}\right\} \tag{2.84}$$

We substitute asymptotic expansions (2.84) into the Navier-Stokes equations and find that the perturbations U', V' and W' satisfy the linearised boundary-layer equations

$$\lambda_1 y_\star \frac{\partial U'}{\partial x_\star} + \lambda_1 V' + \lambda_3 y_\star \frac{\partial U'}{\partial z_\star} = -\frac{\partial P'}{\partial x_\star} + \frac{\partial^2 U'}{\partial y_\star^2}, \tag{2.85}$$

$$\lambda_3 y_\star \frac{\partial W'}{\partial x_\star} + \lambda_3 V' + \lambda_3 y_\star \frac{\partial W'}{\partial z_\star} = -\frac{\partial P'}{\partial z_\star} + \frac{\partial^2 W'}{\partial y_\star^2}, \tag{2.86}$$

$$\frac{\partial P'}{\partial y_\star} = 0, \tag{2.87}$$

$$\frac{\partial U'}{\partial x_\star} + \frac{\partial V'}{\partial y_\star} + \frac{\partial W'}{\partial z_\star} = 0. \tag{2.88}$$

We need to formulate appropriate boundary conditions for the problem. Now that the viscous term is present on the right hand side of (2.85) and (2.86), we can satisfy the no-slip condition

$$u = v = w = 0, \quad y_\star = \epsilon\, \eta(x_\star, z_\star). \tag{2.89}$$

The expansions (2.84) can be expressed on the surface of the roughness as

$$\begin{aligned}(u, v, w)\,|_{y_\star = y_w} = \mathrm{Re}^{-1/6}\, \epsilon\big(\lambda_1 \eta(x_\star, z_\star), 0, \lambda_3 \eta(x_\star, z_\star)\big) + \\ + \epsilon^\star \big(U'(x_\star, 0, z_\star), \mathrm{Re}^{-1/6}\, V'(x_\star, 0, z_\star), W'(x_\star, 0, z_\star)\big) + \cdots .\end{aligned}$$

We can substitute this into the no-slip condition (2.89) and, provided that $\epsilon^\star = \mathrm{Re}^{-1/6}\, \epsilon$, it yields

$$\begin{cases} U'(x_\star, 0, z_\star) = -\lambda_1 \eta(x_\star, z_\star), \\ V'(x_\star, 0, z_\star) = 0, \\ W'(x_\star, 0, z_\star) = -\lambda_3 \eta(x_\star, x_\star). \end{cases} \tag{2.90}$$

Before we solve equations (2.85)-(2.88), we should consider the matching conditions with the main part of the boundary layer where expansions (2.78) and scalings (2.79) apply. At

large values of $y_\star$, we look for a solution to equations (2.85)-(2.88) in the form

$$\left.\begin{aligned} U' &= A(x_\star, z_\star) + \frac{D(x_\star, z_\star)}{y_\star} + O\left(\frac{1}{y_\star^2}\right), \\ W' &= B(x_\star, z_\star) + \frac{E(x_\star, z_\star)}{y_\star} + O\left(\frac{1}{y_\star^2}\right), \\ V' &= -\left(\frac{\partial A}{\partial x_\star} + \frac{\partial B}{\partial z_\star}\right) y_\star + C(x_\star, z_\star) + O\left(\frac{1}{y_\star}\right), \\ P' &= P_0 + \cdots . \end{aligned}\right\} \quad \text{as} \quad y_\star \to \infty. \tag{2.91}$$

According to Kaplun's extension theorem, this expansion should be valid in an intermediate region between the viscous sublayer (region 2 in Figure 2.14) and the main part of the boundary layer (region 1 in Figure 2.14), the latter being defined by (2.79). We can then substitute asymptotic expansions (2.91) into (2.84) which leads to

$$\begin{aligned} u &= \lambda_1 y + \epsilon^\star A(x_\star, z_\star) + \epsilon^\star \, \mathrm{Re}^{-1/6} \, \frac{D(x_\star, z_\star)}{y} + \cdots , \\ w &= \lambda_3 y + \epsilon^\star B(x_\star, z_\star) + \epsilon^\star \, \mathrm{Re}^{-1/6} \, \frac{E(x_\star, z_\star)}{y} + \cdots , \\ v &= -\epsilon^\star \left(\frac{\partial A}{\partial x_\star} + \frac{\partial B}{\partial z_\star}\right) y + \epsilon^\star \, \mathrm{Re}^{-1/6} \, C(x_\star, z_\star) + \cdots , \\ p &= \epsilon^\star \, \mathrm{Re}^{-1/6} \, P_0 + \cdots . \end{aligned} \tag{2.92}$$

The asymptotic expansions (2.92) can now be used at the bottom of the main part of the boundary layer, suggesting that the solution should be represented there in the form

$$\left.\begin{aligned} u &= U(\bar{x}, y, \bar{z}) + \epsilon^\star \, \tilde{u}(x, y, z) + \epsilon^\star \, \mathrm{Re}^{-1/6} \, u'(x, y, z) + \cdots , \\ w &= W(\bar{x}, y, \bar{z}) + \epsilon^\star \, \tilde{w}(x, y, z) + \epsilon^\star \, \mathrm{Re}^{-1/6} \, w'(x, y, z) + \cdots , \\ v &= \epsilon^\star \, \tilde{v}(x, y, z) + \epsilon^\star \, \mathrm{Re}^{-1/6} \, v'(x, y, z) + \cdots , \\ p &= \epsilon^\star \, \mathrm{Re}^{-1/6} \, p'(x, y, z) + \cdots . \end{aligned}\right\} \tag{2.93}$$

When we substitute (2.93) into the Navier-Stokes equations, the resulting set of equations are the linearised Euler equations. However the pressure gradient, estimated to be of the order $\epsilon^\star \, \mathrm{Re}^{-1/6}$, disappears at leading order as it appears to be an order of magnitude smaller

than the leading order convective terms, which according to (2.93) are estimated to be of the order $\epsilon^\star$.

This is in contradiction with the equations obtained in Sections 2.2 and 2.3. In order to restore the pressure gradient, we need to assume that $A(x_\star, z_\star) = B(x_\star, z_\star) = 0$ so that all terms of order $\epsilon^\star$ disappear in (2.93). This means that $\tilde{u} = \tilde{v} = \tilde{w} = 0$. This particular behaviour of the boundary layer, where the displacement effect is inexistent, was first discussed by Bogolepov & Lipatov (1985) and is known as 'compensation regime' in Russian literature. The equations for the second order perturbations in (2.93) are then

$$U\frac{\partial u'}{\partial x} + \frac{\partial U}{\partial y}v' + W\frac{\partial u'}{\partial z} = -\frac{\partial p'}{\partial x}, \tag{2.94}$$

$$U\frac{\partial v'}{\partial x} + W\frac{\partial v'}{\partial z} = -\frac{\partial p'}{\partial y}, \tag{2.95}$$

$$U\frac{\partial w'}{\partial x} + \frac{\partial W}{\partial y}v' + W\frac{\partial w'}{\partial z} = -\frac{\partial p'}{\partial z}, \tag{2.96}$$

$$\frac{\partial u'}{\partial x} + \frac{\partial v'}{\partial y} + \frac{\partial w'}{\partial z} = 0. \tag{2.97}$$

These equations are similar to equations (2.24) derived in Section 2.2, with the density of the fluid set to unity. The boundary conditions for (2.94)-(2.97) can be deduced by matching with the asymptotic expansions (2.91) obtained at the edge of the sublayer. We then obtain

$$u', v', w' \to 0 \quad \text{as} \quad x^2 + y^2 + z^2 \to \infty, \tag{2.98}$$

$$\begin{cases} u'(x,y,z) = D(x,z)/y, \\ v'(x,y,z) = C(x,z), \qquad \text{as} \qquad y \to 0 \\ w'(x,y,z) = E(x,z)/y. \end{cases} \tag{2.99}$$

We are thus able to have a non-zero boundary condition for $v'(x,y,z)$, offering an alternative to the impermeability condition used in the inviscid approach described in Section 2.3. Our task is now to find

$$C(x_\star, z_\star) = \lim_{y_\star \to \infty} V'(x_\star, y_\star, z_\star).$$

2.4.2 Analytical solution in the viscous sublayer

In order to calculate the normal velocity $C(x_\star, z_\star)$ at the edge of the viscous sublayer, we should solve the linearised boundary-layer equations (2.85)-(2.88). To this aim, we reduce the original set of PDEs to a single ODE as follows. We differentiate the $x_\star$-momentum equation (2.85) by $x_\star$, the $z_\star$-momentum equation (2.86) by $z_\star$, and then combine them. The continuity equation (2.88) is used to eliminate U' and W', and leads to following equation for V' and P'

$$-y_\star\left(\lambda_1\frac{\partial}{\partial x_\star}+\lambda_3\frac{\partial}{\partial z_\star}\right)\frac{\partial V'}{\partial y_\star}+\left(\lambda_1\frac{\partial}{\partial x_\star}+\lambda_3\frac{\partial}{\partial z_\star}\right)V'= \\ =-\left(\frac{\partial^2}{\partial x_\star^2}+\frac{\partial^2}{\partial z_\star^2}\right)P'-\frac{\partial^3 V'}{\partial y_\star^3}. \qquad (2.100)$$

We differentiate this equation once more now with respect to $y_\star$ and use (2.87) to yield

$$\frac{\partial^4 V'}{\partial y_\star^4}-y_\star\left(\lambda_1\frac{\partial}{\partial x_\star}+\lambda_3\frac{\partial}{\partial z_\star}\right)\frac{\partial^2 V'}{\partial y_\star^2}=0. \qquad (2.101)$$

Let us assume that the roughness shape η is periodic in the $z_\star$ direction and can be written in the form

$$\eta=\mathrm{e}^{i\beta z_\star}\,g(x_\star). \qquad (2.102)$$

Consequently, we decompose V' in the following way

$$V'=\mathrm{e}^{i\beta z_\star}\,\tilde{V}(x_\star,y_\star), \qquad (2.103)$$

and substituting (2.103) into (2.101) yields

$$\frac{\partial^4 \tilde{V}}{\partial y_\star^4}-y_\star\left(\lambda_1\frac{\partial}{\partial x_\star}+i\beta\lambda_3\right)\frac{\partial^2 \tilde{V}}{\partial y_\star^2}=0. \qquad (2.104)$$

In order to eliminate the dependence on $x_\star$, we will use the Fourier transform. Let us define the Fourier transform in $x_\star$ of a function F by the integral

$$\bar{F}(y_\star;\alpha) = \int_{-\infty}^{+\infty} \mathrm{e}^{-i\alpha x_\star}\, F(x_\star, y_\star)\, \mathrm{d}x_\star \tag{2.105}$$

We apply the Fourier transform to equation (2.104), which turns it into

$$\frac{\mathrm{d}^4\bar{V}}{\mathrm{d}y_\star^4} - iy_\star\left(\lambda_1\alpha + \lambda_3\beta\right)\frac{\mathrm{d}^2\bar{V}}{\mathrm{d}y_\star^2} = 0. \tag{2.106}$$

We have now reduced the original set of PDEs to a single 4th order ODE. In order to formulate the four necessary boundary conditions for this equation, we return to the linearised boundary conditions for the perturbations U', V', W', given by (2.90). The first condition is then

$$V'(x_\star, 0, z_\star) = 0.$$

Furthermore, setting $y_\star = 0$ in the continuity equation (2.88) and using (2.90) leads to

$$\left.\frac{\partial V'}{\partial y_\star}\right|_{y_\star=0} = \lambda_1\frac{\partial\eta}{\partial x_\star} + \lambda_3\frac{\partial\eta}{\partial z_\star}.$$

In order to determine a third boundary condition, we look at the asymptotic expansion of V' for large values of $y_\star$, given by

$$V'(x_\star, y_\star, z_\star) = C(x_\star, z_\star) + \cdots, \quad \text{as} \quad y_\star \to \infty,$$

which leads to the conclusion that

$$\frac{\partial V'}{\partial y_\star} \to 0 \quad \text{as} \quad y_\star \to \infty.$$

It should be noted that we augmented the order of the differential equation when we differentiated it by $y_\star$ in the second step. The fourth boundary condition can be found by simply

evaluating (2.100) at $y_\star = 0$, which yields

$$\frac{\partial^3 V'}{\partial y_\star^3} = -\left(\frac{\partial^2}{\partial x_\star^2} + \frac{\partial^2}{\partial z_\star^2}\right) P'. \tag{2.107}$$

The final step in the formulation of appropriate boundary conditions for (2.106) is to apply the Fourier decomposition (2.103) and Fourier Transform (2.105) to these four equations, leading to

$$\begin{cases} \bar{V}\big|_{y_\star=0} = 0, \\ \bar{V}_{y_\star}\big|_{y_\star=0} = \left(\lambda_1 i\alpha + \lambda_3 i\beta\right)\bar{g}, \\ \bar{V}_{y_\star} \to 0 \quad \text{as} \quad y_\star \to \infty, \\ \bar{V}_{y_\star y_\star y_\star}\big|_{y_\star=0} = \left(\alpha^2+\beta^2\right)\bar{p}(0;\alpha,\beta). \end{cases} \tag{2.108}$$

where $\bar{g}$ and $\bar{p}$ represent the Fourier Transforms of the body shape function g and pressure respectively. Equation (2.106) can be reduced to the canonical form of the Airy equation by introducing the new variable ξ defined by

$$y_\star = s\xi = (i\lambda)^{-1/3}\xi, \tag{2.109}$$

with $\lambda = \lambda_1\alpha + \lambda_3\beta$. This turns equation (2.106) into

$$\frac{\mathrm{d}^4\bar{V}}{\mathrm{d}\xi^4} - \xi\frac{\mathrm{d}^2\bar{V}}{\mathrm{d}\xi^2} = 0. \tag{2.110}$$

The boundary conditions (2.108) should be recast in terms of the new variable ξ. We have

$$\begin{cases} \bar{V}\big|_{\xi=0} = 0, \\ \bar{V}_\xi\big|_{\xi=0} = is\lambda\bar{g}, \\ \bar{V}_\xi \to 0 \quad \text{as} \quad \xi \to \infty, \\ \bar{V}_{\xi\xi\xi}\big|_{\xi=0} = s^3\left(\alpha^2+\beta^2\right)\tilde{p}(0). \end{cases} \tag{2.111}$$

The general solution to equation (2.110) is

$$\bar{V}_{\xi\xi} = C_1\,\mathrm{Ai}(\xi) + C_0\,\mathrm{Bi}(\xi), \tag{2.112}$$

where Ai and Bi are the two complementary solutions of the Airy equations. According to the boundary conditions, $\bar{V}_\xi \to 0$ at large values of ξ, which leads to the condition that $\bar{V}_{\xi\xi} \to 0$ as $\xi \to \infty$ as well. Thus, we should set $C_0 = 0$ to remove the exponential growth of the Bi function. Integrating (2.112) once yields

$$\bar{V}_\xi = C_1 \int_0^\xi \mathrm{Ai}(t)\mathrm{d}t + C_2. \tag{2.113}$$

Applying the second boundary conditions, we find

$$C_2 = is\lambda\bar{g}.$$

Letting $y_\star \to \infty$ and using the third boundary condition leads to the relation

$$C_1 = -\frac{C_2}{\int_0^\infty \mathrm{Ai}(t)\mathrm{d}t}, \tag{2.114}$$

and combining these two equations for C_1 and C_2 yields

$$\bar{V}_\xi = \frac{is\lambda\bar{g}\int_\xi^\infty \mathrm{Ai}(t)\mathrm{d}t}{\int_0^\infty \mathrm{Ai}(t)\mathrm{d}t}. \tag{2.115}$$

We use the well-known result $\int_0^\infty \mathrm{Ai}(t)\mathrm{d}t = 1/3$ and we integrate by parts the numerator of equation (2.115), leading to

$$\bar{V}_\xi = 3is\lambda\,\bar{g}\left(-\xi\,\mathrm{Ai}(\xi) - \int_\xi^\infty \mathrm{Ai}'(t)\mathrm{d}t\right). \tag{2.116}$$

Let us now integrate once more and set the integration constant to 0 due to the first boundary condition (2.108), thus yielding

$$\bar{V}(\xi) = -3is\lambda\,\bar{g}\int_0^{\xi} t\,\mathrm{Ai}(t)\mathrm{d}t - 3\,is\lambda\,\bar{g}\int_0^{\xi}\int_{\zeta}^{\infty}\mathrm{Ai}'(t)\mathrm{d}t\mathrm{d}\zeta. \tag{2.117}$$

We are now in measure to find

$$C(x_\star, z_\star) = \lim_{y_\star\to\infty} V'(x_\star, y_\star, z_\star).$$

When taking the limit $\xi \to \infty$, the second term on (2.117) becomes much smaller than the first, and to leading order, we get

$$\lim_{\xi\to\infty}\bar{V} = 3\,is\lambda\bar{g}\int_0^{\infty} t\,\mathrm{Ai}(t)\mathrm{d}t. \tag{2.118}$$

We can simplify this further by substituting $is\lambda = [i\,(\lambda_1\alpha + \lambda_3\beta)]^{2/3}$ and using the identity $\int_0^{\infty} t\,\mathrm{Ai}(t)\mathrm{d}t = -\,\mathrm{Ai}'(0)$. The latter result is well known and can be derived by integrating directly the Airy equation. Thus, we obtain

$$\lim_{\xi\to\infty}\bar{V} = -3\,\mathrm{Ai}'(0)\,[i\,(\lambda_1\alpha + \lambda_3\beta)]^{2/3}\,\bar{g}(\alpha). \tag{2.119}$$

The formula (2.119) is in agreement with the work of Choudhari & Duck (1996). It can be used to derive a new boundary condition for the inviscid problem, instead of the impermeability condition (2.51) used previously. Indeed, the asymptotic matching between the main part of the boundary layer and the viscous sublayer requires[2]

$$v'(x, 0, z) = C(x_\star, z_\star). \tag{2.120}$$

[2]Recall that coordinates $x_\star$ and $z_\star$ are identical to coordinates x and z.

In order to calculate $C(x_\star, z_\star)$, we need to perform the inverse Fourier transform of equation (2.119) , and as a result we obtain

$$C(x_\star, z_\star) = -\frac{3\,\mathrm{Ai}'(0)}{2\pi}\,\mathrm{e}^{i\beta z_\star}\int_{-\infty}^{+\infty}\mathrm{e}^{i\alpha x_\star}\left[i(\lambda_1\alpha+\lambda_3\beta)\right]^{2/3}\bar{g}(\alpha)\mathrm{d}\alpha. \tag{2.121}$$

The integral (2.121) is performed numerically. Once this is done, we can use boundary condition (2.120) throughout the receptivity analysis described in Section 2.3. In particular, recall that the amplitude of the eigenmode was found to take the form

$$A = \frac{v_1(0)\hat{v}_0\,'(0)}{q_0(0)\int_0^{+\infty}\Lambda\,\hat{v}_0/q_0\,\mathrm{d}y}. \tag{2.122}$$

The term $v_1(0)$ should be replaced here by the Laplace transform of equation (2.121). As a consequence, we find that the amplitude $\mathcal{A}_{\text{vis}}$ of the crossflow vortex, obtained using the no-slip boundary condition, is given by

$$\mathcal{A}_{\text{vis}} = -\frac{3\,\mathrm{Ai}'(0)\left[\int_0^{+\infty}\mathrm{e}^{-\sigma_0 x_\star}\int_{-\infty}^{+\infty}\mathrm{e}^{i\alpha x_\star}\left[i(\lambda_1\alpha+\lambda_3\beta)\right]^{2/3}\bar{g}(\alpha)\mathrm{d}\alpha\mathrm{d}x_\star\right]\hat{v}_0'(0)}{2\pi\,q_0(0)\int_0^{+\infty}\Lambda\,\hat{v}_0/q_0\,\mathrm{d}y}. \tag{2.123}$$

The dependence of the magnitude of the amplitude function (2.123) on the wave number β is plotted in Figure 2.15. The calculations were performed using the same profile and roughness shape as in Section 2.3.

The function $|\mathcal{A}_{\text{vis}}(\beta)|$ exhibits a similar behaviour as $|\mathcal{A}_{\text{inv}}(\beta)|$ for values of $\beta < 0.125$. After a period of rapid growth, the amplitude reaches this time a global maximum at $\beta = 0.125$. This is followed by a sudden decrease of the amplitude until $\beta = 0.45$. It then seems to reach a horizontal asymptote. On Figure 2.16, we plot the amplitude at locations further down the wing. Similarly as in Section 2.3, the amplitude shape is magnified, with its maximum increasing in magnitude, and occurring at higher values of the wavenumber β. Figure 2.15 and 2.16 were compared with the plots obtained in Choudhari & Duck (1996) and showed good agreement.

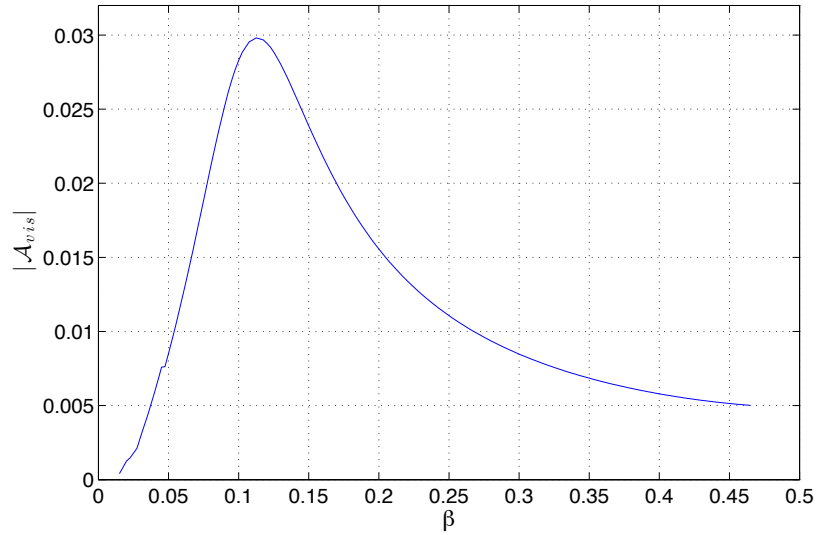

Figure 2.15: Amplitude of crossflow vortex $\mathcal{A}_{\text{vis}}$ as a function of the wavenumber β.

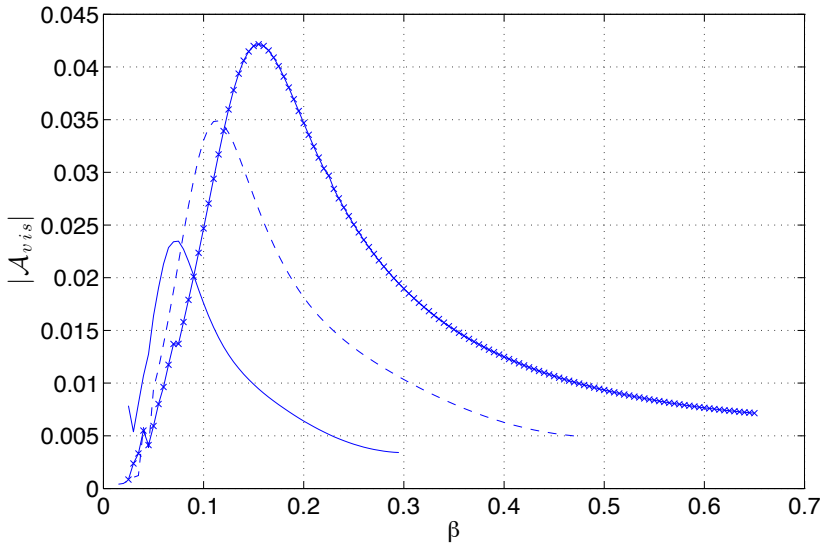

Figure 2.16: Amplitude of crossflow vortex at different locations along the wing (no-slip): $s = 0.0004167, M_\infty = 0.0442322$ (—); $s = 0.0006759, M_\infty = 0.0731715$ (−−); $s = 0.0009823, M_\infty = 0.1094626$ (-×-).

Chapter 3

Accelerating Subsonic Flow past a Curved Ramp

We now move away from the field of transition to turbulence and turn towards viscous-inviscid interaction of two-dimensional boundary layers. In the introduction, we mentioned that separation of boundary layers is linked to singularities in the pressure gradient. The singularities can be caused due to abrupt changes in the object's shape, such as corners or surface discontinuities on a wing, or by physical changes in the properties of the flow such as shock waves. This mathematical singularity should be smoothed out by the viscous-inviscid interaction.

The local study of the inviscid flow past corners or discontinuities typically gives rise to algebraic singularities of the form

$$\frac{\mathrm{d}p}{\mathrm{d}x} = \kappa(-x)^{\lambda}, \quad \text{as} \quad x \to 0^{-}, \tag{3.1}$$

where it is assumed that the origin of the coordinate system is centred at the discontinuity point and κ, which can be small or order one, is a control parameter related to the strength of the discontinuity. An example of such a flow would be the Prandtl-Meyer transonic flow over a convex corner (Ruban, Wu & Pereira 2006), when parameter $\lambda = -3/5$, or transonic flow separating from a corner point (Ruban & Turkyilmaz 2000) when $\lambda = -2/3$.

Another interesting example of a flow giving rise to such a pressure gradient is the study

of the transonic fluid flow past a discontinuity in curvature, where it is further assumed that the sonic point coincides with the point of discontinuity. It was shown (Buldakov & Ruban 2002) in that case that parameter $\lambda = -1/3$. It turns out that this specific value of λ corresponds to a bifurcation in parameter space for the boundary-layer flow. Indeed, let us set $\lambda = -1/3 + \delta$ and further assume that $\kappa = \kappa(\epsilon) \ll 1$. In this case the curvature discontinuity only produces small perturbations to the incoming Blasius flow. It can then be shown that the stream function upstream of the discontinuity takes the form

$$\psi(x, Y) = (-x)^{2/3} \left(\frac{1}{2}\tau_w \eta^2 + \kappa(\epsilon)(-x)^{\delta} f(\eta) + \cdots \right), \quad \text{as} \quad x \to 0^-, \tag{3.2}$$

where $\eta = Y/(-x)^{1/3} = O(1)$. Thus, when $\delta > 0$, the perturbations always decay and no flow separation takes place. If $\delta < 0$, despite the small coefficient $\kappa(\epsilon)$, the perturbations will grow and might become of the same order as the leading order term, which can lead to separation.

This leads to the conclusion that $\delta = 0$ (corresponding to $\lambda = -1/3$) represents indeed an important change in the qualitative property of the solution of the boundary-layer problem. Furthermore, it can be shown that as $\delta \to 0$, the function $f(\eta)$ contains a term growing like $\Gamma(\delta)$[1] and in the limit, logarithmic terms should be added in the coordinate asymptotic expansion (3.2) of the streamfunction's perturbation to account for this effect.

Surprisingly, a similar behaviour is observed when we assume that $\kappa = O(1)$. In that case, the pressure gradient is strong enough to affect the flow upstream of the interaction region and logarithmic terms should be included at leading order in the asymptotic expansion of the stream function. We aim to present the viscous-inviscid interaction problem and its solution for subsonic and transonic flows subject to the pressure gradient

$$\frac{\mathrm{d}p}{\mathrm{d}x} = \kappa(-x)^{-1/3}, \quad \text{as} \quad x \to 0^-. \tag{3.3}$$

[1]Here, $\Gamma(t)$ is the standard Gamma function

$$\Gamma(t) = \int_0^\infty x^{t-1}\, \mathrm{e}^{-x}\, \mathrm{d}x,$$

with the asymptotic property $\Gamma(t) \sim 1/t$ as $t \to 0$.

In the former case, the specific pressure gradient (3.3) can be generated by suitable choice of the body shape. Linear equations will be derived in both the upper and lower deck of the interaction region, allowing for an analytic solution. For the latter case, we will show in Chapter 4 that the flow naturally develops the required singularity. The equation in the upper deck will be found to reduce to the Kármán-Guderley equation, which is nonlinear. This problem will then be solved numerically.

3.1 General formulation

Let us investigate the fluid flow past a body shape with flat leading section of length L. The body then bends up or down as shown in Figure 3.1.

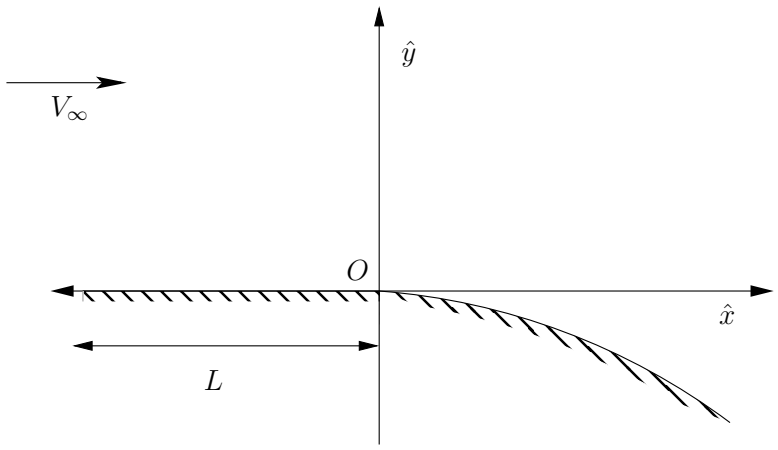

Figure 3.1: Layout of the problem.

We chose $\hat{x}$ to be parallel and $\hat{y}$ to be perpendicular to the flat part of the body contour. The origin O is chosen to coincide with the point where the body starts to bend. The flow, assumed to be steady, two-dimensional and incompressible, is governed by the Navier-

Stokes equations

$$\begin{aligned} \hat{u}\frac{\partial \hat{u}}{\partial \hat{x}} + \hat{v}\frac{\partial \hat{u}}{\partial \hat{y}} &= -\frac{1}{\rho}\frac{\partial \hat{p}}{\partial \hat{x}} + \nu\left(\frac{\partial^2 \hat{u}}{\partial \hat{x}^2} + \frac{\partial^2 \hat{u}}{\partial \hat{y}^2}\right), \\ \hat{u}\frac{\partial \hat{v}}{\partial \hat{x}} + \hat{v}\frac{\partial \hat{v}}{\partial \hat{y}} &= -\frac{1}{\rho}\frac{\partial \hat{p}}{\partial \hat{y}} + \nu\left(\frac{\partial^2 \hat{v}}{\partial \hat{x}^2} + \frac{\partial^2 \hat{v}}{\partial \hat{y}^2}\right), \\ \frac{\partial \hat{u}}{\partial \hat{x}} + \frac{\partial \hat{v}}{\partial \hat{y}} &= 0. \end{aligned} \tag{3.4}$$

The velocity components are denoted by $\hat{u}$ and $\hat{v}$, and the pressure by $\hat{p}$. The density ρ and kinematic viscosity coefficient ν are assumed to be constant throughout the flow. Let us introduce non-dimensional variables

$$\begin{cases} \hat{x} = Lx, \quad \hat{y} = Ly, \\ \hat{u} = V_\infty u, \quad \hat{v} = V_\infty v, \quad \hat{p} = p_\infty + \rho V_\infty^2 p, \end{cases} \tag{3.5}$$

where V_∞ and p_∞ represent the free stream velocity and pressure respectively. After substituting (3.5) into (3.4), the Navier-Stokes equations take the form

$$\begin{aligned} u\frac{\partial u}{\partial x} + v\frac{\partial u}{\partial y} &= -\frac{\partial p}{\partial x} + \frac{1}{\mathrm{Re}}\left(\frac{\partial^2 u}{\partial x^2} + \frac{\partial^2 u}{\partial y^2}\right), \\ u\frac{\partial v}{\partial x} + v\frac{\partial v}{\partial y} &= -\frac{\partial p}{\partial y} + \frac{1}{\mathrm{Re}}\left(\frac{\partial^2 v}{\partial x^2} + \frac{\partial^2 v}{\partial y^2}\right), \\ \frac{\partial u}{\partial x} + \frac{\partial v}{\partial y} &= 0, \end{aligned} \tag{3.6}$$

with the Reynolds number defined as

$$\mathrm{Re} = \frac{V_\infty L}{\nu}.$$

We assume that in a vicinity of the origin, we may express the wall shape y_w in the form

$$y_w = \begin{cases} 0 & : x < 0, \\ \kappa x^{5/3} & : x > 0. \end{cases} \tag{3.7}$$

This condition is necessary in order to generate the pressure gradient (3.3) for subsonic flows, as was mentioned in the introduction. Depending on the sign of κ, the body can bend up or down. The boundary conditions are the no-slip conditions on the wall, which

are written as

$$u = v = 0, \quad y = y_w, \tag{3.8}$$

and the free stream conditions

$$u = 1, \quad v = 0, \quad p = 0 \quad \text{as} \quad x^2 + y^2 \to \infty. \tag{3.9}$$

To study the flow, we will follow Prandtl's Hierarchical strategy. We start by analysing the external inviscid flow, ignoring the presence of viscosity, and will then turn to the analysis of the boundary layer. The singularity in the pressure gradient will lead to the introduction of an interaction region which takes the standard triple deck form.

3.2 Analysis of the external inviscid flow

We start with the flow in the inviscid region, where

$$x = O(1), \quad y = O(1). \tag{3.10}$$

In this case, the Navier-Stokes equations (3.6) reduce to the Euler equations

$$\begin{aligned} u\frac{\partial u}{\partial x} + v\frac{\partial u}{\partial y} &= -\frac{\partial p}{\partial x}, \\ u\frac{\partial v}{\partial x} + v\frac{\partial v}{\partial y} &= -\frac{\partial p}{\partial y}, \\ \frac{\partial u}{\partial x} + \frac{\partial v}{\partial y} &= 0. \end{aligned} \tag{3.11}$$

We drop the no-slip conditions in favour of the impermeability condition on the body surface, which takes the form

$$\left.\frac{v}{u}\right|_{y=y_w} = \frac{\mathrm{d}y_w}{\mathrm{d}x}. \tag{3.12}$$

Additionally, we must specify the free stream conditions

$$u = 1, \quad v = p = 0 \quad \text{as} \quad x^2 + y^2 \to \infty. \tag{3.13}$$

The flow is assumed to be incompressible and irrotational, which enables us to introduce the complex potential

$$w(x+iy) = \phi(x,y) + i\psi(x,y).$$

Here, $\psi(x,y)$ represents the stream-function of the flow, and $\phi(x,y)$ the potential function, both satisfying Laplace equation. In a vicinity of the origin, we can assume that $|\kappa x| \ll 1$, in which case the impermeability condition (3.12) can be linearised and reduces to

$$v(x,0) = \begin{cases} 0 & : x < 0, \\ \dfrac{5}{3}\kappa x^{2/3} & : x > 0. \end{cases} \tag{3.14}$$

Guided by this, we look for a solution in the form

$$w(x+iy) = z + Cz^{5/3} + \cdots \quad \text{as} \quad z \to 0, \tag{3.15}$$

where the constant C is assumed to be complex and should be suitably chosen in order to satisfy the boundary conditions. Differentiating with respect to z yields

$$w' = u - iv = 1 + \frac{5}{3}\left(C_r + iC_i\right) z^{2/3} + \cdots . \tag{3.16}$$

We let $z = re^{i\theta}$, and identifying real and imaginary parts, the velocity components become

$$u(x,y) = 1 + \frac{5}{3}\left(C_r \cos\left(\frac{2}{3}\theta\right) - C_i \sin\left(\frac{2}{3}\theta\right)\right) r^{2/3} + \cdots , \tag{3.17}$$

$$v(x,y) = -\frac{5}{3}\left(C_r \sin\left(\frac{2}{3}\theta\right) + C_i \cos\left(\frac{2}{3}\theta\right)\right) r^{2/3} + \cdots . \tag{3.18}$$

We now apply the boundary condition (3.14) and note that $x \lesseqgtr 0$ is equivalent to $\theta = \pi, 0$, which leads to

$$C_r = \frac{1}{\sqrt{3}} C_i, \quad C_i = -\kappa.$$

In order to find the pressure distribution, we use the Bernoulli equation which gives

$$p(x,y) = 1 - \frac{1}{2}|\bar{w}'|^2 = -\frac{5}{3}\left(C_r \cos\left(\frac{2}{3}\theta\right) - C_i \sin\left(\frac{2}{3}\theta\right)\right) r^{2/3} + \cdots \quad \text{as} \quad r \to 0.$$

In particular, on the body surface upstream of the origin, we have

$$p(x,0) = \chi(-x)^{2/3} + \cdots, \quad \text{as} \quad x \to 0^-. \tag{3.19}$$

The parameter χ is defined by the equation

$$\chi = \frac{5}{3}\kappa\left[\frac{1}{\sqrt{3}}\cos\left(\frac{2}{3}\pi\right) - \sin\left(\frac{2}{3}\pi\right)\right] = -\frac{10}{3\sqrt{3}}\kappa. \tag{3.20}$$

When $\kappa < 0$, the pressure gradient is favourable and we expect the flow in the boundary layer to be accelerated. We will in fact show in the following section that solutions can only be constructed for $\kappa < 0$.

3.3 Subsonic boundary layer upstream of the curved ramp

Let us now turn our attention to the flow in the boundary layer. We introduce the usual coordinates (x, Y) defined by

$$x = x, \quad y = \mathrm{Re}^{-1/2}\, Y. \tag{3.21}$$

The asymptotic analysis of the Navier-Stokes equations (3.6) is based on the limit

$$x = O(1), \quad Y = O(1) \quad \text{as} \quad \mathrm{Re} \to \infty.$$

The solution is sought in the asymptotic form

$$\left.\begin{aligned} u &= U(x,Y) + \cdots, \\ v &= \mathrm{Re}^{-1/2}\, V(x,Y) + \cdots, \\ p &= P(x,Y) + \cdots. \end{aligned}\right\} \tag{3.22}$$

Substituting (3.21) and (3.22) into the Navier-Stokes equations leads to the classical boundary-layer equations

$$\begin{aligned} U\frac{\partial U}{\partial x} + V\frac{\partial U}{\partial Y} &= -\frac{\partial P}{\partial x} + \frac{\partial^2 U}{\partial Y^2}, \\ \frac{\partial P}{\partial Y} &= 0, \\ \frac{\partial U}{\partial x} + \frac{\partial V}{\partial Y} &= 0. \end{aligned} \tag{3.23}$$

The second equation in (3.23) indicates that pressure remains constant across the boundary layer and only depends on x. Asymptotic matching with the inviscid region thus requires that $P(x, Y) = p_e(x)$, where $p_e(x)$ denotes the inviscid wall pressure (3.19). Hence, the pressure gradient in the boundary layer is given by equation

$$\frac{\mathrm{d}p_e}{\mathrm{d}x} = -\frac{2}{3}\chi(-x)^{-1/3}. \tag{3.24}$$

We introduce the stream function $\psi(x, Y)$, defined by the equations

$$U = \frac{\partial \psi}{\partial Y}, \quad V = -\frac{\partial \psi}{\partial x}, \tag{3.25}$$

which then enables us to write the boundary-layer equations in the form

$$\frac{\partial \psi}{\partial Y}\frac{\partial^2 \psi}{\partial x \partial Y} - \frac{\partial \psi}{\partial x}\frac{\partial^2 \psi}{\partial Y^2} = -\frac{\mathrm{d}p_e}{\mathrm{d}x} + \frac{\partial^3 \psi}{\partial Y^3}. \tag{3.26}$$

This equation should be solved together with the no-slip conditions

$$\psi = \frac{\partial \psi}{\partial Y} = 0 \quad \text{on} \quad Y = 0, \tag{3.27}$$

as well as a matching condition with the inviscid flow. Under the influence of the strong favourable pressure gradient (3.24), the boundary layer typically splits into two regions, which we will denote region $2a$ and region $2b$, depicted in Figure 3.2.

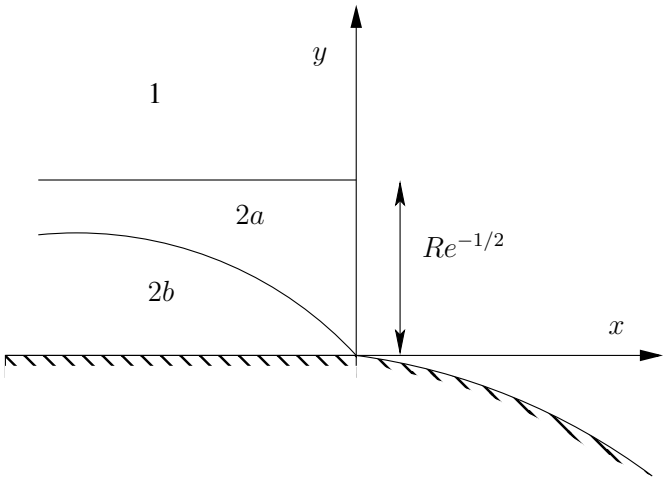

Figure 3.2: Two-tiers structure of the boundary layer.

3.3.1 Region $2b$ - Viscous sublayer

The slow fluid particles near the wall are the most affected by the singular pressure gradient (3.24). In order to apply the no-slip condition, the convective terms on the left hand side should balance with the pressure gradient as well as the viscous term. We thus need

$$\frac{\psi^2}{xY^2} \sim \frac{\mathrm{d}p_e}{\mathrm{d}x} \sim \frac{\psi}{Y^3}. \tag{3.28}$$

This system of estimates can easily be solved to yield

$$Y \sim (-x)^{1/3}, \quad \psi \sim (-x)^{2/3}. \tag{3.29}$$

The effects of viscosity then seem to be restricted to a small region near the wall, hence the appellation 'viscous sublayer'. This suggests the introduction of the similarity variable

$$\eta = \frac{Y}{(-x)^{1/3}} = O(1),$$

and motivates us to seek the solution to (3.26) in the form

$$\psi(x, Y) = (-x)^{2/3} f(\eta) + \cdots, \quad \text{as} \quad x \to 0^-. \tag{3.30}$$

Substituting this into (3.26) leads to the nonlinear ordinary differential equation

$$f''' - \frac{2}{3} f f'' + \frac{1}{3}\big(f'\big)^2 + \frac{2}{3}\chi = 0, \tag{3.31}$$

which should be solved with no-slip conditions

$$f(0) = f'(0) = 0, \tag{3.32}$$

and the requirement that $f(\eta)$ does not grow exponentially as $\eta \to \infty$. The latter condition is necessary in order to match with the main part of the boundary layer. This equation admits an exact solution of the form

$$f(\eta) = A\eta^2 + B\eta + C, \tag{3.33}$$

provided that constants A, B and C satisfy

$$B^2 - 4AC + 2\chi = 0.$$

However, the no-slip conditions (3.32) require $B = C = 0$, implying that no polynomial solutions exist. Balancing the terms in the equations shows that it allows exponentially growing solutions, but these are incompatible with the third boundary condition. In order to get more insight, we let

$$\frac{\mathrm{d}p_e}{\mathrm{d}x} = \kappa(-x)^{-1/3+\delta}, \quad \text{as} \quad x \to 0^-,$$

where δ is assumed small. Balancing terms in the boundary-layer equation leads to the solution being sought in the form

$$\psi(x, Y) = (-x)^{2/3+\delta/4} f(\eta) + \cdots, \quad \text{as} \quad x \to 0^-, \tag{3.34}$$

where the similarity variable $\eta = Y/(-x)^{1/3-\delta/4}$. The function f now satisfies the nonlinear ordinary differential equation

$$f''' - \left(\frac{2}{3} + \frac{\delta}{4}\right) f f'' + \left(\frac{1}{3} + \frac{\delta}{2}\right) \left(f'\right)^2 + \kappa = 0, \tag{3.35}$$

subject to the boundary conditions

$$f(0) = f'(0) = 0, \tag{3.36}$$

and the requirement that $f(\eta)$ does not grow exponentially. At large values of η, we can write

$$f = A(\delta)\eta^{(8+3\delta)/(4-3\delta)} + B(\delta)\eta^{(8+3\delta)/(4-3\delta)-1} + \cdots, \tag{3.37}$$

and it can be shown that $A(\delta) \sim \delta^{-3/4}$ as $\delta \to 0$, indicating that the limiting case is indeed singular. Terms growing faster than polynomials but slower than exponentials should be added in the asymptotic expansion for the stream function. This is done by introducing logarithmic terms in (3.30). Due to the equations being nonlinear, in order to balance every term, the thickness of the viscous sublayer and thus the definition of the similarity variable η should be modified to also include those logarithmic terms. Returning to the original boundary-layer equation (3.26), we now look for a solution of the form

$$Y \sim (-x)^{1/3}\big(-\log(-x)\big)^{-\alpha}, \quad \psi \sim \big(-\log(-x)\big)^{\alpha}(-x)^{2/3}. \tag{3.38}$$

Accordingly, the similarity variable η should now take the form

$$\eta = \big(-\log(-x)\big)^{\alpha} \frac{Y}{(-x)^{1/3}}. \tag{3.39}$$

We chose the parameter α in such a way that the pressure gradient only appears in the second order approximation, in which case we should set $\alpha = 1/4$. This allows us to construct a solution to the problem. Consequently, we look for a solution to equation

(3.26) in the form of the coordinate asymptotic expansion

$$\psi = \big(-\log(-x)\big)^{1/4}(-x)^{2/3}\left(f_0(\eta) + \frac{f_1(\eta)}{\big(-\log(-x)\big)} + \cdots\right), \quad \text{as} \quad x \to 0^-. \tag{3.40}$$

We substitute (3.40) and (3.39) into equation (3.26), and the leading order equation appears to be

$$f_0''' - \frac{2}{3}f_0 f_0'' + \frac{1}{3}\left(f_0'\right)^2 = 0, \tag{3.41}$$

subject to

$$f_0(0) = f_0'(0) = 0, \tag{3.42}$$

and the requirement that $f_0(\eta)$ does not grow exponentially. This equation is similar to (3.31), but it doesn't contain the terms coming from the pressure gradient, and thus allows for a simple polynomial solution

$$f_0(\eta) = \frac{1}{2}A\eta^2, \tag{3.43}$$

which is now compatible with boundary conditions (3.42). The constant A remains arbitrary at this stage, but should be found as part of the solution. The next order equation incorporates both the forcing from the singular pressure gradient and the terms from the leading order solution

$$f_1''' - \frac{1}{3}A\eta^2 f_1'' + \frac{2}{3}A\eta f_1' - \frac{2}{3}A f_1 + \frac{2}{3}\chi = \frac{3}{8}A^2\eta^2. \tag{3.44}$$

The boundary conditions for f_1 are also given by (3.42). Equation (3.44) is linear and can be solved exactly in the following way. We first differentiate it once, leading to

$$f_1'''' - \frac{1}{3}A\eta^2 f_1''' = \frac{3}{4}A^2\eta, \tag{3.45}$$

which has complementary solution

$$f_1'''(\eta) = B\exp\left(\frac{1}{9}A\eta^3\right).$$

We then use the method of undetermined coefficients and let $B = B(\eta)$, which upon substitution into (3.45), leads to the equation

$$B(\eta) = \int_0^\eta \frac{3}{4} A^2 \xi \, \mathrm{e}^{-\frac{1}{9}A\xi^3} \, \mathrm{d}\xi + C. \tag{3.46}$$

When we differentiated equation (3.44), we added another constant of integration and we thus require an additional boundary condition. It is found by evaluating equation (3.44) at $\eta = 0$, which yields

$$f_1'''(0) = -\frac{2}{3}\chi.$$

This fixes the integration constant C in (3.46). The general solution contains the exponentially growing term $\exp\left(\frac{1}{9}\eta^3\right)$, which should be eliminated in order to satisfy the third boundary condition (3.42). This can be done by imposing the condition $B \to 0$ as $\eta \to \infty$, which is possible if

$$\frac{2}{3}\chi = \int_0^\infty \frac{3}{4} A^2 \xi \, \mathrm{e}^{-\frac{1}{9}A\xi^3} \, \mathrm{d}\xi. \tag{3.47}$$

Equation (3.47) then gives us a solvability condition relating A and the body contour curvature κ. The integral on the right hand side can be converted to a Gamma integral, leading to the simplified form

$$A = \frac{2^{9/4}\chi^{3/4}}{3^{7/4}\Gamma(2/3)^{3/4}}. \tag{3.48}$$

In particular, we observe that if the curvature $\kappa > 0$, which means according to (3.20) that parameter $\chi < 0$, the constant A becomes complex. This indicates that the solution doesn't exist in the case of convex walls. It turns out that when $|\kappa| \ll 1$, then the problem can be linearised and solutions can be constructed for both positive and negative κ.

In order to obtain the solution for f_1, we start from the equation

$$f_1''' = \frac{3}{4} A^2 \, \mathrm{e}^{\frac{A}{9}\eta^3} \int_\infty^\eta t \, \mathrm{e}^{-\frac{A}{9}t^3} \, \mathrm{d}t,$$

and integrate this three times, leading to

$$f_1(\eta) = \frac{1}{2}\int_0^\eta (\eta - \xi)^2 \int_\infty^\zeta \frac{3}{4} A^2 \zeta \, \mathrm{e}^{\frac{1}{9}A(\xi^3 - \zeta^3)} \, \mathrm{d}\zeta \mathrm{d}\xi + D\eta^2. \tag{3.49}$$

Constant D is arbitrary at this stage and needs to be found by considering higher order problem. Of specific interest is the behaviour of f_1 at large values of η. Integrating by parts equation (3.49), we find that

$$f_1 = -\frac{9}{8}A\eta^2\log(\eta) + C_1\eta^2 + C_2\eta + C_3 + O\left(\frac{1}{\eta}\right) \quad \text{as} \quad \eta \to \infty. \tag{3.50}$$

While the constant C_1 remains arbitrary at this stage, we find that

$$C_2 = -\frac{9^{5/6}}{4}A^{2/3}\Gamma(2/3)^2, \quad C_3 = \frac{\chi}{A}. \tag{3.51}$$

The aim of the analysis of the sublayer is to determine the slope θ that the streamlines make at the edge of region $2b$ to estimate the displacement effect of the sublayer. By definition,

$$\theta = \lim_{\eta\to\infty} \mathrm{Re}^{-1/2}\,\frac{V}{U}, \tag{3.52}$$

and substituting (3.50) into (3.40) and (3.25), we obtain

$$\theta = \mathrm{Re}^{-1/2}\Big(-\log(-x)\Big)^{-5/4}(-x)^{-2/3}\frac{2}{3}C_2 + \cdots. \tag{3.53}$$

This concludes our analysis of the viscous sublayer, and we now turn to the main part of the boundary layer.

3.3.2 Region $2a$ - Main part of the boundary layer

The analysis of the main part of the boundary layer is based on the limit

$$x \to 0^-, \quad Y = O(1). \tag{3.54}$$

In order to estimate ψ in the main part of the boundary layer, we substitute asymptotic expansion (3.50) into (3.40). As a result, the asymptotic expansion for ψ in region $2a$ takes the form

$$\psi = (-\log(-x))^{3/4}\,\psi_0(Y) + \cdots, \quad \text{as} \quad x \to 0^-.$$

We estimate each term of the boundary-layer equation (3.26) as

$$\frac{\partial\psi}{\partial Y}\frac{\partial^2\psi}{\partial x\partial Y}\sim\frac{\Delta\psi_0^2}{\Delta x(\log\Delta x)^{1/4}\Delta Y^2},\quad \frac{\mathrm{d}p_e}{\mathrm{d}x}\sim\frac{1}{\Delta x^{1/3}},\quad \frac{\partial^3\psi}{\partial Y^3}\sim\frac{\Delta\psi_0}{\Delta Y^3}. \tag{3.55}$$

According to the scalings (3.54), we see that in region $2a$ the convective terms dominate. The boundary-layer equation (3.26) then reduces to

$$\frac{\partial\psi}{\partial Y}\frac{\partial^2\psi}{\partial x\partial Y}-\frac{\partial\psi}{\partial x}\frac{\partial^2\psi}{\partial Y^2}=0. \tag{3.56}$$

This can be rewritten as

$$\frac{\partial}{\partial Y}\left(\frac{\partial\psi/\partial x}{\partial\psi/\partial Y}\right)=0, \tag{3.57}$$

indicating that the streamline slope remains unchanged in the main part of the boundary layer. According to Kaplun's extension principle, formula (3.53) obtained at the edge of region $2b$ is also applicable to the bottom of region $2a$, and according to (3.57), it is actually valid throughout the whole region.

Thus, the displacement effect generated by the change in streamline slope occurring at the edge of region $2b$ is transmitted to the inviscid region through the 'buffer' region $2a$. This produces pressure perturbations Δp to the inviscid flow which, for subsonic flows, are proportional to θ. We can then write

$$\Delta p\sim\mathrm{Re}^{-1/2}\Big(-\log(-x)\Big)^{-5/4}(-x)^{-2/3}.$$

Despite the small coefficient $\mathrm{Re}^{-1/2}$, the pressure perturbations experience unbounded growth as $x\to0^-$. If these perturbations become comparable with the inviscid pressure p_e, our assumption that the pressure gradient is independent of what happens in the boundary layer breaks down and an interaction region should be introduced. This happens when

$$p_e\sim\Delta p\Leftrightarrow(-x)^{2/3}\sim\mathrm{Re}^{-1/2}\Big(-\log(-x)\Big)^{-5/4}(-x)^{-2/3}. \tag{3.58}$$

Thus, the solution to the transcendental equation

$$x|\log x|^{15/16} = \mathrm{Re}^{-3/8}, \tag{3.59}$$

gives the longitudinal extent of the interaction region, and we denote this solution by σ.

3.4 Formulation of the interaction problem

We now turn to the description of the interaction region, which takes the standard triple deck form as depicted on Figure 3.3. We start with the analysis of the lower deck and move up towards the inviscid region.

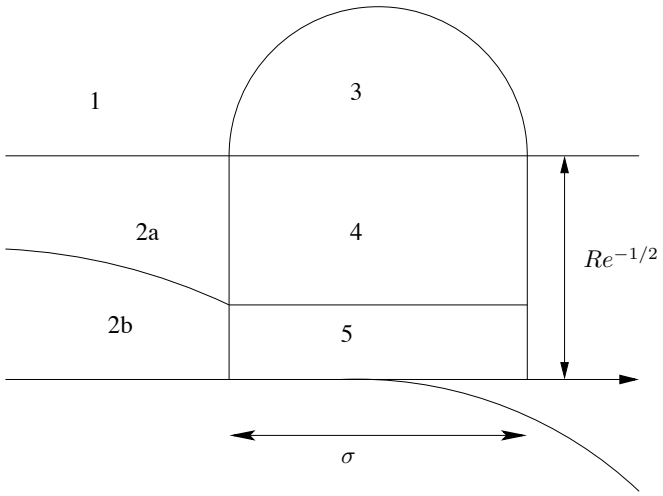

Figure 3.3: Triple deck structure of interaction region.

3.4.1 Region 5: the viscous sublayer

The lower deck is the continuation of the viscous sublayer $2b$, where the similarity variable η is an order one quantity. This relation must hold as well in region 5. Hence, the thickness of the viscous sublayer can be found by substituting $x = \sigma$ in the equation (3.39) and

expanding assuming $\sigma \ll 1$. The analysis of region 5 is then based on the scalings

$$x = \sigma X_\star, \quad Y = \sigma^{1/3} |\log \sigma|^{-1/4} Y_\star. \tag{3.60}$$

According to Kaplun's extension theorem, the asymptotic expansion (3.40) for ψ is valid in the overlap region between region $2b$ and region 5. Hence, in order to find the form of the solution in region 5, we rewrite (3.40) in terms of the variables $X_\star$ and $Y_\star$ leading to

$$\psi = |\log(\sigma)|^{1/4} \sigma^{2/3} \left(\frac{1}{2} A Y_\star^2 + \frac{(-X_\star)^{2/3}}{|\log(\sigma)|} \left(f_1(\eta_\star) - \frac{3A}{8} \log(-X_\star) \eta_\star^2 \right) + \cdots \right) \tag{3.61}$$

where we define the new similarity variable $\eta_\star$

$$\eta_\star = \frac{Y_\star}{(-X_\star)^{1/3}} = O(1).$$

This suggests that the solution in region 5 should be sought in the form

$$\psi = |\log \sigma|^{1/4} \sigma^{2/3} \left(\psi_0^\star(X_\star, Y_\star) + \frac{1}{|\log \sigma|} \psi_1^\star(X_\star, Y_\star) + \cdots \right). \tag{3.62}$$

Recall that the pressure in the boundary layer far upstream is given by $P = \chi(-x)^{2/3}$. Substituting $x = \sigma X_\star$, we find that the pressure in the interaction region should be sought in the form

$$P = \sigma^{2/3} P_\star(X_\star), \tag{3.63}$$

and the matching condition with the upstream boundary layer is

$$P_\star = \chi(-X_\star)^{2/3} \quad \text{as} \quad X_\star \to -\infty. \tag{3.64}$$

Substitution of (3.60)-(3.63) into the boundary-layer equation leads to the following equation for $\psi_0^\star$

$$\frac{\partial \psi_0^\star}{\partial Y_\star} \frac{\partial^2 \psi_0^\star}{\partial X_\star \partial Y_\star} - \frac{\partial \psi_0^\star}{\partial X_\star} \frac{\partial^2 \psi_0^\star}{\partial Y_\star^2} = \frac{\partial^3 \psi_0^\star}{\partial Y_\star^3}. \tag{3.65}$$

This equation should be solved subject to the no-slip condition on the wall

$$\psi_0^\star = \frac{\partial \psi_0^\star}{\partial Y_\star} = 0, \quad Y_\star = 0,$$

together with the matching condition with the upstream boundary layer flow

$$\psi_0^\star = \frac{1}{2} A Y_\star^2 \quad \text{as} \quad X_\star \to -\infty.$$

It is not surprising that the solution to this equation compatible with these boundary condition is simply

$$\psi_0^\star = \frac{1}{2} A Y_\star^2.$$

The constant A is not arbitrary but is instead fixed by the matching condition with the upstream flow, and its value is

$$A = \frac{2^{9/4} \chi^{3/4}}{3^{7/4} \Gamma(2/3)^{3/4}}.$$

The leading order solution in the interaction region just mimics the behaviour of the flow upstream. The interaction with the inviscid flow comes through pressure, which occurs at second order in the asymptotic expansion. In order to study this effect, we turn to the equation for $\psi_1^\star$, which is linear

$$A Y_\star \frac{\partial^2 \psi_1^\star}{\partial X_\star \partial Y_\star} - A \frac{\partial \psi_1^\star}{\partial X_\star} = -\frac{\mathrm{d} P_\star}{\mathrm{d} X_\star} + \frac{\partial^3 \psi_1^\star}{\partial Y_\star^3}. \tag{3.66}$$

It should be solved with the no-slip boundary conditions on the wall and the asymptotic matching witch the upstream flow

$$\begin{cases} \psi_1^\star(X_\star, 0) = 0, & \left.\dfrac{\partial \psi_1^\star}{\partial Y_\star}\right|_{Y_\star = 0} = \begin{cases} 0 & X_\star < 0, \\ -A\kappa X_\star^{5/3} & X_\star > 0. \end{cases} \\ \psi_1^\star \to (-X_\star)^{2/3} \left(f_1(\eta_\star) - \dfrac{3A}{8} \log(-X_\star) \eta_\star^2 \right) \quad \text{as} \quad X_\star \to -\infty. \end{cases} \tag{3.67}$$

The boundary-layer equations are parabolic, and in order to solve them, the asymptotic behaviour of $\psi_1^\star$ for $Y_\star \to \infty$ should also be specified. We substitute (3.50) into the last equation in (3.67), leading to

$$\psi_1^\star = -\frac{9}{8}AY_\star^2 \log Y_\star + \frac{1}{2}C_1 Y_\star^2 + C_2(-X_\star)^{1/3}Y_\star + \cdots . \tag{3.68}$$

This suggests that

$$\psi_1^\star = -\frac{9}{8}AY_\star^2 \log Y_\star + \frac{1}{2}C_1 Y_\star^2 + A_\star(X_\star)Y_\star + \cdots , \quad \text{as} \quad Y_\star \to \infty, \tag{3.69}$$

The function $A_\star(X_\star)$ is called the displacement function, and it should satisfy the condition

$$A_\star(X_\star) \to C_2(-X_\star)^{1/3} + \cdots \quad \text{as} \quad X_\star \to -\infty. \tag{3.70}$$

The formulation of the problem in the viscous sublayer thus consists of the linearised boundary-layer equation (3.66), together with the no-slip condition (3.67) and the asymptotic behaviour of the flow specified for $X_\star \to -\infty$ (3.67) and $Y_\star \to \infty$ (3.69). The displacement function $A_\star(X_\star)$ should be found as part of the interaction solution.

3.4.2 Region 4: the buffer layer

We now turn our attention to the middle deck, where

$$x = \sigma X_\star, \quad Y_\star = \sigma^{-1/3}|\log\sigma|^{1/4}Y. \tag{3.71}$$

At the edge of region 5, the asymptotic expansion for the stream function takes the form

$$\begin{aligned}\psi = &\frac{1}{2}|\log\sigma|^{1/4}\sigma^{2/3}AY_\star^2 + \\ &+|\log\sigma|^{-3/4}\sigma^{2/3}\left(-\frac{9}{8}AY_\star^2\log Y_\star + \frac{1}{2}C_1Y^2 + A_\star(X_\star)Y_\star\right) + \cdots .\end{aligned} \tag{3.72}$$

This can be deduced from the asymptotic expansion for ψ in region 5, given by (3.62), and the asymptotic expansion of $\psi_1^\star$ given by (3.69). According to Kaplun's extension theorem,

this asymptotic expansion is also valid at the bottom of region 4. We now rewrite this in terms of the variables of region 4 by substituting (3.71) into equation (3.72), which leads to

$$\psi = \frac{7A}{8}|\log\sigma|^{3/4}Y^2 + |\log\sigma|^{-1/4}\left(\frac{1}{2}C_1Y^2 - \frac{9A}{8}Y^2\log Y\right) - \frac{9A}{8}\frac{\log|\log\sigma|^{1/4}}{|\log\sigma|^{1/4}}Y^2 + |\log\sigma|^{-1/2}\sigma^{1/3}A_\star(X_\star)Y + \cdots . \tag{3.73}$$

This suggests that we look for a solution in region 4 in the asymptotic form

$$\left.\begin{aligned}\psi &= |\log\sigma|^{3/4}\psi_{40}(Y) + \cdots + |\log\sigma|^{-1/2}\sigma^{1/3}\psi_{41}(X_\star, Y) + \cdots .\\ P &= \sigma^{2/3}P_4(X_\star) + \cdots .\end{aligned}\right\} \tag{3.74}$$

The matching conditions with region 5 are then given by

$$\left.\begin{aligned}\psi_{40} &= \frac{7A}{8}Y^2 + \cdots\\ \psi_{41} &= A_\star(X_\star)Y + \cdots\end{aligned}\right\} \quad \text{as} \quad Y \to 0. \tag{3.75}$$

Substituting (3.71) and (3.74) into the Navier-Stokes equations leads to

$$\frac{\mathrm{d}\psi_{40}}{\mathrm{d}Y}\frac{\partial^2\psi_{41}}{\partial X_\star \partial Y} - \frac{\partial\psi_{41}}{\partial X_\star}\frac{\mathrm{d}^2\psi_{40}}{\mathrm{d}Y^2} = 0. \tag{3.76}$$

This further reduces to

$$\frac{\partial}{\partial Y}\left(\frac{\partial\psi_{41}/\partial X_\star}{\mathrm{d}\psi_{40}/\mathrm{d}Y}\right) = 0, \tag{3.77}$$

indicating that to leading order, the streamline slope remains the same as we go through region 4. The solution to (3.76) subject to boundary conditions (3.75) is given by

$$\frac{\partial\psi_{41}}{\partial X_\star} = C(X_\star)\frac{\mathrm{d}\psi_{40}}{\mathrm{d}Y}. \tag{3.78}$$

with $C(X_\star) = \dfrac{\mathrm{d}A_\star}{\mathrm{d}X_\star}$ in order to satisfy matching conditions (3.75). In particular, note that the streamline slope in this region is given by

$$\theta = -\,\mathrm{Re}^{-1/2}\,\frac{v}{u} = -|\log\sigma|^{-5/4}\sigma^{-2/3}\,\mathrm{Re}^{-1/2}\,\frac{\mathrm{d}A^\star}{\mathrm{d}X_\star} + \cdots \tag{3.79}$$

which is in accordance with the scalings. The role of region 4 is then to simply transmit the streamline slope at the edge of the viscous sublayer to the upper inviscid deck, which gives it the name of 'buffer region'.

3.4.3 Region 3: the upper inviscid layer

Finally, we consider the upper region of the triple deck. This region is the extension of the triple deck into the inviscid flow. The flow is assumed to be subsonic, so we introduce the coordinate scalings

$$x = \sigma x_\star, \quad y = \sigma y_\star, \tag{3.80}$$

and the fluid dynamics functions are scaled as

$$\left.\begin{aligned} u &= 1 + \tau u_1(x_\star, y_\star) + \cdots, \\ v &= \tau v_1(x_\star, y_\star) + \cdots, \\ p &= \tau p^\star(x_\star, y_\star) + \cdots. \end{aligned}\right\} \tag{3.81}$$

The small parameter τ is given by the equation

$$\tau = |\log\sigma|^{-5/4}\sigma^{-2/3}\,\mathrm{Re}^{-1/2}\,. \tag{3.82}$$

We substitute this into the Navier-Stokes equations (3.6), which reduce to the linearised Euler equations

$$\frac{\partial u_1}{\partial x_\star} = -\frac{\partial p^\star}{\partial x_\star}, \quad \frac{\partial v_1}{\partial x_\star} = -\frac{\partial p^\star}{\partial y_\star}, \tag{3.83}$$

$$\frac{\partial u_1}{\partial x_\star} + \frac{\partial v_1}{\partial y_\star} = 0. \tag{3.84}$$

The streamline slope at the bottom of region 3 has to match with the slope at the edge of region 4, the latter being given by equation (3.79). It follows from (3.81) that in region 3, the streamline slope takes the form

$$\theta_w = \lim_{y_\star \to 0} \frac{v}{u} = |\log \sigma|^{-5/4} \sigma^{-2/3} \operatorname{Re}^{-1/2} v_1(x_\star, 0). \tag{3.85}$$

This leads to the conclusion that

$$v_1(x_\star, 0) = -\frac{\mathrm{d}A_\star}{\mathrm{d}x_\star}. \tag{3.86}$$

The condition

$$u_1 - i v_1 = C z_\star^{2/3} + \cdots \quad \text{as} \quad x_\star + i y_\star \to \infty \tag{3.87}$$

should be added in order to match with the inviscid flow upstream, with constant C given by

$$C = -\kappa \left(\frac{1}{\sqrt{3}} + i \right).$$

3.5 Analytical solution of the interaction problem for subsonic flow

The formulation of the interaction problem for subsonic flow consists of linear equation in both the upper and lower deck, which allows us to derive an analytical solution for the pressure distribution.

3.5.1 Inviscid region

We start with the inviscid region. Equations (3.83) and (3.84) show that $p^\star$ satisfies the Laplace equation

$$\frac{\partial^2 p^\star}{\partial x_\star^2} + \frac{\partial^2 p^\star}{\partial y_\star^2} = 0. \tag{3.88}$$

It has to be solved with the boundary conditions

$$\left. \frac{\partial p^\star}{\partial y_\star} \right|_{y_\star = 0} = \frac{\mathrm{d}^2 A_\star}{\mathrm{d}x_\star^2}, \qquad p^\star \to 0 \quad \text{as} \quad x_\star^2 + y_\star^2 \to \infty. \tag{3.89}$$

Let us introduce the streamwise Fourier transform of a function $f(x, y)$ as

$$\tilde{f}(k; y) = \int_{-\infty}^{+\infty} f(x, y) e^{-ikx} \mathrm{d}x. \tag{3.90}$$

Applying this transform to equation (3.88) leads to the equation

$$\frac{\mathrm{d}^2 \tilde{p}^\star}{\mathrm{d}y_\star^2} - k^2 \tilde{p}^\star = 0. \tag{3.91}$$

Turning to the boundary condition (3.89), we find that

$$\tilde{p}^\star \to 0 \quad \text{as} \quad y_\star \to \infty, \qquad \left.\frac{\mathrm{d}\tilde{p}^\star}{\mathrm{d}y_\star}\right|_{y_\star=0} = -k^2 \tilde{A}_\star(k), \tag{3.92}$$

where $\tilde{A}_\star$ denotes the Fourier transform of the displacement function $A_\star(x_\star)$. The solution to (3.91)-(3.92) is given by

$$\tilde{p}^\star = |k| \tilde{A}_\star(k) e^{-|k|y}. \tag{3.93}$$

3.5.2 Viscous region

Our task is now to solve the linearised boundary-layer equation (3.66), with the pressure $P^\star$ given in terms of (3.93) as

$$P^\star = \frac{1}{2\pi} \int_{-\infty}^{+\infty} \tilde{p}^\star(k, Y_\star) e^{ikX_\star} \mathrm{d}k. \tag{3.94}$$

The first step is to take the Fourier transform on both sides of (3.66), leading to the equation

$$ikAY_\star \frac{\mathrm{d}\tilde{\psi}^\star}{\mathrm{d}Y_\star} - ikA\tilde{\psi}^\star = -ik\tilde{p}^\star(k) + \frac{\mathrm{d}^3\tilde{\psi}^\star}{\mathrm{d}Y_\star^3}. \tag{3.95}$$

We then differentiate (3.95) with respect to $Y_\star$ to eliminate the pressure $\tilde{p}^\star$, which leads to

$$\frac{\mathrm{d}^4\tilde{\psi}^\star}{\mathrm{d}Y_\star^4} - ikAY_\star \frac{\mathrm{d}^2\tilde{\psi}^\star}{\mathrm{d}Y_\star^2} = 0. \tag{3.96}$$

This is a fourth order ordinary differential equation, and thus needs four boundary conditions. The first two are found by applying the Fourier Transform to the set of boundary conditions (3.67) which turn into

$$\tilde{\psi}^\star(k;0) = 0, \quad \left.\frac{\mathrm{d}\tilde{\psi}^\star}{\mathrm{d}Y_\star}\right|_{Y_\star=0} = -A\tilde{f}(k), \tag{3.97}$$

where $\tilde{f}(k)$ is the Fourier Transform of the wall shape, given explicitly by

$$\tilde{f}(k) = \kappa\,\Gamma(8/3)(ik)^{-8/3}. \tag{3.98}$$

We also remind that A (not to be confused with $A_\star$) is a given constant with value

$$A = \frac{2^{9/4}\chi^{3/4}}{3^{7/4}\Gamma(2/3)^{3/4}}.$$

In order to derive the remaining two boundary conditions, we turn to the expansion of $\psi^\star$ for $Y_\star \to \infty$, given by (3.69). Differentiating this with respect to $X_\star$ and $Y_\star$, and then applying the Fourier Transform leads to

$$\lim_{Y_\star\to\infty} \frac{\mathrm{d}\tilde{\psi}^\star}{\mathrm{d}Y_\star} = \tilde{A}_\star(k) + \cdots. \tag{3.99}$$

One more boundary condition is deduced by setting $Y_\star = 0$ in equation (3.95), and applying the Fourier transform

$$\left.\frac{\mathrm{d}^3\tilde{\psi}^\star}{\mathrm{d}Y_\star^3}\right|_{Y_\star=0} = ik\tilde{p}^\star(k), \tag{3.100}$$

with $\tilde{p}^\star(k) = |k|\tilde{A}_\star$.

Equation (3.96) can be reduced to the canonical form of the Airy equation by introducing a new independent variable s defined by $Y_\star = (ikA)^{-1/3}s$. As a result, equation (3.96) turns into

$$\frac{\mathrm{d}^4\tilde{\psi}^\star}{\mathrm{d}s^4} - s\frac{\mathrm{d}^2\tilde{\psi}^\star}{\mathrm{d}s^2} = 0. \tag{3.101}$$

In terms of variable s, the boundary conditions (3.97)-(3.100) are written as

$$\left.\begin{aligned} \tilde{\psi}^\star &= 0, \\ \tilde{\psi}^\star_s &= -(ik)^{-1/3}A^{2/3}\tilde{f}(k), \\ \tilde{\psi}^\star_{sss} &= A^{-1}\tilde{p}(k), \end{aligned}\right\} \qquad \text{at} \quad s = 0. \tag{3.102}$$

$$\tilde{\psi}^\star_s = (ikA)^{-1/3}\tilde{A}_\star(k) + \cdots, \qquad \text{as} \quad s \to \infty. \tag{3.103}$$

The general solution to equation (3.101) is

$$\tilde{\psi^\star}_{ss} = C_1\,\mathrm{Ai}(s) + C_2\,\mathrm{Bi}(s). \tag{3.104}$$

We cannot allow exponential growth in the solution for large $Y_\star$, or correspondingly to large s. We need to apply some restrictions on parameter k in order to use the asymptotic expansions for $\mathrm{Ai}(s)$ and $\mathrm{Bi}(s)$ at large value of the complex independent variable s. More specifically, we need

$$|\arg(s)| = |\arg\left((ik)^{1/3}Y_\star\right)| < \frac{\pi}{3} \quad \text{as} \quad Y_\star \to \infty.$$

We will thus allow k to be complex, and write $k = |k|e^{i\phi}$, with $\phi = \arg k$. The inequality above can then be solved to yield

$$-\frac{3\pi}{2} < \phi < \frac{\pi}{2}.$$

We introduce a branch cut in the complex k plane along the positive imaginary axis. Using this restriction, we are able to use the asymptotic expansions for Ai and Bi in Abramowitch & Stegun (1972). The Bi function grows exponentially in this sector, and we thus set $C_2 = 0$, leading to

$$\tilde{\psi}^\star_{ss} = C_1\,\mathrm{Ai}(s). \tag{3.105}$$

This equation can be differentiated once, in order to apply the third boundary condition of

(3.102), giving the first relation between C_1 and $\tilde{A}_\star(k)$

$$C_1 \operatorname{Ai}'(0) = A^{-1}|k|\tilde{A}_\star(k). \tag{3.106}$$

Equation (3.105) is now integrated once, yielding

$$\tilde{\psi}_s^\star(s) = C_1 \int_0^s \operatorname{Ai}(\xi)\mathrm{d}\xi + \tilde{\psi}_s^\star(0), \tag{3.107}$$

where $\tilde{\psi}_s^\star(0)$ is zero according to (3.102). The second relation between C_1 and $\tilde{A}_\star(k)$ is found by investigating the limit of equation (3.107) for large values of s, and using the first of boundary condition (3.103)

$$(Aik)^{-1/3}\tilde{A}_\star(k) = C_1 \int_\gamma \operatorname{Ai}(\xi)\mathrm{d}\xi - (ik)^{-1/3}A^{2/3}\tilde{f}(k), \tag{3.108}$$

where γ is the line extending from the origin to infinity along a ray that makes an angle $\arg\left[(ik)^{1/3}\right]$ with the real axis. Combining (3.106) and (3.108) and solving for the displacement function $\tilde{A}_\star$ gives

$$\tilde{A}_\star = \frac{3A^{2/3}\operatorname{Ai}'(0)}{(ik)^{1/3}|k| - 3A^{2/3}\operatorname{Ai}'(0)}\tilde{f}, \quad C_1 = \frac{|k|\tilde{A}_\star}{A\operatorname{Ai}'(0)}. \tag{3.109}$$

In particular, the pressure on the wall in Fourier space is given by

$$\tilde{p}(0;k) = \tilde{A}_\star(k)|k|. \tag{3.110}$$

Returning back to physical space, we find that the pressure distribution across the interaction region is given by

$$P_\star(X_\star) = \frac{1}{2\pi}\int_{-\infty}^{+\infty} \mathrm{e}^{ikX_\star}\frac{3A^{2/3}\operatorname{Ai}'(0)|k|}{|k|(ik)^{1/3} - 3A^{2/3}\operatorname{Ai}'(0)}\tilde{f}(k)\mathrm{d}k. \tag{3.111}$$

The integral (3.111) is calculated numerically. The behaviour of the pressure gradient in the

boundary layer is plotted in Figure 3.4. This shows very good agreement with the upstream asymptotics. The perturbations to the wall skin friction are displayed on Figure 3.5.

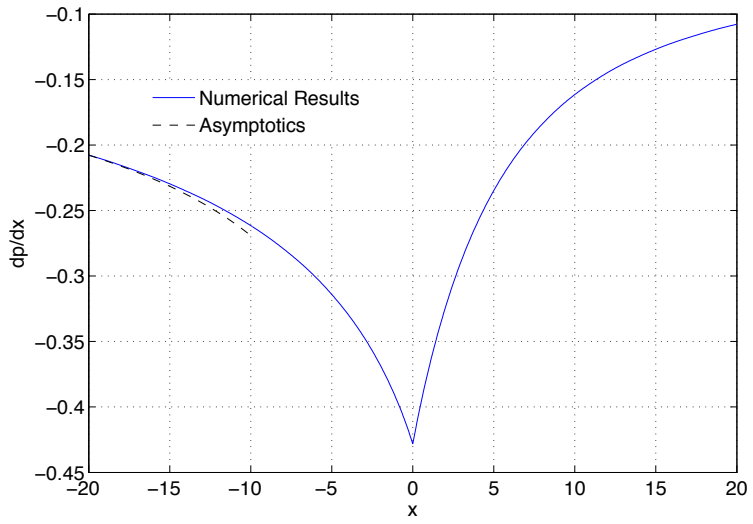

Figure 3.4: Pressure gradient and corresponding asymptotics across the interaction region.

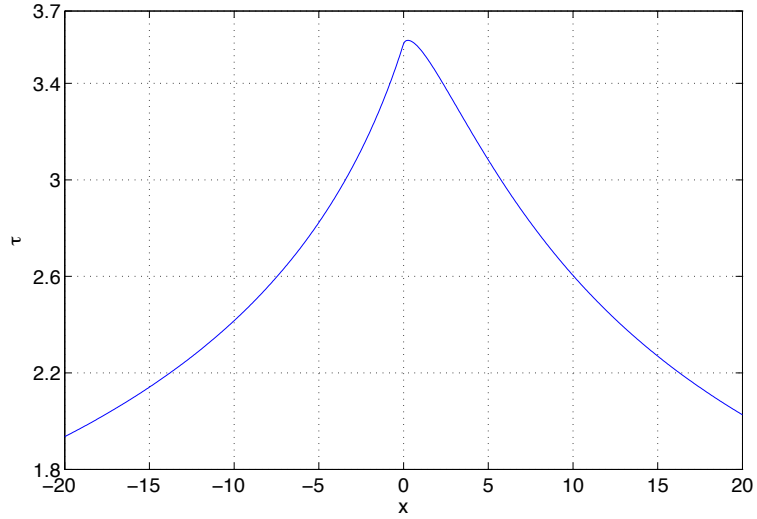

Figure 3.5: Skin friction perturbation across the interaction region.

We have obtained the required effect: the curvature discontinuity has the effect of accelerating the flow near the body surface. The pressure singularity that resulted is smoothed out by the interaction process between the accelerating potential flow and the linear boundary layer, which in turn leads to an increase in the skin friction, shown on Figure 3.5. We also present a graph of the pressure distribution across the interaction region for various values of the curvature κ on Figure 3.6. We will compare this with the distribution obtained in the transonic flow case.

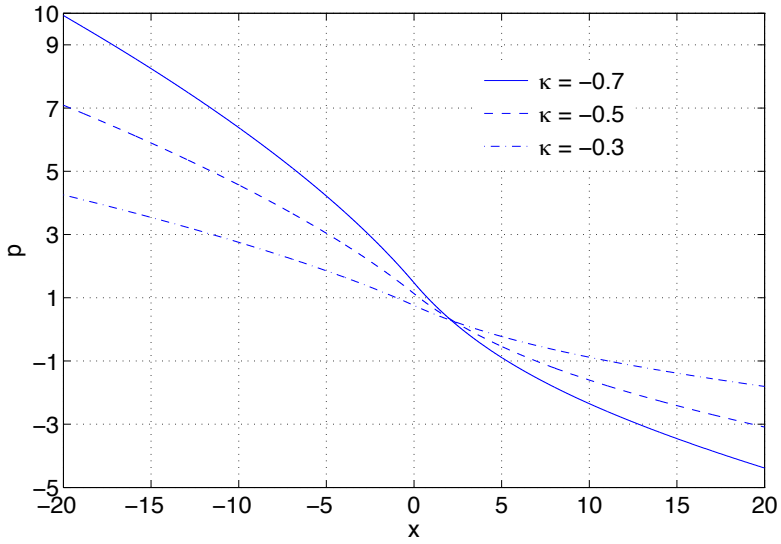

Figure 3.6: Pressure distribution across the interaction region.

We now check that the solution (3.111) matches with the upstream condition (3.64). In order to do this, we will evaluate the inverse Fourier transform of the pressure gradient at large negative values of $X_\star$ and prove that it matches with the condition

$$\frac{\mathrm{d}P_\star}{\mathrm{d}X_\star} = -\frac{2}{3}\chi(-X_\star)^{-1/3} \quad \text{as} \quad X_\star \to -\infty,$$

given in the previous section. According to (3.110), the pressure gradient in Fourier space is given by

$$\mathcal{F}\left(\frac{\mathrm{d}P_\star}{\mathrm{d}X_\star}\right) = ik|k|\tilde{A}_\star. \tag{3.112}$$

The Fourier inversion theorem then states that

$$\frac{\mathrm{d}P_\star}{\mathrm{d}X_\star} = \frac{1}{2\pi}\int_{-\infty}^{+\infty} \mathrm{e}^{ikX_\star}\,\frac{3A^{2/3}\,\mathrm{Ai}'(0)\,|k|ik}{|k|(ik)^{1/3} - 3A^{2/3}\,\mathrm{Ai}'(0)}\,\tilde{f}(k)\mathrm{d}k. \tag{3.113}$$

Recall that

$$\tilde{f} = \kappa\,\Gamma\left(\frac{8}{3}\right)(ik)^{-8/3}, \tag{3.114}$$

so introducing the constants $B_1 = 3A^{2/3}\,\mathrm{Ai}'(0)\Gamma(8/3)\,\kappa$ and $B_2 = 3A^{2/3}\,\mathrm{Ai}'(0)$, the integral (3.113) reduces to

$$I(x) = \frac{1}{2\pi}\int_{-\infty}^{+\infty} \frac{B_1|k|\,\mathrm{e}^{ikX_\star}}{(ik)^{5/3}\big[|k|(ik)^{1/3} - B_2\big]}\,\mathrm{d}k. \tag{3.115}$$

We split this into two integrals, one for negative k and one for positive k

$$I(x) = -\frac{1}{2\pi}\int_{-\infty}^{0} \frac{B_1 k\,\mathrm{e}^{ikX_\star}}{(ik)^{5/3}\big[-k(ik)^{1/3} - B_2\big]}\,\mathrm{d}k + \frac{1}{2\pi}\int_{0}^{+\infty} \frac{B_1 k\,\mathrm{e}^{ikX_\star}}{(ik)^{5/3}\big[k(ik)^{1/3} - B_2\big]}\,\mathrm{d}k. \tag{3.116}$$

We first consider the second integral. We extend k to the complex plane and remember that we introduced a branch cut on the positive imaginary axis. Due to the presence of the modulus of k, we need to introduce a second branch cut along the negative imaginary axis.

We consider the contour Γ, sketched on Figure 3.7, which consists of

1. γ_1, the line segment from ϵ to R,
2. γ_2, the arc of circle of radius R, with $\theta \in [0, -\pi/2]$,
3. γ_3, the line segment from $-iR$ to $-i\epsilon$ on the right hand side of the branch cut,
4. γ_4, the arc of circle of radius ϵ, with $\theta \in [-\pi/2, 0]$.

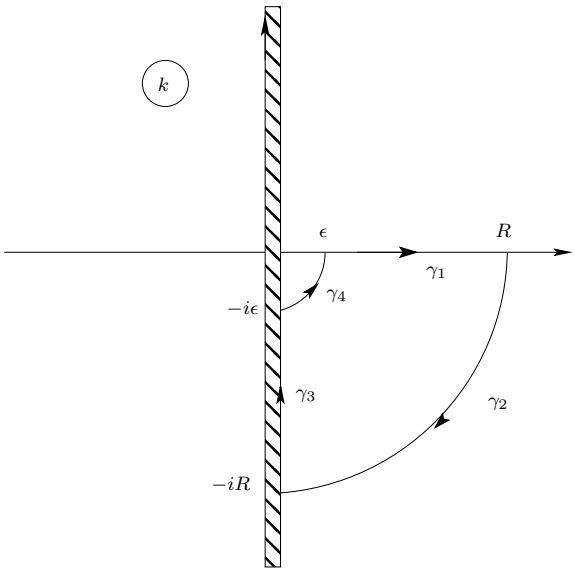

Figure 3.7: Contour of integration for (3.116).

We then write

$$\int_\Gamma \Lambda(k)\,\mathrm{e}^{ikX_\star}\,\mathrm{d}k = \left(\int_{\gamma_1} + \int_{\gamma_2} + \int_{\gamma_3} + \int_{\gamma_4}\right) \Lambda(k)\,\mathrm{e}^{ikX_\star}\,\mathrm{d}k,$$

where

$$\Lambda(k) = \frac{B_1 k}{(ik)^{5/3}\left[k(ik)^{1/3} - B_2\right]},$$

and consider each of the integrals in turn.

Notice first of all that $\int\limits_{\gamma_1} \Lambda(k)\,\mathrm{e}^{ikX_\star}\,\mathrm{d}k$ recovers the original integral as $\epsilon \to 0, R \to \infty$. On γ_2, we let $k = R\,\mathrm{e}^{i\theta}$, and we estimate

$$\left|\Lambda\left(R\,\mathrm{e}^{i\theta}\right)\right| \sim \frac{1}{R^2} \quad \text{as} \quad R \to \infty.$$

The function $\Lambda(k)$, the contour γ_2 and parameter x all satisfy the conditions necessary to apply Jordan's Lemma. Accordingly, we can then assert that

$$\left|\int_{\gamma_2} \Lambda(k)\,\mathrm{e}^{ikX_\star}\,\mathrm{d}k\right| \to 0 \quad \text{as} \quad R \to \infty.$$

On γ_4, we write $k = \epsilon\,\mathrm{e}^{i\theta}$, where it is assumed that $\epsilon \ll 1$, and we can estimate

$$\left|\Lambda\left(\epsilon\,\mathrm{e}^{i\theta}\right)\mathrm{e}^{ikX_\star}\right| \sim \epsilon^{-2/3}, \quad \text{as} \quad \epsilon \to 0.$$

Thus, we have the following bound

$$\left|\int_{\gamma_4}\Lambda(k)\,\mathrm{e}^{ikX_\star}\,\mathrm{d}k\right| \leq |\gamma_4|\left|\Lambda\left(\epsilon\,\mathrm{e}^{i\theta}\right)\mathrm{e}^{ikX_\star}\right| \sim \frac{\epsilon\pi}{2}\epsilon^{-2/3} \sim \epsilon^{1/3} \quad \text{as} \quad \epsilon \to 0.$$

The contribution from the integral along γ_4 is then negligible. Finally, on γ_3, we write $k = iy$, leading to

$$\mathcal{I} = \int_{-\epsilon}^{-R} \frac{B_1 y\,\mathrm{e}^{-yX_\star}}{(-y)^{5/3}\left[iy(-y)^{1/3} - B_2\right]}\mathrm{d}y. \tag{3.117}$$

We make the change of variable $u = -y$, which leads to

$$\mathcal{I} = \int_{\epsilon}^{R} \frac{B_1 u\,\mathrm{e}^{uX_\star}}{u^{5/3}\left[-iu^{4/3} - B_2\right]}\mathrm{d}u. \tag{3.118}$$

Recall that we are interested in the behaviour of this integral at large negative values of $X_\star$. Thus, $\mathcal{I}$ is of Laplace type. The main contribution comes from a vicinity of $u = \epsilon$, where to leading order

$$\frac{B_1 u}{u^{5/3}\left[-iu^{4/3} - B_2\right]} \sim -\frac{B_1}{B_2}u^{-2/3}.$$

We can then extend the range of the integral to infinity, and write

$$\mathcal{I} \sim \frac{B_1}{B_2}\int_{\epsilon}^{\infty} u^{-2/3}\,\mathrm{e}^{uX_\star}\,\mathrm{d}u. \tag{3.119}$$

Using the substitution $uX_\star = -t$, this is converted into

$$\mathcal{I} \sim \frac{B_1}{B_2}(-X_\star)^{-1/3}\int_{-X_\star\epsilon}^{-X_\star\infty} t^{-2/3}\,\mathrm{e}^{-t}\,\mathrm{d}t. \tag{3.120}$$

For any negative fixed $X_\star$ no matter how large, the integral on the right hand side of (3.120)

tends to $\Gamma(1/3)$ when $\epsilon \to 0$. Finally, we can use the Residue Theorem to write

$$\int_\Gamma \Lambda(k)\, \mathrm{e}^{ikX_\star}\, \mathrm{d}k = 2\pi i \sum_{a\in\Gamma} \text{Res}\, \left(\Lambda(k)\, \mathrm{e}^{ikX_\star}, a\right). \tag{3.121}$$

However, the contour Γ doesn't contain any poles so the right hand side of (3.121) is zero. Taking the limits $\epsilon \to 0, R \to \infty$, we then get

$$\frac{1}{2\pi} \int_0^{+\infty} \frac{B_1 k\, \mathrm{e}^{ikX_\star}}{(ik)^{5/3}\,(k(ik)^{1/3} - B_2)}\, \mathrm{d}k = \frac{1}{2\pi}\frac{B_1}{B_2}\Gamma(1/3)(-X_\star)^{-1/3} + \cdots, \quad \text{as} \quad X_\star \to -\infty. \tag{3.122}$$

The other integral in (3.116) is performed in a similar way and leads to the same answer. Using the definition of B_1, B_2 and relations[2]

$$\Gamma(8/3)\Gamma(1/3) = \frac{20\sqrt{3}}{27}\pi, \quad \kappa = -\frac{9}{10\sqrt{3}}\,\chi,$$

we conclude that

$$\frac{\mathrm{d}P}{\mathrm{d}X_\star} = -\frac{2}{3}\chi(-X_\star)^{-1/3} + \cdots, \quad X_\star \to -\infty. \tag{3.123}$$

This is exactly the matching condition from the upstream viscous sublayer.

[2]The second equality simply comes from the definition of χ.

Chapter 4

Accelerating Transonic Flow past a Discontinuity of Wall Curvature

The previous study focused on the case where the external flow was subsonic. Our interest was to present the behaviour of the boundary layer subjected to the pressure gradient

$$\frac{\mathrm{d}p_e}{\mathrm{d}x} \sim (-x)^{-1/3}, \tag{4.1}$$

in a simplified context, in particular with regards to the formulation and solution of the interaction problem. To that aim we introduced a body shape satisfying a specific power law, namely

$$y_w = \begin{cases} 0 & : x < 0, \\ \kappa x^{5/3} & : x > 0. \end{cases}$$

This enabled us to generate the required pressure gradient. The solution in both the upper deck and lower deck of the interaction region were found in closed-form.

We now show how this theory can be extended to the transonic regime. It turns out that pressure gradient (4.1) is naturally generated in the vicinity of curvature discontinuities. The analysis of the external inviscid flow needs now to account for compressibility and transonic effects. We will show that when studying the viscous sublayer, we may still use the incompressible boundary-layer equations derived in Section 3.3. The scalings for the interaction region will however have to be amended. Additionally, the inviscid upper deck

will be governed by the Kármán-Guderley equations, which are nonlinear, and the problem will thus have to be solved numerically.

4.1 Inviscid transonic flow

Let us consider the flow of an inviscid compressible fluid over a curved surface, where a discontinuity in the curvature is present at a point x_s. We denote the curvature upstream of point x_s by κ^-, and downstream by κ^+. We introduce a set of coordinate axes $(\hat{x}, \hat{y})$ such that the origin coincides with point x_s and the x-axis is tangent to the body surface at point x_s, as shown on Figure 4.1.

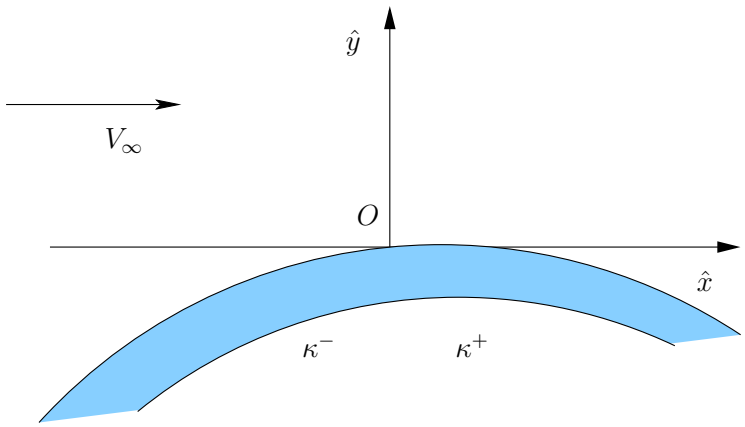

Figure 4.1: Body surface discontinuity in curvature.

The velocity components in these coordinates are denoted by $\hat{u}$ and $\hat{v}$, and the speed of sound is denoted by $\hat{a}$. It is known that any two-dimensional steady inviscid flow of a perfect gas is governed by the equation

$$\left(\hat{a}^2 - \hat{u}^2\right) \frac{\partial \hat{u}}{\partial \hat{x}} + \left(\hat{a}^2 - \hat{v}^2\right) \frac{\partial \hat{v}}{\partial \hat{y}} = \hat{u}\hat{v} \left(\frac{\partial \hat{u}}{\partial \hat{y}} + \frac{\partial \hat{v}}{\partial \hat{x}} \right). \tag{4.2}$$

The speed of sound $\hat{a}$ is related to the velocity components $\hat{u}$ and $\hat{v}$ via the Bernoulli

equation

$$\frac{\hat{a}^2}{\gamma-1}+\frac{\hat{u}^2+\hat{v}^2}{2}=\frac{\hat{a}_\infty^2}{\gamma-1}+\frac{\hat{V}_\infty^2}{2}, \tag{4.3}$$

where γ is the ratio of specific heats and $\hat{V}_\infty$ and $\hat{a}_\infty$ represent the gas velocity and the speed of sound in the unperturbed flow upstream. Provided that the flow upstream is uniform and free of shock waves, or the shock waves are weak, which is true for all transonic flows, the inviscid flow remains irrotational

$$\frac{\partial\hat{u}}{\partial\hat{y}}-\frac{\partial\hat{v}}{\partial\hat{x}}=0. \tag{4.4}$$

This allows us to introduce the potential function $\hat{\Phi}(\hat{x},\hat{y})$ defined by

$$\hat{u}=\frac{\partial\hat{\Phi}}{\partial\hat{x}},\quad \hat{v}=\frac{\partial\hat{\Phi}}{\partial\hat{y}}.$$

The pressure $\hat{p}$ and density $\hat{\rho}$ are related to the speed of sound through the well known formula

$$\hat{a}^2=\gamma\frac{\hat{p}}{\hat{\rho}}. \tag{4.5}$$

Substituting this into the Bernoulli equation (4.3) yields

$$\frac{\gamma}{\gamma-1}\frac{\hat{p}}{\hat{\rho}}+\frac{\hat{u}^2+\hat{v}^2}{2}=\frac{\gamma}{\gamma-1}\frac{\hat{p}_\infty}{\hat{\rho}_\infty}+\frac{\hat{V}_\infty^2}{2}, \tag{4.6}$$

which enables us to find $\hat{p}$ and $\hat{\rho}$ once $\hat{u}$ and $\hat{v}$ are known. Finally, the entropy conservation law takes the form

$$\frac{\hat{p}}{\hat{\rho}^\gamma}=\frac{\hat{p}_\infty}{\hat{\rho}_\infty^\gamma}. \tag{4.7}$$

Let us assume that the velocity at the origin coincides with the speed of sound; this is to ensure that the flow treated is of transonic nature. In order to study the flow, we introduce the non-dimensional variables

$$\begin{cases} \hat{x}=Lx,\quad \hat{y}=Ly,\quad \hat{\Phi}=a_*L\Phi,\\ \hat{u}=a_*u,\quad \hat{v}=a_*v,\quad \hat{a}=a_*a,\\ \hat{p}=p_*+\rho_*a_*^2p,\quad \hat{\rho}=\rho_*\rho. \end{cases} \tag{4.8}$$

Here, L represents the characteristic dimension of the body, a_* is the speed of sound at the origin, and p_* and ρ_* are the values of pressure and density at the origin. Under this transformation, equations (4.2)-(4.7) become

$$\left(a^2-u^2\right)\frac{\partial u}{\partial x}+\left(a^2-v^2\right)\frac{\partial v}{\partial y}=uv\left(\frac{\partial u}{\partial y}+\frac{\partial v}{\partial x}\right), \tag{4.9}$$

$$a^2=\frac{\gamma+1}{2}-\frac{\gamma-1}{2}\left(u^2+v^2\right), \tag{4.10}$$

$$\frac{1}{\rho}\left(1+\gamma p\right)+\frac{\gamma-1}{2}\left(u^2+v^2\right)=\frac{\gamma+1}{2}, \tag{4.11}$$

$$1+\gamma p=\rho^{\gamma}. \tag{4.12}$$

We are interested in the asymptotic solution of (4.9)-(4.12) as we approach the singularity. In the vicinity of point O, we do not expect the values of u and v to differ much from their value at the point i.e. $u\sim 1+\delta u, v\sim \delta v$. Balancing terms in equation (4.4), we find $\delta u/y\sim \delta v/x$. Equation (4.10) gives $a\sim 1+\delta u$. Substituting this in equation (4.9) and balancing the first two terms on the left hand side gives $\delta u^2/x\sim \delta v/y$. Solving these estimates for u and v yields

$$u-1\sim\left(\frac{x}{y}\right)^2,\quad v\sim\left(\frac{x}{y}\right)^3.$$

The potential function Φ can then be estimated as

$$\Phi\sim x+x\left(\frac{x}{y}\right)^2. \tag{4.13}$$

Let us assume that as $x\to 0$, coordinate $y\to 0$ according to $y^k\sim x$, i.e. the quantity $\xi=\dfrac{x}{y^k}$ remains order-one as x and y simultaneously tend to zero. This suggests that we look for a solution of (4.9)-(4.12) in the self-similar form

$$\Phi=x+y^{3k-2}\phi(\xi)+\cdots,\quad y\to 0. \tag{4.14}$$

4.1.1 Self-similar solution

We now proceed to derive an equation for ϕ. We start by computing the velocity components u and v, which take the following form

$$u = \frac{\partial \Phi}{\partial x} = 1 + y^{2k-2}\phi'(\xi) + \cdots, \tag{4.15}$$

$$v = \frac{\partial \Phi}{\partial y} = y^{3k-3}\left[(3k-2)\phi(\xi) - k\xi\phi'(\xi)\right] + \cdots. \tag{4.16}$$

The speed of sound a is given by the Bernoulli equation (4.10)

$$a = 1 - \frac{\gamma - 1}{2} y^{2k-2}\phi'(\xi) + \cdots. \tag{4.17}$$

An estimation for the pressure and density can then be found by solving equations (4.12) and (4.11) for p and ρ. We have

$$p = -y^{2k-2}\phi'(\xi) + \cdots, \tag{4.18}$$

$$\rho = 1 - y^{2k-2}\phi'(\xi) + \cdots. \tag{4.19}$$

Substituting (4.15)-(4.17) into (4.9) leads to the following ordinary differential equation

$$\left[k^2\xi^2 - (\gamma+1)\phi'\right]\phi'' - 5k(k-1)\xi\phi' + 3(k-1)(3k-2)\phi = 0. \tag{4.20}$$

This equation was first derived by Frankl (1947) and Guderley (1957) in the study of the far field behaviour of transonic flow past an aerofoil. It can be seen from (4.15) and (4.16) that we should then chose $k < 1$ so that the perturbations decay at infinity. On the contrary, we are interested in the case where $y \to 0$ in our study, and we should thus chose $k > 1$.

To formulate the boundary conditions for our problem, we first introduce function y_w describing the shape of the surface. In the vicinity of the origin, we can Taylor expand the wall shape and write

$$y_w = \begin{cases} -\frac{1}{2}\kappa^- x^2 + \cdots & : x < 0, \\ -\frac{1}{2}\kappa^+ x^2 + \cdots & : x > 0. \end{cases} \tag{4.21}$$

The impermeability condition on the body surface requires that

$$v(x, y_w) = u(x, y_w)\frac{\mathrm{d}y_w}{\mathrm{d}x}. \tag{4.22}$$

Since we are looking at a vicinity of the sonic point, we can assume $|\kappa^{\pm}x| \ll 1$ so that the boundary condition may be transferred from $y = y_w$ to $y = 0$. As $y \to 0$, the similarity variable ξ tends to $\pm\infty$ depending on the sign of x. The impermeability condition then takes the form

$$\begin{cases} \lim\limits_{\xi\to-\infty} \left[(3k-2)\phi(\xi) - k\xi\phi'(\xi)\right] y^{3k-3} = -\kappa^{-}x, \\ \lim\limits_{\xi\to+\infty} \left[(3k-2)\phi(\xi) - k\xi\phi'(\xi)\right] y^{3k-3} = -\kappa^{+}x. \end{cases} \tag{4.23}$$

The boundary conditions (4.23) suggest that we should investigate the asymptotic behaviour of function ϕ at large values of ξ. We look for an asymptotic solution of equation (4.20) at large negative values of ξ in the form

$$\phi(\xi) = d(-\xi)^{\lambda} + \cdots \quad \text{as} \quad \xi \to -\infty. \tag{4.24}$$

Substituting this into equation (4.20) and assuming, subject to subsequent confirmation, that $\lambda < 3$ leads to the algebraic equation

$$k^2\lambda^2 - \left[k^2 + 5k(k-1)\right]\lambda + 3(k-1)(3k-2) = 0,$$

with solutions

$$\lambda = 3 - 3/k \quad \text{or} \quad \lambda = 3 - 2/k.$$

Since $k > 0$, these solutions both satisfy $\lambda < 3$. Hence, the asymptotic expansion of ϕ at large negative values of ξ takes the form

$$\phi(\xi) = d_0(-\xi)^{3-2/k} + d_1(-\xi)^{3-3/k} + \cdots, \quad \xi \to -\infty. \tag{4.25}$$

In order to compute the similarity parameter k and the unknown coefficients d_0 and d_1, we

turn to the boundary conditions (4.23). Substituting (4.25) into (4.23) leads to

$$d_1(-x)^{3-3/k} + \cdots = \kappa^-(-x). \tag{4.26}$$

This can only be satisfied if $d_1 = \kappa^-$ and $3 - 3/k = 1$. The similarity parameter k is thus uniquely defined as

$$k = \frac{3}{2}.$$

A similar analysis shows that the asymptotic behaviour of ϕ at large positive values of ξ takes the form

$$\phi(\xi) = c_0\xi^{3-2/k} + c_1\xi^{3-3/k} + \cdots, \quad \xi \to \infty. \tag{4.27}$$

Substituting this into the impermeability condition (4.23) yields the relation

$$\kappa^+ = -c_1. \tag{4.28}$$

Coefficients d_0 and c_0 remain unknown at that point, and should be found by solving the problem numerically on the whole interval $\xi \in (-\infty, +\infty)$. The formulation of the problem in the inviscid part of the flow consists of the nonlinear ordinary differential equation (4.20), now written as

$$\left(\frac{9}{4}\xi^2 - (\gamma+1)\,\phi'\right)\phi'' - \frac{15}{4}\xi\phi' + \frac{15}{4}\phi = 0, \tag{4.29}$$

and the boundary conditions

$$\begin{cases} \lim\limits_{\xi\to-\infty}\left[\dfrac{5}{2}\phi(\xi) - \dfrac{3}{2}\xi\phi'(\xi)\right] = -\kappa^-\xi, \\ \lim\limits_{\xi\to+\infty}\left[\dfrac{5}{2}\phi(\xi) - \dfrac{3}{2}\xi\phi'(\xi)\right] = -\kappa^+\xi. \end{cases} \tag{4.30}$$

It should be noted that these boundary conditions are equivalent to specifying

$$d_1 = \kappa^-, \quad c_1 = -\kappa^+,$$

in asymptotic expansions (4.25) and (4.27). This problem is non-trivial and should be

solved numerically. Depending on the ratio of curvatures κ^+/κ^-, a wide variety of behaviours can be observed. In order to analyse and understand the numerical results, we need the insight of the phase plane analysis, which we proceed to describe.

4.1.2 Phase plane analysis

A good way to analyse nonlinear second order ordinary differential equations is to study their behaviour in the phase plane. Following the dimensional analysis of the previous section, let us introduce functions F and G defined by

$$\left.\begin{aligned} u &= 1 + \frac{1}{\gamma+1}\, y^{2k-2} F(\xi) + \cdots \\ v &= \frac{1}{\gamma+1}\, y^{3k-3} G(\xi) + \cdots \end{aligned}\right\} \quad \text{as} \quad y \to 0. \tag{4.31}$$

Substituting this into equation (4.9) and the irrotationality condition (4.4) enables us to reduce the problem to a system of two first order ODE

$$\left\{\begin{aligned} \frac{\mathrm{d}F}{\mathrm{d}\xi} &= (k-1)\frac{3G - 2k\xi F}{F - k^2\xi^2}, \\ \frac{\mathrm{d}G}{\mathrm{d}\xi} &= (k-1)\frac{2F^2 - 3k\xi G}{F - k^2\xi^2}. \end{aligned}\right. \tag{4.32}$$

The functions F and G are related to the potential function ϕ through the equations

$$F(\xi) = (\gamma+1)\phi'(\xi), \quad G(\xi) = (\gamma+1)\big[(3k-2)\phi(\xi) - k\xi\phi'(\xi)\big]. \tag{4.33}$$

Note that the system (4.32) admits the invariant transformation

$$\xi^\star = A\xi, \quad F^\star = A^2 F, \quad G^\star = A^3 G, \tag{4.34}$$

for any constant A. In order to make the solution independent on A, we normalise F and G through the transformation

$$F(\xi) = k^2\xi^2 f(\xi), \quad G(\xi) = k^3\xi^3 g(\xi). \tag{4.35}$$

This leads to the system

$$\begin{cases} \dfrac{\mathrm{d}f}{\mathrm{d}\xi} = \dfrac{3(k-1)g + 2f - 2kf^2}{(f-1)k\xi}, \\ \dfrac{\mathrm{d}g}{\mathrm{d}\xi} = \dfrac{2(k-1)f^2 - 3kfg + 3g}{(f-1)k\xi}. \end{cases} \tag{4.36}$$

Finally, in order to make the system autonomous, we introduce a new independent variable χ such that

$$\mathrm{d}\chi = \frac{\mathrm{d}\xi}{(f-1)k\xi}. \tag{4.37}$$

Thus, an equivalent formulation of ODE (4.29) is the following non-singular autonomous system

$$\begin{cases} \dfrac{\mathrm{d}f}{\mathrm{d}\chi} = 3(k-1)g + 2f - 2kf^2, \\ \dfrac{\mathrm{d}g}{\mathrm{d}\chi} = 2(k-1)f^2 - 3kfg + 3g. \end{cases} \tag{4.38}$$

Each solution of (4.29) can be treated as a trajectory in the phase plane, and represents a family of solutions for all possible values of A (as defined in (4.34)). An example of such a trajectory is depicted on Figure 4.2, along with the stationary points of (4.38), discussed a bit further.

It can be seen from (4.37) that the transformation of the independent variable is singular at

$$\xi = 0, \quad f = 1.$$

As the old variable ξ passes through 0 as it increases from $-\infty$ to $+\infty$, variable χ changes direction. The phase plane is thus divided into two sheets which meet at infinity, one for $\xi < 0$ and another for $\xi > 0$. A typical trajectory thus starts on one sheet, reflects back at infinity and comes back on the other sheet.

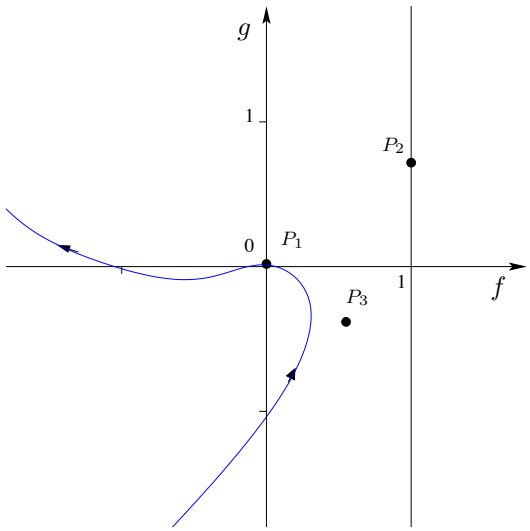

Figure 4.2: A trajectory and the stationary points of (4.38).

Furthermore, each sheet contains the singular line $f = 1$, which corresponds to the singular point

$$\phi' = \frac{k^2\xi^2}{(\gamma+1)}$$

of the ODE (4.20). When a trajectory hits this line in the phase plane, it corresponds to a turning point for the physical variable ξ, which has no physical meaning. The only exception is the point P_2 in the phase plane, where $f = 1$ and $g = 2/3$, which is one of the stationary points of system (4.38). Crossing at this point is allowed - it is related to the characteristics curves of the original equation (4.9) (Buldakov & Ruban 2002).

Of particular interest to us are the stationary points of (4.38). They are

$$P_1 = (0,0), \quad P_2 = \left(1, \frac{2}{3}\right), \quad P_3 = \left(\frac{1}{k^2}, -\frac{2}{3k^3}\right).$$

Identifying the type of each stationary point is important in order to understand the physical meaning of trajectories in their vicinity. Linearising around these three points show that for $k = 3/2$

1. P_1 is a node,

2. P_2 is a node,

3. P_3 is a saddle point.

According to definition (4.35), point P_1 is reached as $|\xi| \to \infty$, suggesting that it corresponds to the behaviour of the flow on the wall. Thus, trajectories in the phase plane must start and return back to the origin, as shown on Figure 4.2. The importance and meaning of the saddle point P_3 will be demonstrated in one of our examples. For an in-depth analysis of the physical meaning of P_2 and P_3, the reader can refer to Buldakov & Ruban (2010).

Armed with this knowledge, our aim is to construct a few solutions and interpret their meaning. The equations (4.38) are nonlinear and should be integrated numerically with suitable boundary conditions. An equivalent method that we use here is to solve directly equation (4.29) and then convert the solution ϕ into the phase-plane variables F and G using (4.33). The corresponding solution curves can then be subsequently plotted in a phase-plane portrait.

4.1.3 Numerical solution

We now describe the numerical solution to problem (4.29)-(4.30). Since the boundary conditions are specified at $\xi = -\infty$ and $\xi = +\infty$, it should be treated as a boundary-value problem. We can however turn it into an initial value problem, which is more convenient for the purpose of the analysis. For fixed $k = 3/2$, we start from the asymptotic expansion

$$\phi = d_0(-\xi)^{5/3} + d_1(-\xi) + \cdots, \quad \text{as} \quad \xi \to -\infty. \tag{4.39}$$

The second constant on the right hand side of (4.39) is fixed by the upstream boundary condition (4.26). The first constant is taken arbitrary in the first step of the calculation, which consists in integrating the problem numerically on the interval $\xi = [-\xi_\infty, \xi_\infty]$ using a simple predictor-corrector scheme. Once we have the data for large ξ_∞, we find constants c_0 and c_1 by solving the system of linear equations

$$\begin{cases} \phi(\xi_\infty) = c_0\xi_\infty^{5/3} + c_1\xi_\infty, \\ \phi'(\xi_\infty) = \left(3 - \dfrac{2}{k}\right) c_0\xi_\infty^{2/3} + \left(3 - \dfrac{3}{k}\right) c_1. \end{cases} \tag{4.40}$$

One can see that for each different starting value of d_0, a different set $\{c_0, c_1\}$, and thus a different value for κ^+ will be generated. Only one such value will satisfy the downstream boundary condition (4.28), and we need to iterate on d_0 until we find the correct one.

We can thus establish a one-to-one relation between coefficient d_0 and the downstream curvature κ_+. If κ_+ is specified at the onset, we should iterate on d_0 to satisfy the correct boundary condition. Alternatively, we can fix d_0 and find the 'allowed' downstream curvature κ_+ (by solving (4.40)) as part of the solution. The latter method has a big advantage, in that the problem is extremely sensitive to the ratio κ_-/κ_+. It is not guaranteed that the solution will converge or even exist for an arbitrary pair $\{\kappa_-, \kappa_+\}$. Specifying d_0 rather than κ_+ thus gives us more control on the stability of the calculations.

As a starting point for the numerical calculations, we observe that the ODE

$$\left(\frac{9}{4}\xi^2 - (\gamma+1)\,\phi'\right)\phi'' - \frac{15}{4}\xi\phi' + \frac{15}{4}\phi = 0 \tag{4.41}$$

admits the simple solution

$$\phi = C\xi.$$

The boundary conditions (4.30) are then satisfied provided that $\kappa_- = \kappa_+ = -C$. This solution thus corresponds to the situation when there is no discontinuity in the body curvature. The asymptotic expansion for large values of ξ then takes the trivial form

$$\begin{cases} \phi = C(-\xi), & \text{as} \quad \xi \to -\infty, \\ \phi = C\xi, & \text{as} \quad \xi \to +\infty, \end{cases} \tag{4.42}$$

indicating that the coefficients d_0 and c_0 of asymptotic expansion (4.25)-(4.27) are identically equal to 0.

In order to generate a first set of non-trivial solutions, we then perturb this 'basic' solution around d_0. The sign of d_0 has an important meaning. Let us recall that

$$u = 1 + y^{2k-2}\phi'(\xi) + \cdots .$$

Inserting above the asymptotic expansion (4.25), which is valid at large negative values of

ξ, and substituting $k = 3/2$, we find that

$$u = 1 - \frac{5}{3} d_0 (-\xi)^{2/3} + \cdots, \quad \text{as} \quad \xi \to -\infty, \tag{4.43}$$

suggesting that the flow upstream is subsonic provided $d_0 > 0$. Conversely, if we take $d_0 < 0$, the flow upstream will be supersonic. We will study the flow behaviour for both positive and negative values of d_0. We will interpret the physical meaning of the resulting phase plane curves and specify the important parameters.

1. The first set of solutions that we present is obtained when we set the upstream curvature $\kappa^- = 0.5$, and chose d_0 to range from 0 to 0.29. The corresponding solutions $\phi'(\xi)$, which represent the perturbations to the streamwise velocity, are depicted on the left of Figure 4.3. The blue line corresponds to $d_0 = 0$, which is equivalent to the case $\kappa^+ = \kappa^-$ described earlier. As expected for $d_0 > 0$, the flow is initially subsonic, which is characterised by $\phi'(\xi) < 0$. The flow then accelerates, and finally becomes supersonic at some distance from the origin. The corresponding values for c_0, c_1 are plotted on Figure 4.4.

   The solutions in phase-plane variables are plotted on the right of Figure 4.3. The blue line also represents the solution for equal curvatures. When $d_0 > 0$, the solution curves start at the origin in the subsonic ($f < 0$) side of the plane, corresponding to the left hand side of the diagram, and they are situated above the blue line. After going off to infinity as $\xi \to 0$ (which is not shown on the graph), they reflect in the $g = 0$ axis and jump back to $g = -\infty, f = -\infty$. They come back under the blue line and move towards the supersonic region $f > 0$ and finally end up back at the origin. All solutions stay away from the saddle point P_2 and node point P_3 (represented by the black and yellow circle respectively) provided that $d_0 < 0.29$.

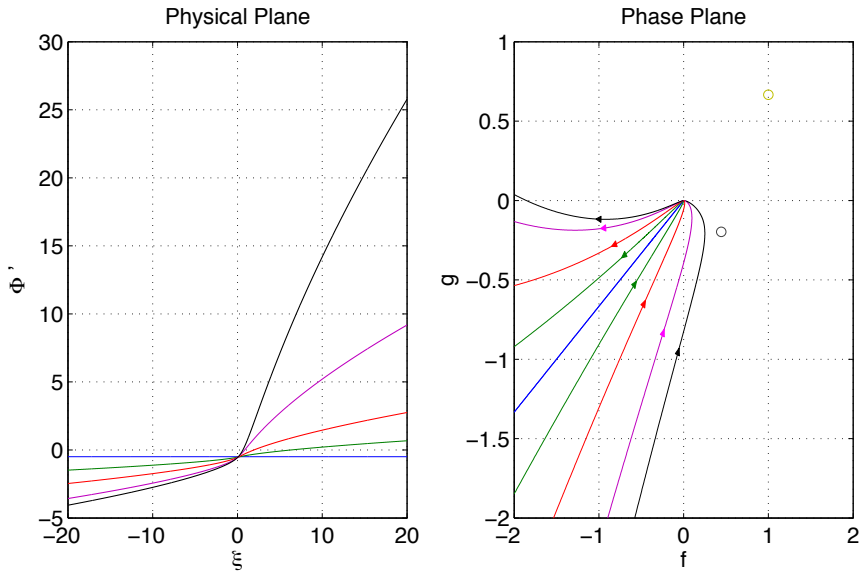

Figure 4.3: Small difference between upstream and downstream curvature.

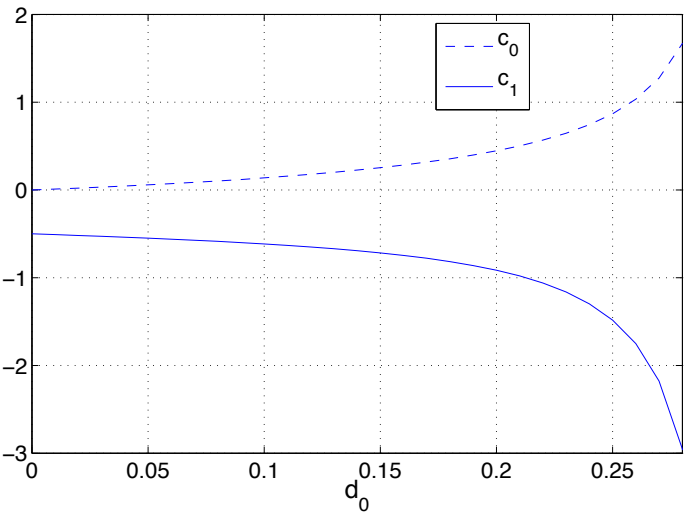

Figure 4.4: Behaviour of coefficients c_0 and c_1 as a function of d_0 - subsonic.

For larger values of d_0, the solution curves in the phase plane come back on the wrong

side of the nullcline of saddle point P_2. They are then deflected towards the singular line $f = 1$. This has no physical meaning. There exists however a special value for d_0 where the solution comes back exactly along the nullcline of saddle point P_2. It turns out that this does have a physical meaning - it corresponds to the flow reaching supersonic speed through a Prandtl-Meyer expansion fan. An example of such a flow was presented in Ruban, Wu & Pereira (2006).

2. Let us now consider the opposite situation, when $d_0 < 0$ which means that the flow upstream is supersonic. The flow is decelerating, and only for a specific range of κ^+ will we be able to observe solutions without shock. Once again setting $\kappa^- = 0.5$, we get a set of solutions which are displayed on Figure 4.5. The corresponding values for c_0 and c_1 are displayed on Figure 4.6.

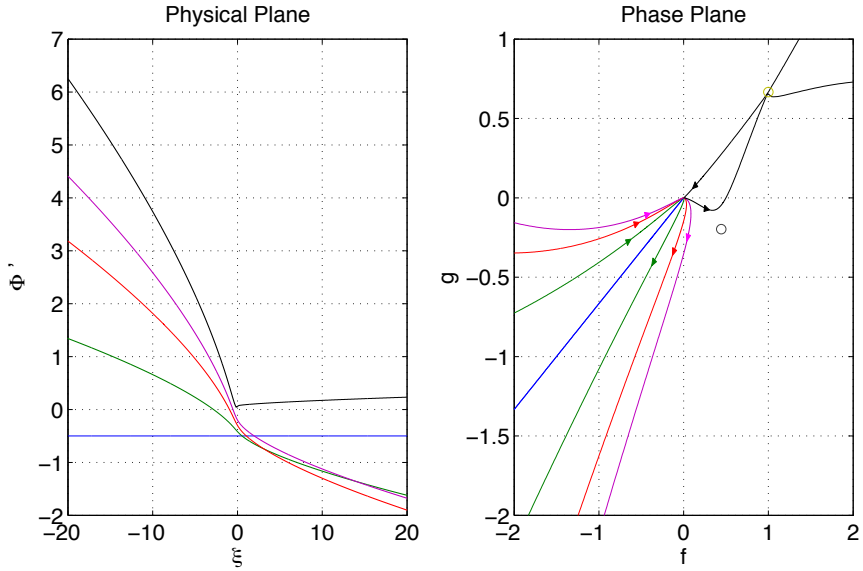

Figure 4.5: Supersonic flow decelerating without a shock wave.

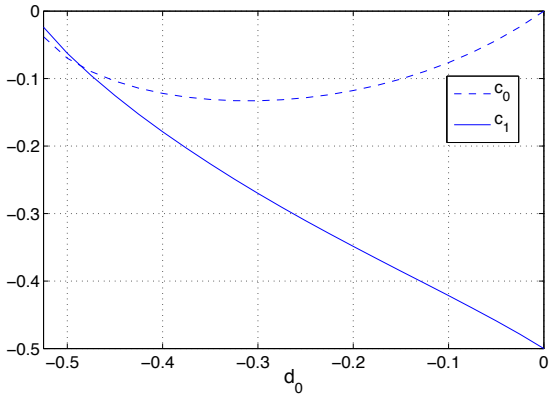

Figure 4.6: Behaviour of coefficients c_0 and c_1 as a function of d_0 - supersonic.

Observe that for some $d_0 > d_{\text{crit}}$, one of the solutions in the physical plane (here the black curve) develops a singularity. The behaviour is best explained in the phase plane, on the right of Figure 4.5. The trajectories start once again at the origin, but this time on the right hand side of the plane, corresponding to the supersonic region $f > 0$, and under the blue line. Straight away after leaving the origin, the trajectories approach the saddle point P_2. For $d_0 < d_{\text{crit}}$, trajectories are sent to $f = -\infty, g = -\infty$ along the nullcline of P_2. After going to infinity, they reflect and come back to the origin in the subsonic side. However, we see that some trajectories (black curve) are deflected to the other side of the saddle point and then attracted towards the node P_3. The discontinuity that the solution develops is associated with the formation of a shock-wave as the flow decelerates from high supersonic speed to low subsonic speeds. Thus, the remaining part of the solution curve linking point P_3 back to the origin is inaccurate and should be modified to account for the shock. Examples of such flows can be found in Buldakov & Ruban (2002).

3. Finally, we look for solutions as $\kappa^- \to 0$, which corresponds to the situation when we have a flat plate upstream, thus emulating the study of Chapter 3 but for transonic flows. We assume that the flow upstream is subsonic, so that the solutions start once again on the left hand side of the phase plane. After jumping to the other sheet, the trajectories come back much closer to the nullcline of saddle point P_3. For some

critical value of the parameter d_0, the trajectories comes back to the wrong side of the saddle point, and are then deflected towards the line $f = 1$. The black curve is an example of such a trajectory, and one can see that in the physical plane, the solution develops a discontinuity. As mentioned before, these solutions do not have a physical meaning. However, special solutions can be constructed that come back exactly along the nullcline. These correspond to Prandtl-Mayer expansion fan, as described in Yumashev (2010) and Ruban, Wu & Pereira (2006).

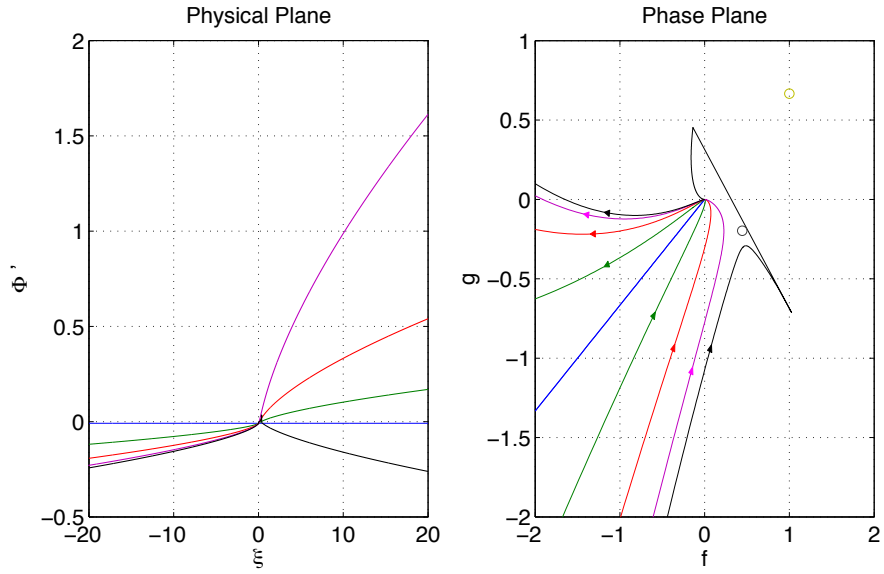

Figure 4.7: Prandtl-Meyer flow obtained in the limit as $\kappa^- \to 0$.

This concludes our analysis of the behaviour in the phase plane. It gave us insight into the actual physics of the flow and provides indication on how to calibrate the parameters $\kappa^{\pm}$ for future numerical calculations.

4.1.4 Pressure distribution in the inviscid region

The final step in the inviscid analysis is to derive an expression for the pressure gradient. We recall that using the Bernoulli equation, we were able to find

$$p_0 = -y^{2k-2}\phi'(\xi) + \cdots . \tag{4.44}$$

Differentiating once with respect to x, it follows that the pressure gradient can be written

$$\frac{\partial p_0}{\partial x} = -y^{k-2}\phi''(\xi) + \cdots .$$

In order to obtain an expression for the pressure gradient on the wall, we need to set $y = 0$, which corresponds to $\xi \to \pm\infty$ depending on the sign of x. We are interested in the behaviour upstream of the singularity, in which case we should take $x < 0$. Using the asymptotic expansion (4.25) for ϕ at large negative values of ξ, we find that

$$\left.\frac{\partial p_0}{\partial x}\right|_{y=0,x<0} = -\frac{10}{9}d_0(-x)^{-1/3} + \cdots . \tag{4.45}$$

Thus, this shows that in the vicinity of a discontinuity in curvature, transonic flows naturally generate the singular pressure gradient used throughout Chapter 3. It is also important to note that the pressure gradient is favourable provided that $d_0 > 0$, which corresponds to an incoming subsonic flow.

4.2 Transonic boundary layer upstream of the discontinuity

In order to analyse the behaviour of the boundary layer on the aerofoil surface, it is convenient to introduce orthogonal curvilinear coordinates $\hat{x}', \hat{y}'$ where $\hat{x}'$ is measured along the body contour and $\hat{y}'$ normal to it. The velocity components in these coordinates will be denoted by $\hat{u}'$ and $\hat{v}'$. The pressure and gas density are written as $\hat{p}$ and $\hat{\rho}$. Furthermore, we need to consider the enthalpy $\hat{h}$ and the dynamic viscosity $\hat{\mu}$. The non-dimensional

variables are introduced in a similar fashion as (4.8)

$$\left\{\begin{array}{l} \hat{x}' = Lx', \quad \hat{y}' = Ly', \\ \hat{u}' = a_* u', \quad \hat{v}' = a_* v', \quad \hat{p} = p_* + \rho_* a_*^2 p, \\ \hat{\rho} = \rho_* \rho, \quad \hat{h} = a_*^2 h, \quad \hat{\mu} = \hat{\mu}_* \mu. \end{array}\right. \tag{4.46}$$

The suffix '$*$' serves to denote the values of quantities immediately outside the boundary layer at point O, where the fluid velocity is equal to the speed of sound. The analysis of the flow is based on the asymptotic expansion

$$\left.\begin{array}{ll} u' = U_0(x', Y') + \cdots, & v' = \mathrm{Re}^{-1/2} V_0(x', Y') + \cdots, \\ p = P_0(x', Y') + \cdots, & \rho = \rho_0(x', Y') + \cdots, \\ h = H_0(x', Y') + \cdots, & \mu = \mu_0(x', Y') + \cdots, \end{array}\right\} \tag{4.47}$$

where the Reynolds number

$$\mathrm{Re} = \frac{\hat{\rho}_* \hat{V}_* L}{\hat{\mu}_*}, \tag{4.48}$$

is assumed to be large, and the normal coordinate is scaled as usual as

$$y' = \mathrm{Re}^{-1/2} Y'.$$

Substitution of (4.46)-(4.47) into the Navier-Stokes equations leads to the compressible boundary-layer equations

$$\rho_0 \left(U_0 \frac{\partial U_0}{\partial x'} + V_0 \frac{\partial U_0}{\partial Y'} \right) = -\frac{\partial P_0}{\partial x'} + \frac{\partial}{\partial Y'} \left(\mu_0 \frac{\partial U_0}{\partial Y'} \right), \tag{4.49}$$

$$\rho_0 \left(U_0 \frac{\partial H_0}{\partial x'} + V_0 \frac{\partial H_0}{\partial Y'} \right) = U_0 \frac{\partial P_0}{\partial x'} + \frac{\partial}{\partial Y'} \left(\frac{\mu_0}{Pr} \frac{\partial H_0}{\partial Y'} + \mu_0 \frac{Pr - 1}{Pr} U_0 \frac{\partial U_0}{\partial Y'} \right), \tag{4.50}$$

$$\frac{\partial \rho_0 U_0}{\partial x'} + \frac{\partial \rho_0 V_0}{\partial Y'} = 0, \tag{4.51}$$

$$H_0 = \frac{1}{(\gamma - 1)\rho_0} + \frac{\gamma}{\gamma - 1} \frac{P_0}{\rho_0}. \tag{4.52}$$

These equations are in turn the momentum equation projected upon the longitudinal coordinate x', the energy equation with Pr the Prandtl number, the continuity equation and the

state equation. Substituting (4.46)-(4.47) into the y'-component of the momentum equation leads to the conclusion that the pressure gradient in the boundary layer does not change across the boundary layer to leading order

$$\frac{\partial P_0}{\partial Y'} = 0. \tag{4.53}$$

According to (4.45), the pressure gradient inside the boundary layer is thus given by

$$\frac{\partial P_0}{\partial x'} = -\frac{10}{9} d_0 (-x')^{-1/3}. \tag{4.54}$$

In the following analysis, we will denote the value of the non-dimensional enthalpy H_0 at the 'bottom' of the boundary layer at point O by H_w, and the corresponding values of the non-dimensional density ρ_0 and viscosity μ_0 by ρ_w and μ_w respectively. Assuming that the body surface is not artificially heated or cooled, ρ_w and μ_w are order-one quantities. Since the flow is two dimensional, it is convenient to introduce the stream function $\Psi_0(x', Y')$ such that

$$\frac{\partial \Psi_0}{\partial Y'} = \rho_0 U_0, \quad \frac{\partial \Psi_0}{\partial x'} = -\rho_0 V_0, \tag{4.55}$$

which enables us to automatically satisfy the continuity equation.

Under the action of the singular pressure gradient (4.54), the boundary layer splits into two subregions, the main part of the boundary layer shown in Figure 4.8 as region $2a$, and a near-wall sublayer $2b$. We shall start with the sublayer $2b$.

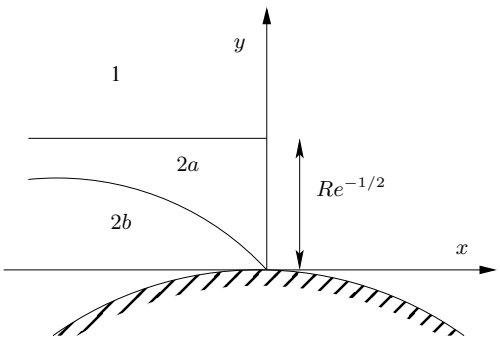

Figure 4.8: Two-tiers structure of the boundary layer.

4.2.1 Upstream boundary layer flow

The flow in region $2b$ experiences an extreme acceleration caused by the singular favourable pressure gradient (4.54). The convective terms on the left hand side of the momentum equation should then be of the same order of magnitude as the pressure gradient on the right hand side. Taking into account that to leading order $\rho_0 = \rho_w + \cdots$, this is expressed as

$$\frac{\partial \Psi_0}{\partial Y'} \frac{\partial^2 \Psi_0}{\partial x' \partial Y'} \sim \frac{\partial P_0}{\partial x'}. \tag{4.56}$$

In order for the solution in region $2b$ to satisfy the no-slip condition

$$\Psi_0 = \frac{\partial \Psi_0}{\partial Y'} = 0 \quad \text{at} \quad Y' = 0, \tag{4.57}$$

the convective terms on the left hand side should balance with the viscous term on the right hand side. Recalling that to leading order $\mu_0 = \mu_w + \cdots$, this is expressed as

$$\frac{\partial \Psi_0}{\partial Y'} \frac{\partial^2 \Psi_0}{\partial x' \partial Y'} \sim \frac{\partial^3 \Psi_0}{\partial Y'^3}. \tag{4.58}$$

Taking into account the form of the pressure gradient (4.54), it should be clear that equations (4.56)-(4.58) are the same as the ones derived in Chapter 3. In a similar fashion, we introduce logarithmic terms in the asymptotic expansion of the stream function Ψ_0

$$\Psi_0 \sim (-\log(-x'))^{1/4} (-x')^{2/3}. \tag{4.59}$$

This is substituted in (4.58), which enables us to estimate the thickness of region $2b$ as

$$Y' \sim (-x')^{1/3} (-\log(-x'))^{-1/4}. \tag{4.60}$$

This suggests that the asymptotic expansion of the stream function in the viscous sublayer $2b$ should be sought in the form

$$\psi = \big(-\log(-x)\big)^{1/4} (-x)^{2/3} \left(f_0(\eta) + \frac{f_1(\eta)}{\big(-\log(-x)\big)} + \cdots \right), \quad \text{as} \quad x \to 0^-, \tag{4.61}$$

where, on account of (4.60), we introduce the similarity variable η

$$\eta = \big(-\log(-x')\big)^{1/4} \frac{Y'}{(-x')^{1/3}}. \tag{4.62}$$

The asymptotic expansion for the density ρ_0 and dynamic viscosity μ_0 can be determined by estimating the temperature variations in region $2b$. To this aim, we turn to the energy equation (4.50). Balancing the heat transfer term on the right hand side of this equation with the mechanical energy dissipation

$$\frac{\partial}{\partial Y'}\left(\mu_0 \frac{\partial H_0}{\partial Y'}\right) \sim \mu_0 \left(\frac{\partial U_0}{\partial Y'}\right)^2,$$

we see that the variations of the enthalpy

$$|H_0 - H_w| \sim U_0^2 \sim \log(-x')(-x')^{2/3}.$$

Using the state equation (4.52), we can further assert that

$$|\rho_0 - \rho_w| \sim \log(-x')(-x')^{2/3},$$

and, since the viscosity μ_0 is a function of the enthalpy (Goldstein 1930),

$$|\mu_0 - \mu_w| \sim \log(-x')(-x')^{2/3}.$$

The asymptotic expansion of the density and viscosity in region $2b$ may thus be represented in the form

$$\left.\begin{aligned} \rho_0(x', Y') &= \rho_w + \log(-x')(-x')^{2/3}\tilde{\rho}(\eta) + \cdots \\ \mu_0(x', Y') &= \mu_w + \log(-x')(-x')^{2/3}\tilde{\mu}(\eta) + \cdots \end{aligned}\right\} \quad \text{as} \quad x' \to 0^-. \tag{4.63}$$

Thus, in the viscous sublayer, it suffices to know the leading order terms, and the solution for the corrections $\tilde{\rho}$ and $\tilde{\mu}$ need to be worked out. We can eliminate the constants ρ_w and

μ_w from the equation by applying the affine transformation

$$\psi = \rho_w^{-3/2}\mu_w^{1/2}\bar{\psi}, \quad x' = \rho_w^{-3/2}\mu_w^{3/4}\bar{x}, \quad Y' = \rho_w^{-1/2}\mu_w^{1/4}\bar{Y}. \tag{4.64}$$

Substitution of (4.64), (4.63) , (4.62) and (4.61) into (4.55) and then into (4.49) leads to a set of ordinary differential equations. We obtain the following equation and boundary conditions in the leading order approximation

$$f_0''' - \frac{2}{3}f_0 f_0'' + \frac{1}{3}\big(f_0'\big)^2 = 0, \quad f_0(0) = f_0'(0) = 0, \tag{4.65}$$

and the requirement that $f_0(\eta)$ does not grow exponentially as $\eta \to \infty$. This equation admits a simple solution $f_0 = \frac{1}{2}A\eta^2$ which satisfies all the boundary conditions. The constant A is arbitrary and should be found as part of the next order problem.

The latter is written

$$f_1''' - \frac{1}{3}A\eta^2 f_1'' + \frac{2}{3}A\eta f_1' - \frac{2}{3}A f_1 + \frac{10}{9}d_0 = \frac{3}{8}A^2\eta^2. \tag{4.66}$$

The set of boundary conditions formulated in (4.65) applies to $f_1(\eta)$ as well. In Chapter 3, we found the solution to equation (4.66) to be given by the integral

$$f_1(\eta) = \frac{1}{2}\int_0^\eta (\eta-\xi)^2 \int_\infty^\zeta \frac{3}{4}A^2\zeta\, \mathrm{e}^{\frac{1}{9}A(\xi^3-\zeta^3)}\,\mathrm{d}\zeta\mathrm{d}\xi + D\eta^2. \tag{4.67}$$

The constant D is arbitrary and, as before, should be found by considering the next order problem for f_2. In the process of solving equation (4.66), we find that we need to impose the condition

$$A = \frac{5^{3/4}2^{9/4}d_0^{3/4}}{3^{10/4}\Gamma(2/3)^{3/4}},$$

in order to obtain a valid solution. This solvability condition takes a similar form as the one derived in Chapter 3. Recall that for subsonic flows, constant A was a function of the downstream curvature κ. The transonic version of constant A also depends on the downstream curvature through constant d_0. The asymptotic expansion of f_1 at large values

of η was found to be

$$f_1 = -\frac{9}{8}A\eta^2\log(\eta) + C_1\eta^2 + C_2\eta + C_3 + O\left(\frac{1}{\eta}\right) \quad \text{as} \quad \eta \to \infty, \tag{4.68}$$

with the constants C_2 and C_3 given by the equations

$$C_2 = -\frac{9^{5/6}}{4}A^{2/3}\Gamma(2/3)^2, \quad C_3 = \frac{5}{3}\frac{d_0}{A}. \tag{4.69}$$

The behaviour of f_1 at large values of η enables us to calculate the streamline slope at the edge of the viscous sublayer. Since we are using curvilinear coordinates (x', Y'), the streamline slope θ should be calculated as

$$\theta = -\operatorname{Re}^{-1/2}\frac{\partial\psi}{\partial x'}\bigg/\frac{\partial\psi}{\partial Y'} = -\operatorname{Re}^{-1/2}\left(\frac{\partial\psi}{\partial x'}\bigg/\frac{\partial\psi}{\partial Y} - f'(x')\right). \tag{4.70}$$

We substitute expansion (4.68), which leads to

$$\theta = -\operatorname{Re}^{-1/2}\left(\left(-\log(-x')\right)^{-5/4}(-x')^{-2/3}\frac{2}{3}C_2 + \cdots\right) + \operatorname{Re}^{-1/2}f'(x'). \tag{4.71}$$

This expression is independent of Y. This suggests that the main part of the boundary layer, region $2a$, acts once again as a buffer region whose aim is to transmit the streamline slope at the edge of region $2b$ back to the inviscid region 1.

One can see that the equations and upstream asymptotics that we obtained in Chapter 3 are still applicable to the description and formulation of the viscous sublayer of the interaction region, as well as the 'buffer' layer. However, the length-scale σ of the triple deck should be amended to account for transonic effects.

Indeed, in transonic flows, we find that the pressure perturbations Δp in the inviscid region, caused by the displacement θ of the boundary layer, are stronger than their subsonic and supersonic counterparts, namely of the order of $\theta^{2/3}$. The process of boundary-layer interaction occurs when the pressure perturbations become of the same order as the original

inviscid pressure p_e. Thus, for transonic flows, the interaction occurs when

$$p_e \sim \theta^{2/3} \Leftrightarrow (-x)^{2/3} \sim \left(\mathrm{Re}^{-1/2}\log(-x)^{-5/4}(-x)^{-2/3}\right)^{2/3}. \tag{4.72}$$

The width σ of the interaction region is now given by the solution of the transcendental equation

$$x|\log x|^{3/4} = \mathrm{Re}^{-3/10}\,. \tag{4.73}$$

4.3 Formulation of the viscous-inviscid interaction region

Let us now turn to the interaction region that forms in the vicinity of the surface discontinuity. It takes the standard triple-deck form, the lowest deck (region 5) being a continuation of the viscous sublayer $2b$. The middle deck (region 4) is the continuation of the main part of the boundary layer, while the upper deck (region 3) sits in the inviscid transonic part of the flow. This is sketched in Figure 4.9.

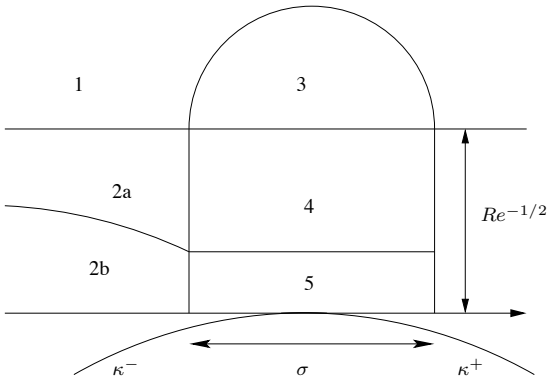

Figure 4.9: Triple deck structure of interaction region.

4.3.1 The viscous lower deck

In order to formulate the interaction problem, we proceed as in Section 3.4.1 and introduce the scalings

$$\bar{x} = \sigma X_\star, \quad \bar{Y} = \sigma^{1/3}|\log\sigma|^{-1/4}Y_\star. \tag{4.74}$$

where σ is the solution of (4.73). The solution in the viscous sublayer is then sought in the asymptotic form

$$\begin{cases} \psi = |\log\sigma|^{1/4}\sigma^{2/3}\left(\dfrac{1}{2}AY_\star^2 + \dfrac{\psi_1^\star(X_\star,Y_\star)}{|\log\sigma|} + \cdots\right), \\ P = \sigma^{2/3}P_\star(X_\star) + \cdots, \end{cases} \tag{4.75}$$

leading to the linearised boundary-layer equations

$$AY_\star\frac{\partial^2\psi_1^\star}{\partial X_\star\partial Y_\star} - A\frac{\partial\psi_1^\star}{\partial X_\star} = -\frac{\mathrm{d}P_\star}{\mathrm{d}X_\star} + \frac{\partial^3\psi_1^\star}{\partial Y_\star^3}. \tag{4.76}$$

Equation (4.76) should be solved with the boundary conditions

$$\begin{cases} \psi_1^\star = \dfrac{\partial\psi_1^\star}{\partial Y_\star} = 0, & \text{at} \quad Y_\star = 0, \\ \psi_1^\star \to (-X_\star)^{2/3}\left(f_1(\eta_\star) - \dfrac{3A}{8}\log(-X_\star)\eta_\star^2\right) & \text{as} \quad X_\star \to -\infty, \\ \psi_1^\star = -\dfrac{9}{8}AY_\star^2\log Y_\star + \dfrac{1}{2}C_1Y_\star^2 + A_\star(X_\star)Y_\star + \cdots, & \text{as} \quad Y_\star \to \infty. \end{cases} \tag{4.77}$$

These are respectively the no-slip condition on the body surface, the matching with the flow upstream of the interaction region and the flow behaviour at the edge of the viscous sublayer.

The similarity variable $\eta_\star$ is defined as $\eta_\star = Y_\star/(-X_\star)^{1/3} = O(1)$ and the function f_1 is the solution to the ordinary differential equation

$$f_1''' - \frac{1}{3}A\eta^2 f_1'' + \frac{2}{3}A\eta f_1' - \frac{2}{3}Af_1 + \frac{10}{9}d_0 = \frac{3}{8}A^2\eta^2, \tag{4.78}$$

subject to the boundary conditions

$$f_1(0) = f_1'(0) = 0,$$

and the requirement that $f_1(\eta)$ does not grow exponentially as $\eta \to \infty$. The displacement

function $A_\star(X_\star)$ satisfies the matching condition

$$A_\star(X_\star) \to C_2\,(X_\star)^{1/3} + \cdots, \quad \text{as} \quad X_\star \to -\infty, \tag{4.79}$$

and should be found as part of the solution to the interaction problem. Finally, the streamline slope is estimated as

$$\theta = \mathrm{Re}^{-1/2}\,\sigma^{-2/3}|\log\sigma|^{-5/4}. \tag{4.80}$$

The analysis of the flow in the buffer region 4, between the viscous layer and the inviscid upper deck remains the same as in the previous chapter and is not repeated here.

4.3.2 The inviscid upper deck

The analysis of the inviscid upper deck is the fundamental difference with the work of Chapter 2, since we now need to account for transonic effects. The flow in this region is governed by the transonic small perturbation theory. The scaling in the x-direction remains the same as for region 5, so we set $x = \sigma x_\star$. The y-coordinate should be scaled as

$$y = \frac{\sigma}{\alpha}\,y_\star,$$

where α is expected to be determined as a result of the analysis of the upper deck flow. This scaling is typical of transonic flows, which need to account for an extended region of influence. We look for a solution in the form

$$\begin{cases} u(x,y) = 1 + \tau\,u_1(x_\star, y_\star) + \cdots, \\ v(x,y) = \gamma\,v_1(x_\star, y_\star) + \cdots, \end{cases} \tag{4.81}$$

with parameters τ and γ assumed to be small. Substitution of (4.81) into the irrotationality condition gives

$$\tau\alpha\frac{u_1}{y_\star} \sim \gamma\frac{v_1}{x_\star},$$

indicating that we should set $\gamma = \tau\alpha$. In order to estimate the speed of sound a, we use the Bernoulli equation (4.10) written for a

$$a^2 = \frac{1}{M_\infty^2} + \frac{\gamma - 1}{2}\left(1 - \left(u^2 + v^2\right)\right),$$

where we set $M_\infty^2 = 1 + \zeta M_1$, $\zeta \ll 1$ in order to make sure the flow is transonic. Inserting the asymptotic expansion (4.81) leads to

$$a^2 = 1 - 2\zeta M_1 - (\gamma - 1)\tau u_1 + \cdots . \tag{4.82}$$

We thus chose $\zeta = \tau$ to avoid degeneration. Substituting asymptotic expansions (4.81) and (4.82) into the transonic equation (4.9) leads to the following estimates

$$\begin{aligned}
\left(a^2 - u^2\right) u_x &\sim \left(-2M_1 - (\gamma + 1)\right)\frac{\tau^2}{\xi} u_1 \frac{\partial u_1}{\partial x_\star} + \cdots , \\
\left(a^2 - v^2\right) v_y &\sim \frac{\tau\alpha^2}{\xi}\frac{\partial v_1}{\partial y_\star} + \cdots , \\
2uvu_y &\sim \frac{\tau^2\alpha^2}{\xi} v_1 \frac{\partial u_1}{\partial y_\star} + \cdots .
\end{aligned} \tag{4.83}$$

Since $\tau \ll 1$, the third term is small compared to the second one and should be disregarded. According to the principle of least degeneration, we should then set $\alpha^2 = \tau$. Taking this into account and introducing the potential function

$$u_1 = \frac{\partial \phi_\star}{\partial x_\star}, \quad v_1 = \frac{\partial \phi_\star}{\partial y_\star},$$

the transonic equation (4.9) reduces to

$$\left(2M_1 + (\gamma + 1)\frac{\partial \phi_\star}{\partial x_\star}\right)\frac{\partial^2 \phi_\star}{\partial x_\star^2} - \frac{\partial^2 \phi_\star}{\partial y_\star^2} = 0, \tag{4.84}$$

which is known as the Kármán-Guderley equation. We can estimate the pressure by substituting (4.81) into the Bernoulli equation (4.10), which leads to the following scaling

$$p(x, y) = \alpha^2 p_\star(x_\star, y_\star) + \cdots .$$

It remains to find the relationship between α and σ. The pressure gradient in the inviscid flow and in the viscous flow have to match, leading to the condition

$$\frac{\alpha^2}{\sigma}\frac{\mathrm{d}p^\star}{\mathrm{d}x_\star} = \sigma^{-1/3}\frac{\mathrm{d}P_\star}{\mathrm{d}X_\star}.$$

Solving for the order of magnitude leads to $\alpha = \sigma^{1/3}$.

Let us now turn to the boundary conditions for equation (4.84). The matching condition of the velocity components at the edge of region 3 and 4 is written

$$v_1(x_\star, 0) = \lim_{Y\to\infty}\frac{V}{U} = -\big(A'_\star(x_\star) - f'(x_\star)\big). \tag{4.85}$$

A far-field condition should be added for this equation. It follows from the asymptotic matching with the upstream transonic flow analysis carried out in Section 4.1. We have

$$\phi_\star = y_\star^{5/2}\phi(\xi_\star) + \cdots, \quad \text{as} \quad y_\star \to \infty, \tag{4.86}$$

where the variable $\xi_\star$ is defined by

$$\xi_\star = \frac{x_\star}{y_\star^{3/2}}.$$

The formulation of the upper transonic problem thus consists of the scalings

$$x = \sigma x_\star, \quad y = \sigma^{2/3} y_\star, \tag{4.87}$$

$$\begin{cases} u(x,y) = 1 + \sigma^{2/3}u_1(x_\star, y_\star) + \cdots, \\ v(x,y) = \sigma v_1(x_\star, y_\star) + \cdots, \\ p(x,y) = \sigma^{2/3}p_\star(x_\star, y_\star) + \cdots, \end{cases} \tag{4.88}$$

and the Kármán-Guderley equations, together with the impermeability condition and far-field matching

$$\left(2M_1 + (\gamma+1)\frac{\partial\phi_\star}{\partial x_\star}\right)\frac{\partial^2\phi_\star}{\partial x_\star^2} - \frac{\partial^2\phi_\star}{\partial y_\star^2} = 0, \tag{4.89}$$

$$\begin{cases} \left.\dfrac{\partial \phi_\star}{\partial y_\star}\right|_{y_\star=0} = -\left[A_\star'(x_\star) - f'(x_\star)\right], \\ \lim\limits_{x_\star^2+y_\star^2\to\infty} \phi_\star = y_\star^{5/2}\phi\left(\xi_\star\right), \quad \xi_\star = \dfrac{x_\star}{y_\star^{3/2}}. \end{cases} \tag{4.90}$$

We remind the reader that σ is the solution of the transcendental equation

$$x|\log x|^{3/4} = \mathrm{Re}^{-3/10}, \tag{4.91}$$

and the function $\phi(\xi_\star)$ is the solution to

$$\left(\frac{9}{4}\xi^2 - (\gamma+1)\phi'\right)\phi'' - \frac{15}{4}\xi\phi' + \frac{15}{4}\phi = 0, \tag{4.92}$$

subject to

$$\begin{cases} \lim\limits_{\xi\to-\infty}\left[\dfrac{5}{2}\phi(\xi) - \dfrac{3}{2}\xi\phi'(\xi)\right] = -\kappa^-\xi, \\ \lim\limits_{\xi\to+\infty}\left[\dfrac{5}{2}\phi(\xi) - \dfrac{3}{2}\xi\phi'(\xi)\right] = -\kappa^+\xi. \end{cases} \tag{4.93}$$

In order to analyse the full viscous-inviscid interaction, this should be solved in conjunction with the linearised boundary-layer equation derived in Section 4.3.1.

4.4 Numerical solution of the interaction problem

In Chapter 3, the equations governing the viscous-inviscid interaction were linear, which enabled us to obtain analytical solutions. The corresponding equations for transonic flow are nonlinear and should be solved numerically. The numerical calculations are done in three stages. The first one consists in solving the viscous sublayer equations (4.76)-(4.77). We then solve the equations (4.89)-(4.90) of the transonic upper deck. The last step consists in organising the interaction between the boundary layer and the transonic flow.

4.4.1 Boundary-layer calculations

The flow in the viscous sublayer is governed by the linearised boundary-layer equations (4.76). For the purpose of the numerical calculation, we recast them in terms of the velocity

components U and V

$$\begin{aligned} AY_\star \frac{\partial U}{\partial X_\star} + AV &= -\frac{\mathrm{d}P_\star}{\mathrm{d}X_\star} + \frac{\partial^2 U}{\partial Y_\star^2}, \\ \frac{\partial U}{\partial X_\star} + \frac{\partial V}{\partial Y_\star} &= 0. \end{aligned} \tag{4.94}$$

The no-slip and matching conditions are

$$\begin{cases} U = V = 0 & \text{at} \quad Y_\star = 0, \\ U = -\dfrac{3}{4} A Y_\star \log(-X_\star) + (-X_\star)^{1/3} f_1'(\eta_\star) + \cdots, & \text{as} \quad X_\star \to -\infty, \\ U = -\dfrac{9}{4} A Y_\star \log Y_\star - \dfrac{9}{8} A Y_\star + A_\star(X_\star) + \cdots, & \text{as} \quad Y_\star \to \infty. \end{cases} \tag{4.95}$$

We recall that the similarity variable $\eta_\star$ is defined as $\eta_\star = Y_\star/(-X_\star)^{1/3}$ and that the constant A is given by

$$A = \frac{5^{3/4} 2^{9/4} d_0^{3/4}}{3^{10/4} \Gamma(2/3)^{3/4}}.$$

The function f_1 satisfies the linear equation

$$f_1''' - \frac{1}{3} A \eta_\star^2 f_1'' + \frac{2}{3} A \eta_\star f_1' - \frac{2}{3} A f_1 + \frac{10}{9} d_0 = \frac{3}{8} A^2 \eta_\star^2,$$

with boundary conditions $f_1(0) = f_1'(0) = 0$ and no exponential growth for large $\eta_\star$. It has the asymptotic behaviour

$$f_1 = -\frac{9}{8} \eta_\star^2 \log \eta_\star + C_2 \eta_\star + C_3 + O\left(\frac{1}{\eta_\star}\right), \quad \text{as} \quad \eta_\star \to \infty.$$

The constants C_2 and C_3 are given analytically by

$$C_2 = -\frac{9^{5/6}}{4} A^{2/3} \Gamma(2/3)^2, \quad C_3 = \frac{5}{3} \frac{d_0}{A}.$$

Finally, the displacement function $A_\star$ has the following asymptotic behaviour upstream

$$A_\star(X_\star) = C_2 (-X_\star)^{1/3} + \cdots, \quad \text{as} \quad X_\star \to -\infty.$$

In order to calculate the pressure distribution in the viscous sublayer, we introduce a discrete mesh (x_i, y_j), with $i = 1, ..., NX; j = 1, ..., NY_{\text{vis}}$. Here, subscript 'vis' refers to the viscous mesh for normal coordinate $Y_\star$. We denote the values of the displacement function $A_\star$ and the pressure gradient $dp(x)$ at the points x_i by the vectors $\boldsymbol{A_0}$ and $\boldsymbol{dp}$. We solve the boundary-layer equations (4.94) by marching from position x_i to the position x_{i+1} as described in Kravtsova, Zametaev & Ruban (2005). At each cross-section of the boundary layer at x_i, starting from $i = 3$, we formulate a set of linear operator equations

$$\Phi_j = 0, \quad j = 1, ..., NY_{\text{vis}} - 1, \tag{4.96}$$

based on the $X_\star$-momentum equation. On the left edge of the mesh, at $i = 1, 2$, we use the matching condition for the velocity profile profile U given by (4.95). Additionally, the values of the displacement function and pressure gradient at the initial cross-sections are known from the asymptotics

$$A_{0i} = C_2(-x_i)^{1/3}, \quad dp_i = -\frac{10}{9} d_0 (-x_i)^{-1/3}, \quad i = 1, 2.$$

The vertical velocity V is calculated using the continuity equation. It is written in finite-difference form as follows

$$\frac{1}{2}\left(\frac{U_{i-2,j} - 4U_{i-1,j} + 3U_{i,j}}{2\Delta x} + \frac{U_{i-2,j-1} - 4U_{i-1,j-1} + 3U_{i,j-1}}{2\Delta x}\right) + \\ + \frac{V_{i,j} - V_{i,j-1}}{\Delta y} = 0. \tag{4.97}$$

We solve this equation for $V_{i,j}$ and use it for progressively increasing $j = 2, ..., M$, starting from the wall where according to the no-slip condition $V_{i,1} = 0$. For a given vector $\boldsymbol{A_0}$, the set of linear equations (4.96) serves to determine the longitudinal velocity component $U_{i,j}$ for $j = 2, ..., NY_{\text{vis}} - 1$ and the pressure gradient $\boldsymbol{dp_i}$ at the cross-sections x_i, for $i = 3, .., NX$. To compute the pressure distribution, we integrate numerically $\boldsymbol{dp_i}$ starting from $i = 1, ..., NX$.

We note here that the problem in the viscous sublayer can still be solved using Fourier transform methods assuming an unknown pressure distribution $P(x)$. Following the same

method used in Section 3.5.2, we are able to derive the following relation between the displacement function $\tilde{A}_\star$ and the pressure $\tilde{p}_\star$ in Fourier space

$$\tilde{A}_\star(k) = \frac{(ik)^{1/3}}{3A^{2/3}\,\mathrm{Ai}'(0)}\,\tilde{p}_\star. \tag{4.98}$$

We used this formula as a check that the boundary-layer code described above works. To this aim, we solved the problem with the artificial displacement function

$$A_\star(X_\star) = C_2\left(1 + X_\star^2\right)^{1/6},$$

which provides the correct upstream asymptotic behaviour described in equation (4.79). Figure 4.10 shows the difference between the pressure gradient obtained by taking the inverse Fourier Transform of formula (4.98) with given $\tilde{A}_\star$ and the numerical code. The asymptotic behaviour for the pressure

$$\frac{\mathrm{d}P_\star}{\mathrm{d}X_\star} = -\frac{10}{9}d_0(-X_\star)^{-1/3}, \quad \text{as} \quad X_\star \to -\infty$$

was plotted on top of the solution. It shows excellent agreement, indicating that the code described works well.

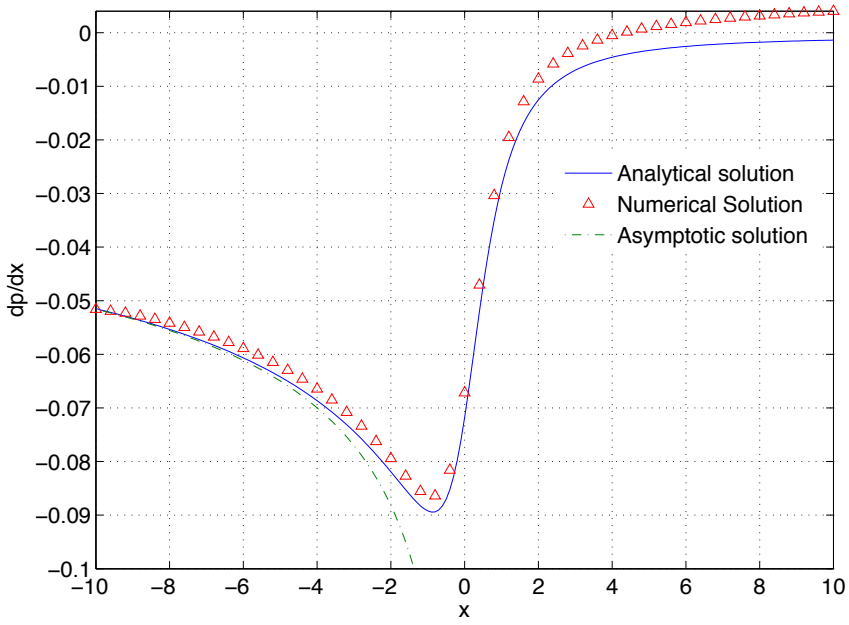

Figure 4.10: Comparison between analytical, numerical and asymptotical results for the pressure gradient distribution across the interaction region.

4.4.2 Kármán-Guderley calculations

The flow in the transonic inviscid upper deck is governed by the Kármán-Guderley equations

$$\left(K-(\gamma+1)\frac{\partial\phi_\star}{\partial x_\star}\right)\frac{\partial^2\phi_\star}{\partial x_\star^2}+\frac{\partial^2\phi_\star}{\partial y_\star^2}=0, \tag{4.99}$$

subject to the matching condition with the viscous flow

$$\left.\frac{\partial\phi_\star}{\partial y_\star}\right|_{y_\star=0}=-\frac{\mathrm{d}A_\star}{\mathrm{d}x_\star}+\frac{\mathrm{d}f}{\mathrm{d}x_\star}, \tag{4.100}$$

and the far-field boundary conditions

$$\lim_{x_\star^2+y_\star^2\to\infty}\phi_\star=y_\star^{5/2}\phi\left(\xi_\star\right),\quad \xi_\star=\frac{x_\star}{y_\star^{3/2}}. \tag{4.101}$$

The Kármán parameter $K = 2M_1$ and the body shape f has the form

$$f = \begin{cases} -\frac{1}{2}\kappa^- x^2, & x \leq 0, \\ -\frac{1}{2}\kappa^+ x^2, & x > 0. \end{cases} \tag{4.102}$$

The function $\phi(\xi_\star)$ is the solution of the equation

$$\left(\frac{9}{4}\xi^2 - (\gamma+1)\phi'\right)\phi'' - \frac{15}{4}\xi\phi' + \frac{15}{4}\phi = 0, \tag{4.103}$$

subject to

$$\begin{cases} \lim\limits_{\xi\to-\infty}\left[\frac{5}{2}\phi(\xi) - \frac{3}{2}\xi\phi'(\xi)\right] = -\kappa^-\xi, \\ \lim\limits_{\xi\to+\infty}\left[\frac{5}{2}\phi(\xi) - \frac{3}{2}\xi\phi'(\xi)\right] = -\kappa^+\xi. \end{cases} \tag{4.104}$$

For the solution to this equation, we refer to Section 4.1.3.

Given a displacement function $A_\star$ and the body shape (4.102), our task is to solve equations (4.99)-(4.101) to obtain the 'inviscid' pressure distribution

$$p\big|_{y_\star=0} = -\frac{\partial\phi_\star}{\partial x_\star}\bigg|_{y_\star=0}.$$

For this purpose, it is convenient to use the linearised Kármán-Guderley equations, which are obtained by representing all functions in the form

$$\phi_\star = \phi_0 + \phi_1, \quad p_\star = p_0 + p_1, \quad A_\star = A_0,$$

where ϕ_1 and p_1 are assumed to be small. Substituting this into (4.99)-(4.101) leads to the

following leading order problem for ϕ_0

$$\left(K-(\gamma+1)\frac{\partial\phi_0}{\partial x_\star}\right)\frac{\partial^2\phi_0}{\partial x_\star^2}+\frac{\partial^2\phi_0}{\partial y_\star^2}=0, \tag{4.105}$$

$$\begin{cases} \left.\dfrac{\partial\phi_0}{\partial y_\star}\right|_{y_\star=0}=-\dfrac{\mathrm{d}A_0}{\mathrm{d}x_\star}+\dfrac{\mathrm{d}f}{\mathrm{d}x_\star}, \\ \lim\limits_{x_\star^2+y_\star^2\to\infty}\phi_0=y_\star^{5/2}\phi\left(\xi_\star\right). \end{cases} \tag{4.106}$$

The pressure distribution is given by $p_0\big|_{y_\star=0}=-\left.\dfrac{\partial\phi_0}{\partial x_\star}\right|_{y_\star=0}$. For ϕ_1, we need to solve the equations

$$\left(K-(\gamma+1)\frac{\partial\phi_0}{\partial x_\star}\right)\frac{\partial^2\phi_1}{\partial x_\star^2}-(\gamma+1)\frac{\partial^2\phi_0}{\partial x_\star^2}\frac{\partial\phi_1}{\partial x_\star}+\frac{\partial^2\phi_1}{\partial y_\star^2}=0, \tag{4.107}$$

$$\begin{cases} \left.\dfrac{\partial\phi_1}{\partial y_\star}\right|_{y_\star=0}=0, \\ \lim\limits_{x_\star^2+y_\star^2\to\infty}\phi_1=0, \end{cases} \tag{4.108}$$

and the pressure is found through $p_1\big|_{y_\star=0}=-\left.\dfrac{\partial\phi_1}{\partial x_\star}\right|_{y_\star=0}$. We introduce a mesh (x_i,y_j) where $(i=1,...,NX;j=1,...,NY_{\text{inv}})$. The subscript 'inv' refers to the inviscid mesh for the normal coordinate $y_\star$. Guided by the first boundary condition (4.106), we introduce the operator equation

$$F_{i,1}=\frac{-3\phi_{0i,1}+4\phi_{0i,2}-\phi_{0i,3}}{2\Delta y}+\frac{A_{0i+1}-A_{0i-1}}{2\Delta x}-f'_{xi}=0, \tag{4.109}$$

for $j=1$ and all $i=2,...,NX-1$. Note that for given A_0, we have used central difference to approximate the derivative A_0'. According to the second boundary condition (4.106), we hold the values

$$\phi_0=y^{5/2}\phi(\xi_\star),$$

in the nonlinear operator $F_{i,j}$ at the left $(i=1;j=2,...,NY_{\text{inv}}-1)$, top $(i=1,...,NX;j=NY_{\text{inv}})$ and right $(i=NX;j=2,...,NY_{\text{inv}}-1)$ edges of the mesh.

The Kármán-Guderley equation is a mixed elliptic-hyperbolic equation depending on

the sign of

$$\Lambda = K - (\gamma + 1)\frac{\partial \phi_0}{\partial x_\star}. \tag{4.110}$$

In order to ensure the stability of the numerical scheme, we use central or backward finite differences schemes on $x_\star$ depending on the sign of Λ

$$\frac{\partial \phi_0}{\partial x_\star} = \begin{cases} \dfrac{\phi_{0i+1,j} - \phi_{0i-1,j}}{2\Delta x}, & \Lambda > 0, \\ \dfrac{\phi_{0i,j} - \phi_{0i-1,j}}{\Delta x}, & \Lambda \leq 0, \end{cases} \tag{4.111}$$

$$\frac{\partial^2 \phi_0}{\partial x_\star^2} = \begin{cases} \dfrac{\phi_{0i+1,j} - 2\phi_{0i,j} + \phi_{0i-1,j}}{(\Delta x)^2}, & \Lambda > 0, \\ \dfrac{\phi_{0i,j} - 2\phi_{0i-1,j} + \phi_{0i-2,j}}{(\Delta x)^2}, & \Lambda \leq 0. \end{cases} \tag{4.112}$$

We use central finite difference on $y_\star$ for the derivative

$$\frac{\partial^2 \phi_0}{\partial y_\star^2} = \frac{\phi_{0i,j+1} - 2\phi_{0i,j} + \phi_{0i,j-1}}{(\Delta y)^2}. \tag{4.113}$$

Therefore, for $(i = 2, ..., NX; j = 2, ..., NY_{\text{inv}} - 1)$ we express the nonlinear operator equation for (4.105) in the form

$$F_{i,j} = \left[K - (\gamma + 1) \left(\frac{\partial \phi_0}{\partial x_\star} \right)_{i,j} \right] \left(\frac{\partial^2 \phi_0}{\partial x_\star^2} \right)_{i,j} + \left(\frac{\partial^2 \phi_0}{\partial y_\star^2} \right)_{i,j} = 0, \tag{4.114}$$

with the quantities in brackets given by (4.111), (4.112) and (4.113) respectively. We have to satisfy equations (4.109) and (4.114) at each point (x_i, y_j) simultaneously. Following the Newton-Raphson method, to calculate $\phi_{0i,k}$ the operator equation can be expressed as

$$F_{i,j}^k(\phi_0) + \left. \frac{\partial F_{i,j}}{\partial \phi_{0l,m}} \right|^k \left(\phi_{0i,j}^{k+1} - \phi_{0i,j}^k \right) = 0, \tag{4.115}$$

where k is the number of iterations. According to equations (4.109) and (4.114), for known values of ϕ_0^k and given A_0, we compute $(\phi_0)_x$ and $(\phi_0)_{xx}$ and the components of matrix F. Using the linearised Kármán-Guderley equations (4.107) and boundary condition (4.108),

we fill the Jacobian matrix

$$\mathcal{J}_F = \left.\frac{\partial F}{\partial \phi_{0l,m}}\right|_{\phi_{1l,m}=1}, \tag{4.116}$$

of size $(NX-2)(NY_{\text{inv}}-1)\times(NX-2)(NY_{\text{inv}}-1)$. We now need to solve the linear system of equations

$$\mathcal{J}_F^k\,\delta\phi_0^k = -F^k \tag{4.117}$$

for the unknown quantity $\delta\phi_0^k$ and then improve the solution at the next step ϕ_0^{k+1} by setting

$$\phi_0^{k+1} = \phi_0^k + r\delta\phi_0^k, \tag{4.118}$$

using a relaxation parameter r. The iterative process with $r = 0.8$ typically needs 9-11 iterations to get an accuracy of 10^{-6}. Finally, for given A_0 we recover the pressure distribution p_0 using the central difference

$$p_{0i} = -\frac{\phi_{0i+1,1} - \phi_{0i-1,1}}{2\Delta x}. \tag{4.119}$$

4.4.3 Viscous-inviscid interaction calculations

We finally turn to organising the interaction process. For a given A_0, we compute ϕ_0 and the inviscid pressure p_{inv} is found using equation (4.119). Using the same value of A_0 for the calculation of the boundary layer, we obtain the viscous pressure p_{vis}. To organise the 'global' Newton iterations for the interaction code, we represent the viscous and inviscid pressure as

$$p_{\text{vis}} = \mathcal{L}(A_0), \quad p_{\text{inv}} = \mathcal{N}(A_0),$$

where $\mathcal{L}$ is a linear and $\mathcal{N}$ is a nonlinear operator. For a given value of the displacement function A_0, we can write

$$\mathcal{L} = \mathcal{L}(A_0) + \left.\frac{\partial \mathcal{L}}{\partial A}\right|_{A=0}\delta A, \quad \mathcal{N} = \mathcal{N}(A_0) + \left.\frac{\partial \mathcal{N}}{\partial A}\right|_{A=0}\delta A. \tag{4.120}$$

The interaction condition requires

$$\mathcal{L} - \mathcal{N} = 0.$$

We thus have to solve the set of linear equations

$$(\mathcal{J}_{\mathcal{L}} - \mathcal{J}_{\mathcal{N}})\ \delta A = \mathcal{N}(A_0) - \mathcal{L}(A_0) \tag{4.121}$$

for unknown δA and then improve the guess A_0. Here, $\mathcal{J}_{\mathcal{L}}$ and $\mathcal{J}_{\mathcal{N}}$ are the Jacobian matrices of $\mathcal{L}$ and $\mathcal{N}$.

For given A^k_{0i}, let us start by calculating the viscous pressure gradient on the current iteration k and integrate it to obtain $(p_{\text{vis}})^k_i$. We then numerically fill the Jacobian matrix

$$\mathcal{J}_{\mathcal{L}} = \frac{\partial \mathcal{L}}{\partial A},$$

of size $(NX-3)\times(NX-3)$ making a perturbation of A_{0i} by 1, step by step for $i = 3, ..., NX-1$ and writing the perturbed p_{vis} into the corresponding column. For the same value of A^k_{0i}, we compute the quantities $(\phi_{0i,j})^k$, $(p_{\text{inv}})^k_i$ and then fill the matrix

$$\mathcal{J}_{\mathcal{N}} = \frac{\partial \mathcal{N}}{\partial A},$$

using the linear boundary value problem for ϕ_1 given in (4.107)-(4.108).

To this aim, we let $A_{i1} = 0$, perturb it by 1 step by step for $i = 2, ..., NX-1$ and writing the perturbed pressure in the corresponding column of the matrix $\mathcal{J}_{\mathcal{N}}$. We compute the operator equation at $y = 0$ in the same way as in (4.109), using central difference for $\Lambda > 0$

$$F_{i,1} = \frac{-3\phi_{1i,1} + 4\phi_{1i,2} - \phi_{1i,3}}{2\Delta y} + \frac{A_{1i+1} - A_{1i-1}}{2\Delta x} = 0, \tag{4.122}$$

and using backward differences for $\Lambda \leq 0$

$$F_{i,1} = \frac{-3\phi_{1i,1} + 4\phi_{1i,2} - \phi_{1i,3}}{2\Delta y} + \frac{3A_{1i} - 4A_{1i-1} + A_{1i-2}}{2\Delta x} = 0. \tag{4.123}$$

To calculate the perturbed pressure p_1, we use a 3rd order finite difference

$$p_{1i} = -\frac{-2\phi_{1i-1,1} - 3\phi_{1i,1} + 6\phi_{1i+1,1} - \phi_{1i+2,1}}{6\Delta x}. \tag{4.124}$$

The suggested numerical technique allows to adjust the viscous-inviscid interaction, whose

convergence is known to be a major problem. In order to improve the stability of the code, the formulas (4.122)-(4.124) enable us to calculate perturbations which are capable of propagating upstream even in the supersonic case. The global iterative process used for the solution of the interaction problem needed 6-7 iterations to get an accuracy of 10^{-4} using a relaxation parameter $r = 0.8$.

4.4.4 Results

We now present the numerical results for the interaction problem. The calculations were performed on a mesh $NX \times NY_{\text{inv}} = 101 \times 41$ for the upper deck and $NX \times NY_{\text{vis}} = 101 \times 76$ for the boundary layer. We used the step sizes $\Delta x = \Delta y = 0.2$ and the Kármán parameter was set to $K = 0.2$. The upstream curvature κ^- was set to 1. We used the parameter values $d_0 = 0.15, 0.2, 0.21$ corresponding to a downstream curvature of $\kappa^+ = 1.33, 1.56$ and 1.61 respectively.

In Figure 4.11, we show the pressure distribution that results from the viscous-inviscid interaction between an accelerating potential flow and the linear boundary layer.

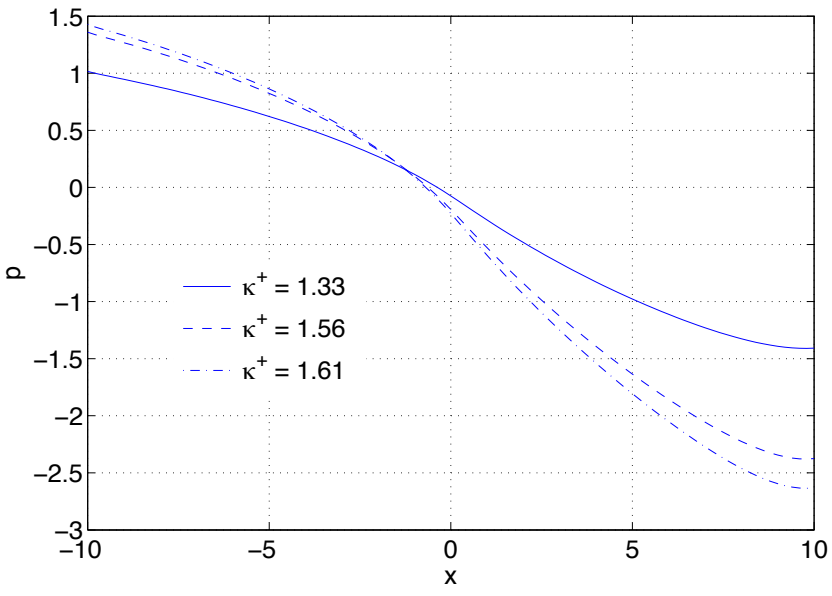

Figure 4.11: Pressure distribution across the interaction region.

The pressure distribution obtained for the transonic case is not dissimilar to the one obtained for subsonic flow, in Figure 3.6. We can see that the pressure decreases across the interaction region and as a result, the flow is accelerated. As parameter d_0 increases, which corresponds to the downstream curvature κ^+ increasing as well, we observe a faster decrease in pressure. The same behaviour was observed in subsonic flows. The flow thus experiences a more intense acceleration, as we can confirm on Figure 4.12, where the skin friction distribution across the interaction region is plotted for the same values of d_0.

This was the aim of this chapter. We showed that by calibrating carefully the parameters $\kappa^{\pm}$, we generate a singular pressure gradient capable of producing an intense acceleration of the flow within the interaction region. This has the effect of both delaying transition to turbulence as well as avoiding separation of the flow.

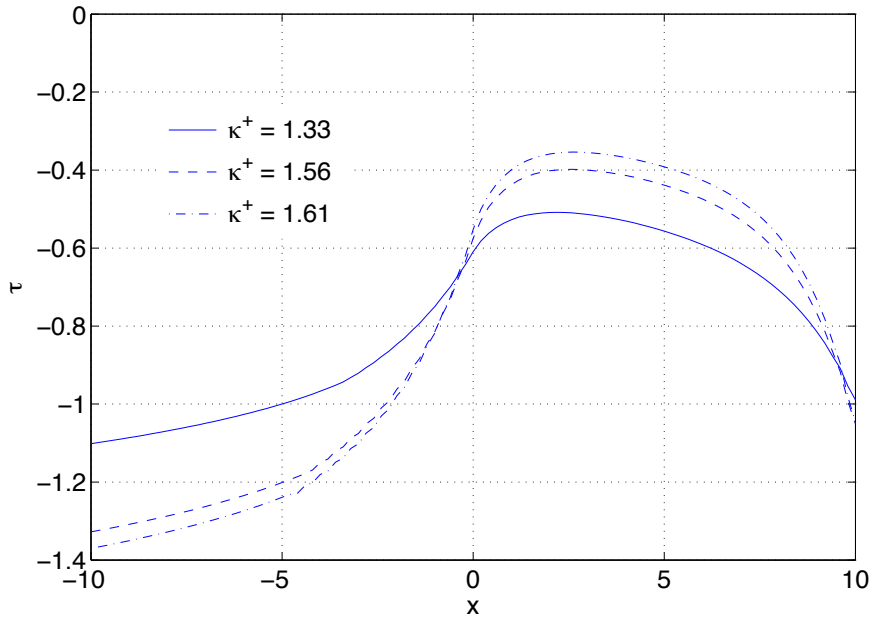

Figure 4.12: Skin friction distribution across the interaction region.

Chapter 5

Conclusion

Despite the progress done in recent years in the field of laminar-turbulent transition, many aspects are still to be studied, in particular the receptivity process. The first chapter of this thesis was devoted to that subject. We investigated compressible flow over a swept wing and started with linear stability analysis. We derived the inviscid stability equations, and subsequently calculated numerically the dispersion relation for inviscid stationary cross-flow vortices. This showed that for some value of the spanwise wavenumber β, we observe growing instability vortices. The receptivity mechanism introduced to generate and analyse these vortices was the addition of a spanwise periodic surface roughness, situated at some distance L from the leading edge. The first important result was that the wavenumber of the perturbations is twice the wavenumber of the surface roughness, and is due to non-linearity in the boundary conditions. A second important result is that in order to observe the inviscid instability, we need to assume that the perturbations scale like the square of the roughness size.

The receptivity analysis that ensued led to the use of the Fredholm Alternative, and a solvability condition was derived, which enabled us to calculate the initial amplitude of the disturbance. The growing vortex propagating downstream of the roughness was found to take the form

$$v'(x,y,z) = \mathcal{K}(\beta) \left[\int_0^\infty \mathrm{e}^{-\sigma_0 x} \left[g(x) \right]^2 \mathrm{d}x \right] \hat{v}_0(y)\, \mathrm{e}^{i\beta z + \sigma_0 x} + \cdots, \quad \text{as} \quad x \to \infty. \tag{5.1}$$

This equation emphasises the dependance of the amplitude of the crossflow vortex on the receptivity coefficient $\mathcal{K}(\beta)$, a global parameter independent of the roughness shape, and on the Laplace transform of the roughness shape.

In order to apply the no-slip conditions, viscosity should be restored to the problem, which can only be done if we impose some restrictions on the roughness size. This led to the introduction of a viscous sublayer, where we derived an analytical formula for the normal velocity flux at the edge of the boundary layer

$$\lim_{y_\star \to \infty} v' = -\frac{3\,\mathrm{Ai}'(0)}{2\pi}\,\mathrm{e}^{i\beta z_\star} \int_{-\infty}^{+\infty} \mathrm{e}^{i\alpha x_\star} \left[i\left(\lambda_1 \alpha + \lambda_3 \beta\right)\right]^{2/3} \bar{g}(\alpha)\mathrm{d}\alpha. \tag{5.2}$$

This condition can be used as a correction to the impermeability condition, and we presented a comparison between the two approaches.

The remaining chapters of the thesis concentrated on the viscous-inviscid interaction occurring in the vicinity of surface discontinuities. It was observed that discontinuities and singularities in the flow lead to singular pressure gradients in the inviscid part of the flow. These usually take the form

$$\frac{\mathrm{d}p}{\mathrm{d}x} = \kappa(-x)^\lambda, \qquad \text{as} \quad x \to 0^-.$$

This singularity should be smoothed by the introduction of an interaction region, which takes the standard triple deck form.

We focused on the special case when $\lambda = -1/3$, which corresponds to the demarcation between decay and growth of the perturbations in the interaction region. This specific pressure gradient arises in the study of the transonic flow past a discontinuity in curvature, where it is further assumed that the sonic point coincides with the point of discontinuity. This unusual singularity leads to the introduction of leading order logarithmic terms in the asymptotic expansion of the stream function upstream of the interaction region.

To get a better understanding of the interaction process, we first presented the problem in the context of subsonic flow. This required us to fix a specific body shape in order to

generate the correct pressure gradient. The simplification in the analysis came from the fact that both the viscous and inviscid part of the interaction region are governed by linear equations, thus allowing for analytical solutions. The key result of the analysis of the flow upstream of the triple deck was that the leading order skin friction on the wall is given by the formula

$$\tau_w = \frac{2^{9/4}\chi^{3/4}}{3^{7/4}\Gamma(2/3)^{3/4}}, \tag{5.3}$$

with χ being related to the curvature κ through $\chi = -3^{-3/2}10\,\kappa$. This indicates that the solution only exists for negative curvatures, a condition that can be relaxed if $|\kappa| \ll 1$. We proceeded to derive appropriate scalings for the triple deck, and found that its longitudinal extent σ satisfied a transcendental equation. In particular, we observed that σ appears smaller than in the classical triple deck approximation. The final formulation of the interaction problem consisted of linear equations both in the lower viscous deck and the upper inviscid deck, which allowed us to construct analytical solutions, expressed in terms of inverse Fourier transforms. These were performed numerically and were found to match very well with the upstream asymptotics.

We then turned back to the original problem, the study of transonic flow in the vicinity of a surface discontinuity. The investigation of the upstream inviscid flow revealed a variety of regimes, which are brought to light through the phase plane analysis. Two noteworthy regimes are the smooth acceleration of subsonic flow to supersonic flow, and the smooth deceleration of supersonic flow to subsonic flow. These only occur for particular values of the curvatures upstream and downstream of the discontinuity. Further increasing their respective values leads to the generation of a Prandtl-Meyer expansion fan or shockwaves.

The analysis of the flow in the upstream boundary layer was similar to the one carried out for subsonic flow, up to some constants. The main difference came from the calculation of the scaling of the triple deck region: we have to account for the fact that pressure perturbations in transonic flows are bigger than their subsonic counterpart. The formulation of the problem in the viscous sublayer of the interaction region turned out to be the same as the subsonic one. However, the inviscid upper deck is now governed by the nonlinear Kármán-Guderley equations. Due to the non-linearity of the equations in the upper deck,

the interaction problem was solved numerically. The pressure distribution resulting from the transonic viscous-inviscid interaction is similar to the one obtained for subsonic flows. As we increase the curvature downstream, the pressure decreases which results in the flow acceleration. Furthermore, the skin friction distribution across the interaction region was shown to increase, which is what we wanted to observe.

Further work

One of the directions in which to extend the results we presented in the crossflow receptivity analysis would be to look at a wider range of velocity profiles and to higher Mach number regimes. In particular, it would be of interest to investigate stability and receptivity characteristics for an incoming transonic flow. So far, only some aspects of the stability analysis have been studied (Mack 1979, 1989) and the receptivity theory remains to be developed.

The last two chapters of this thesis form part of a large chain of effort in understanding the viscous-inviscid interaction in transonic flow from a theoretical point of view, with the main tool being the use of Triple Deck Theory. The starting point was the work of Buldakov & Ruban (2002), who investigated the sonic point on a smooth body surface. Then came the work of Yumashev (2012), who extended this to small curvature discontinuities of the order

$$\mathrm{Re}^{-1/6} \ll \kappa^{\pm} \ll \frac{1}{\log \mathrm{Re}}.$$

Our work was yet another extension, this time to larger curvature discontinuities and favourable pressure gradients. As of yet, no results have been obtained in the case of an adverse pressure gradient, with the curvature $\kappa^{\pm}$ being of the order

$$\kappa^{\pm} \sim \frac{1}{\log \mathrm{Re}}.$$

This is a difficult task from an asymptotic point of view and should be the subject of further research.

References

ABRAMOWITZ, M., STEGUN, I.A. *et al*. (1972) *Handbook of mathematical functions*. Dover New York.

ANDERSON, J.D. (2010) *Fundamentals of Aerodynamics*. McGraw-Hill Science/Engineering/Math.

ARNAL, D., CASALIS, G., COUSTEIX, J. & RENEAUX, J. (1997) Laminar-turbulent transition in subsonic boundary layers-research and applications in france .

BATCHELOR, G.K. (2000) *An introduction to fluid dynamics*. Cambridge university press.

BENMALEK, A. & SARIC, W.S. (1994) Effects of curvature variations on the nonlinear evolution of Görtler vortices. *Physics of Fluids* **6** (10), 3353–3367.

BLASIUS, H. (1908) Grenzschichten in flussigkeiten mit kleiner reibung. *Z Math. Phys* **56** (1), 1–37.

BODONYI, R.J. & KLUWICK, A. (1998) Transonic trailing-edge flow. *The Quarterly Journal of Mechanics and Applied Mathematics* **51** (2), 297–310.

BOGOLEPOV, V.V. & LIPATOV, I.I. (1985) Investigation of three-dimensional local laminar flows. *PMTF Zhurnal Prikladnoi Mekhaniki i Tekhnicheskoi Fiziki* **1**, 28–36.

BROWN, S.N. & STEWARTSON, K. (1969) Laminar separation. *Annual Review of Fluid Mechanics* **1** (1), 45–72.

BULDAKOV, E.V. & RUBAN, A.I. (2002) On transonic viscous–inviscid interaction. *Journal of Fluid Mechanics* **470**, 291–317.

CHAPMAN, D.R., KUEHN, D.M. & LARSON, H.K. (1958) *Investigation of separated flows in supersonic and subsonic streams with emphasis on the effect of transition*, , vol. 1356. NACA.

CHOUDHARI, M. (1994) Roughness-induced generation of crossflow vortices in three-dimensional boundary layers. *Theoretical and Computational Fluid Dynamics* **6** (1), 1–30.

CHOUDHARI, M. & DUCK, P.W. (1996) Nonlinear excitation of inviscid stationary vortex instabilities in a boundary-layer flow. In *IUTAM Symposium on Nonlinear Instability and Transition in Three-Dimensional Boundary Layers*, pp. 409–422. Springer.

CHOUDHARI, M. & STREETT, C. (1990) Boundary layer receptivity phenomena in three-dimensional and high-speed boundary layers. In *AIAA, International Aerospace Planes Conference, 2 nd, Orlando, FL*, p. 1990.

DEYHLE, H. & BIPPES, H. (1996) Disturbance growth in an unstable three-dimensional boundary layer and its dependence on environmental conditions. *Journal of Fluid Mechanics* **316**, 73–113.

FRANKL, F.I. (1947) Studies in the theory of infinite aspect ratio wing moving with the speed of sound. *Dokl. Akad. Nauk SSSR* **57** (2), 1561–1564.

GASTER, M (1965) A simple device for preventing turbulent contamination on swept leading edges(preventing turbulent contamination of laminar flow on highly swept wings by attaching bump on leading edge). *ROYAL AERONAUTICAL SOCIETY, JOURNAL* **69**, 788.

GOLDSTEIN, S. (1930) Concerning some solutions of the boundary layer equations in hydrodynamics. In *Mathematical Proceedings of the Cambridge Philosophical Society*, , vol. 26, pp. 1–30. Cambridge Univ Press.

GOLDSTEIN, S. (1948) On laminar boundary-layer flow near a position of separation. *The Quarterly Journal of Mechanics and Applied Mathematics* **1** (1), 43–69.

GUDERLEY, G. (1957) *The Theory of Transonic Flow (translation)*. Pergamon Press (1962).

GUDERLEY, K.G. (1947) *Considerations of the structure of mixed subsonic-supersonic flow patterns*. Wright-Patterson Air Force Base.

HELMHOLTZ, H. (1868) Über discontinuirliche flüssigkeits-bewegungen. *Monatsber. Akad. Wiss.* **23**, 215–228.

KÁRMÁN, T. (1947) The similarity law of transonic flow. *Journal of Mathematics and Physics* **26** (4), 182–190.

KRAVTSOVA, M.A., ZAMETAEV, V.B. & RUBAN, A.I. (2005) An effective numerical method for solving viscous–inviscid interaction problems. *Philosophical Transactions of the Royal Society A: Mathematical, Physical and Engineering Sciences* **363** (1830), 1157–1167.

LANDAU, L.D. & LIFSHITZ, E.M. (1944) Mechanics of continuous media moscow. *Russia: Gostekhizdat* .

LIN, C.C. (1955) *The theory of hydrodynamic stability*. Cambridge University Press.

MACK, L.M. (1979) On the stability of the boundary layer on a transonic swept wing. *AIAA journal* **79**.

MACK, L.M. (1989) Stability of three-dimensional boundary layers on swept wings at transonic speeds. In *Symposium Transsonicum III*, pp. 209–223. Springer.

MESSITER, A.F. & HU, J.J. (1975) Laminar boundary layer at a discontinuity in wall curvature. *Quarterly of Applied Mathematics* **33**, 175–181.

MORKOVIN, M.V. (1969) On the many faces of transition. In *Viscous drag reduction*, pp. 1–31. Springer.

MUGHAL, M.S. (1998) Active control of wave instabilities in three-dimensional compressible flows. *Theoretical and computational fluid dynamics* **12** (4), 195–217.

NEILAND, V.Y. (1969) Theory of laminar boundary layer separation in supersonic flow. *Fluid Dynamics* **4** (4), 33–35.

RADEZTSKY, R.H., REIBERT, M.S. & SARIC, W.S. (1999) Effect of isolated micron-sized roughness on transition in swept-wing flows. *AIAA journal* **37** (11), 1370–1377.

RAYLEIGH, LORD (1879) On the stability, or instability, of certain fluid motions. *Proceedings of the London Mathematical Society* **1** (1), 57–72.

REED, H.L., SARIC, W.S. & ARNAL, D. (1996) Linear stability theory applied to boundary layers. *Annual review of fluid mechanics* **28** (1), 389–428.

REIBERT, M.S., SARIC, W.S., CARRILLO JR, R.B. & CHAPMAN, K.L. (1996) Experiments in nonlinear saturation of stationary crossflow vortices in a swept-wing boundary layer. *AIAA paper* **184**, 1996.

RESHOTKO, E. (1997) Progress, accomplishments and issues in transition research. In *AIAA, Fluid Dynamics Conference, 28 th, Snowmass Village, CO*.

REYNOLDS, O. (1883) An experimental investigation of the circumstances which determine whether the motion of water shall be direct or sinuous, and of the law of resistance in parallel channels. *Proceedings of the royal society of London* **35** (224-226), 84–99.

RUBAN, A.I. (1984) Acoustic generation of tollmien-schlichting waves. *Akademiia Nauk SSSR Izvestiia Mekhanika Zhidkosti i Gaza* **20**, 44–52.

RUBAN, A.I. & GAJJAR, J. (2014) *Fluid Dynamics: Part 1: Classical Fluid Dynamics*. Oxford University Press.

RUBAN, A.I. & GAJJAR, J. (2016) *Fluid Dynamics: Part 3: Boundary Layers*. OUP Oxford.

RUBAN, A.I. & TURKYILMAZ, I. (2000) On laminar separation at a corner point in transonic flow. *Journal of Fluid Mechanics* **423**, 345–380.

RUBAN, A.I., WU, X. & PEREIRA, R.M.S. (2006) Viscous–inviscid interaction in transonic prandtl–meyer flow. *Journal of Fluid Mechanics* **568**, 387–424.

SARIC, W.S. & REED, H.L. (2003) Crossflow instabilities–theory and technology. *AIAA paper* **771**, 2003.

SARIC, W.S. & REED, H.L. (2004) Toward practical laminar flow control-remaining challenges. *AIAA paper* **2311**, 2004.

SARIC, W.S., REED, H.L. & WHITE, E.B. (2003) Stability and transition of three-dimensional boundary layers. *Annual Review of Fluid Mechanics* **35** (1), 413–440.

SARIC, W.S., WHITE, E.B. & REED, H.L. (1999) Boundary-layer receptivity to freestream disturbances and its role in transition. *AIAA paper* (99-3788).

SMITH, F.T. & BROWN, S.N. (1990) The inviscid instability of a blasius boundary layer at large values of the mach number. *Journal of Fluid Mechanics* **219**, 499–518.

STEWARTSON, K. & WILLIAMS, P.G. (1969) Self-induced separation. *Proceedings of the Royal Society of London. A. Mathematical and Physical Sciences* **312** (1509), 181–206.

SYCHEV, V.V., RUBAN, A.I. & KOROLEV, G. (1987) Asymptotic theory of separated flows. *Moscow Izdatel Nauka* **1**.

TANEDA, S. (1956) Experimental investigation of the wakes behind cylinders and plates at low reynolds numbers. *Journal of the Physical Society of Japan* **11** (3), 302–307.

VAN DYKE, M. (1982) An album of fluid motion .

WHITE, E.B., SARIC, W.S., GLADDEN, R.D. & GABET, P.M. (2001) Stages of swept-wing transition. *AIAA Paper* **271**.

YUMASHEV, D. (2012) Theoretical study of an inviscid transonic flow near a discontinuity in wall curvature (part 1), *MIMS Eprints* .

Appendix A

Asymptotic properties of stability equation

When $y \gg 1$, functions U, W and ρ_b tend to their values at the edge of the boundary layer

$$U(y) \to U_e, \quad \rho_b(y) \to 1 \quad \text{and} \quad W(y) \to W_e,$$

which are found by solving the leading order problem. Recalling that $f = \sigma U + i\beta W$, we estimate

$$\rho_b f^2 \sim \sigma^2 U_e^2 - \beta^2 W_e^2 + 2i\sigma\beta U_e W_e \quad \text{as} \quad y \to \infty.$$

The middle term in equation (2.31) contains derivatives of f and ρ_b, which all vanish at infinity, and are thus set to zero. This gives us the following approximation for large y

$$\bar{p}'' - \lambda^2 \bar{p} = 0, \tag{A.1}$$

where

$$\lambda^2 = \beta^2(1 - M_\infty^2 W_e^2) - \sigma^2(1 - M_\infty^2 U_e^2) + 2M_\infty^2 i\sigma U_e W_e. \tag{A.2}$$

The solution to this equation is

$$\bar{p}(y;\sigma) = A\exp(\lambda y) + B\exp(-\lambda y). \tag{A.3}$$

In the general case, λ is complex so that $\bar{v}$ is a combination of exponentially growing/decaying sinusoids. The boundary condition (2.32) requires us to chose the root whose real part is negative, so that $\bar{p}$ decays at infinity.

Suppose now that $y \ll 1$. We can estimate

$$U(y) \sim W(y) \sim Cy + \cdots \quad \text{as} \quad y \to 0, \tag{A.4}$$

where C is a constant. Expanding the $\log$ term, equation (2.31) can be rewritten as

$$\bar{p}'' - \left(2\frac{f'}{f} + \frac{\rho_b'}{\rho_b}\right)\bar{p}' - \left(M_\infty^2 f^2 \rho_b + \beta^2 - \sigma^2\right)\bar{p} = 0, \tag{A.5}$$

and using estimates (A.4) and ignoring density variations, it reduces to

$$\bar{p}'' - \frac{2}{y}\bar{p}' + \left(\sigma^2 - \beta^2\right)\bar{p} = 0.$$

Let us assume that

$$\bar{p} = ay^\alpha + \cdots, \quad \text{as} \quad y \to 0,$$

with $\alpha \geq 0$. Substituting this in equation (A.5) leads to $\alpha = 0$ or $\alpha = 3$, so that the first term in the asymptotic expansion for small y is either a constant or proportional to y^3. According to boundary condition (2.32), we need $\bar{p}\,(0) = 0$, so this fixes

$$\bar{p} = ay^3 + \cdots \quad \text{as} \quad y \to 0.$$

This is also consistent with $\bar{p}\,'(0) = 0$, and the numerical results in the next section confirm this behaviour.

Appendix B

An example of the adjoint and Fredholm Alternative method

To motivate the technique used in the Section 2.3, we turn to the following model problem.

Find the solution to the problem

$$\phi'' + \lambda^2 \phi = 0, \quad \phi(0) = 0, \ \phi(1) = 0.$$

The general solution is given by

$$\phi = A\cos(\lambda y) + B\sin(\lambda y).$$

Applying the first boundary condition leads to $A = 0$. In order to apply the second boundary condition and not get a trivial solution, we see that we should choose $\lambda = \pi$, leading to

$$\phi = B\sin(\pi y).$$

The amplitude B remains arbitrary. Let's now solve the problem

$$\phi'' + \lambda^2 \phi = 0, \quad \phi(0) = 1, \ \phi(1) = 0.$$

There is an exact solution to this problem given by

$$\phi(y;\lambda) = \cos(\lambda y) - \sec(\lambda)\sin(\lambda y).$$

This is analytic everywhere in the y plane, but exhibits a singularity in the complex σ plane at $\lambda = \pi$. We find that

$$\phi(y) = -\frac{1}{\lambda - \pi}\sin(\lambda y) + \cdots \quad \text{as} \quad \lambda \to \pi.$$

with $\lambda = \pi$ being the eigenvalue of the homogeneous problem.

Now, we can get to the same result using a different technique, which can be used when we do not have an exact analytical expression for $\phi(y;\lambda)$. The reason why we want to do that is because we are interested in calculating an integral of the form

$$\phi'(x,y) = \int_{a-i\infty}^{a+i\infty} \mathrm{e}^{\lambda x}\,\phi(y;\lambda)\mathrm{d}\lambda. \tag{B.1}$$

This integral is evaluated using residues, so that the only thing we need to know is the behaviour of ϕ around its singularities. We thus assume that $\phi(y;\lambda)$ is singular at $\lambda = \lambda_0$, with λ_0 to be found, and we write

$$\phi(y;\lambda) = \frac{1}{\lambda - \lambda_0}\phi_0(y) + \phi_1(y) + \cdots \quad \text{as} \quad \lambda \to \lambda_0. \tag{B.2}$$

This expansion is substituted in the original equation and in the boundary conditions, leading to

$$\phi_0'' + \lambda_0^2\phi_0 + (\lambda - \lambda_0)(\phi_1'' + \lambda_0^2\phi_1 + 2\lambda_0\phi_0) + \cdots = 0, \tag{B.3}$$

where the dots represent terms of order $(\lambda - \lambda_0)^2$. The boundary conditions are then

$$\phi_0(0) = \phi_0(1) = 0, \quad \phi_1(0) = 1, \phi_1(1) = 0. \tag{B.4}$$

The problem for ϕ_0 reduces to the homogeneous one. The solution to the first equation

is then given by

$$\phi_0(y) = A\cos(\lambda_0 y) + B\sin(\lambda_0 y).$$

Applying the boundary conditions, we find that $A = 0$, and we should chose $\lambda_0 = \pi$. The amplitude B of the solution remains undetermined at this stage.

The second equation is

$$\phi_1'' + \pi^2\phi_1 = -2\pi B\sin(\pi y) \tag{B.5}$$

subject to $\phi_1(0) = 1, \phi_1(1) = 0$. It turns out that this problem has a solution only for a specific value of B. We use the adjoint method to find B in the general case. We multiply both sides of the equation by some function $\xi(y)$ and integrate from 0 to 1. The first term on the right hand side is then integrated by parts twice, leading to the equation

$$\phi'(1)\xi(1) - \phi'(0)\xi(0) - \phi(1)\xi'(1) + \phi(0)\xi'(0) + \int_0^1 \phi(y)\left(\xi'' + \pi^2\xi\right)\mathrm{d}y = -2B\pi\int_0^1 \sin(\pi y)\xi(y)\mathrm{d}y. \tag{B.6}$$

We chose the function $\xi(y)$ to satisfy the equation $\xi'' + \pi^2\xi = 0$ with $\xi(0) = \xi(1) = 0$. Thus, equation (B.6) becomes

$$\phi(0)\xi'(0) = -2\pi B\int_0^1 \sin(\pi y)\xi(y)\mathrm{d}y. \tag{B.7}$$

We can then write

$$B = -\frac{\phi(0)\xi'(0)}{2\pi\int_0^1 \sin(\pi y)\xi(y)\mathrm{d}y}. \tag{B.8}$$

In this special case, we see that $\xi(y) = B\sin(\pi y)$, and substituting this gives $B = -1$.

Hence,

$$\phi(y;\lambda) = -\frac{1}{\lambda - \pi}\sin(\lambda y) + \cdots \quad \text{as} \quad \lambda \to \pi$$

as before.